martensite is formed, it rises steeply to >2600 J mol^{-1}. Lee et al [21] conclude that the stored energy in lath martensites may be up to 1150 J mol^{-1} higher than in twinned martensites.

Combination of the free energy and calorimetric data suggests that the net driving force at M_s is very small for lath martensite, but may be appreciable for plate martensite. Indeed, Argent [22] has computed M_s curves for Fe-Cr and Fe-Co alloys on the assumptions that the net driving force is zero (i.e., there is no nucleation barrier), that surface and dislocation entropies may be neglected, and that the stored energy is ∿1000 J mol^{-1}. The values are in reasonable agreement with experiment, and the estimated M_s for pure iron is 855K. Note that the assumption also implies that adiabatic heating [23-24] is not significant for lath martensites.

Lee et al considered the stored energy to arise from dislocations or twin boundaries, but there are also contributions from the interphase interfaces and the coherency strains. For oblate spheroidal plates of dimensions a and c, and for laths with a>b>>c, the interfacial energy per unit volume is $E_s \simeq 3\sigma/2c$ where σ is the specific interfacial free energy. With $\sigma = 200$ mJ m^{-2} and c = 1 μm, E_s is insignificant (0.3 MJ m$^{-3} \simeq 2$ J mol^{-1}), but this term is, of course, important in classical nucleation theory since if c = 1 nm, $E_s \simeq 2$ kJ mol^{-1}. The energy due to internal twinning is similarly $E_t \simeq \sigma^t/t$ where t is the twin separation, and if $\sigma^t = 200$ mJ m^{-2} and t = 20 nm, E_t is only ∿100 J mol^{-1}.

The elastic energy per unit volume of a transformed oblate spheroid with the same shear modulus μ and Poisson's ratio as the isotropic constraining matrix is usually quoted as $E_e = Ac/a$ where [25-26]

$$A = [\pi(2-\nu)/8(1-\nu)]\mu s^2 + (\pi/4)\mu\xi^2 \simeq \mu(s^2 + \xi^2) \qquad (2)$$

1 - ν missing

and s and ξ are the shear and normal strains in the unconstrained invariant plane strain (IPS) shape deformation. With μ = 5.10^{10} Pa, s = 0.18, ξ = 0.05, we obtain E = 85 MJ m$^{-3} \simeq 600$ J mol^{-1} for a typical c/a = 0.05. This may be an overestimate since linear elastic theory has been used for large strains, and the energy may also be decreased by plastic deformation or by formation of plates in groups, or of laths (which otherwise have larger E_e) in self-accommodating packets.

Eqn (2) is derived by replacing the stress-free strains of the martensite plate by the strains of the average or shape deformation, and in the real situation additional strain energy arises from the alternating twins or from the interface dislocations. Mura el al [70] have treated the twin case in which the stress free strain is periodic and they find that the elastic energy does not tend to zero as c/a→0, but rather to a constant value per unit volume given by

$$E_e = f(1-f)(C_{11}-C_{12})(\varepsilon_1-\varepsilon_2)^2 \qquad (2a)$$

where f is the volume fraction of one orientation. C_{11} and C_{12} are the anisotropic elastic stiffnesses of the plate and ε_1, ε_2 are the

principal strains of the lattice (Bain) deformation. Numerical estimates from eqn (2a) give a very large energy of ~ 14 kJ mol^{-1} for steels, and although the use of linear elastic theory severely restricts the accuracy, it is noteworthy that the estimate considerably exceeds the available driving force. An even larger energy was obtained by Kato et al [73] from a somewhat unusual model of slipped martensite.

The reason for the apparent paradox is that for a plate of finite thickness, the additional energy should be incorporated into the surface energy, as is implied but not clearly stated in the work of Khachaturyan and Shatalov [74] who also used anisotropic elasticity and gave the first treatment of the periodic twin structure. They showed that the strain energy caused by the heterogenity of the plate arises from strains located near the habit plane so that it is proportional to the area of this interface. The interface dislocations of a single crystal of "slipped" martensite, or the periodic structure of twinned martensite, thus raise the interfacial free energy from a low value characteristic of a fully coherent interface to an effective value (assumed above to be 200 mJ m^{-2}) appropriate to the semi-coherent interface. If the twin thickness is now held constant as $c \to 0$, the energy per unit volume tends to a large constant value. It follows that the energy of eqn (2a) whilst relevant to some nucleation models, does not enter into the free energy balance for appreciable volumes of transformed product, and it is justifiable for most purposes to use eqn (2) together with an appropriate value for the effective surface free energy. The formulation of the theory developed by Khachaturyan is not restricted to an ellipsoidal shape, and in a later paper [75] he has shown how to calculate the habit plane shape which minimizes the strain energy.

Lath martensites contain dense tangles of lattice dislocations, the untwinned regions of plate martensites contain arrays of screw dislocations, and accompanying plastic deformation causes dislocation tangles and pile-ups in the surrounding austenite. For a dislocation density ρ, the energy is

$$E_d = (\rho \mu b^2/4\pi K)[\ln(R/r_o) + B] \qquad (3)$$

where $1 > K > 1-\nu$, R and r_o are outer and inner cut-off radii and B varies with assumptions about pile-ups. With $\rho = 10^{16-17}$ m^{-2} and $R/r_o = 10^4$, Li et al estimate E_d as 120-2800 J mol^{-1}; the large uncertainty arises mainly from the measured dislocation densities in lath martensites [27] which at the upper limits give very high stored energies. The origin of the dislocations inside laths and partly twinned plates is unknown, but if they are also due to induced plastic deformation, any contribution of E_d to stored energy should be balanced by a greater reduction in E_e. Thus $E_e + E_s + E_t \simeq E_e$ (for macroscopic plates) should represent the upper limit of stored energy, and any difference between laths and plates might only be due to the better elastic accomodation of the latter. The conclusion fails, however, if the dislocations do not accommodate the shape change.

For an Fe-13.7% Ni-0.86% C steel transformed at 297-188K, the

measured enthalpy change at 507K decreases dramatically from 4650 to 1600 J mol^{-1} as the volume of plate martensite increases from 7 to 59% [21]. The implied increase in stored energy is attributed to the high work-hardening and high dislocation densities in regions of deformed austenite which have subsequently to be transformed to martensite. Further experiments we needed to clarify and extend these results.

2.2. Other Martensitic Transformations

ε-martensite forms in some steels at smaller driving forces than α-martensite e.g. 270 J mol^{-1} in Fe-Mn [8] and 210 J mol^{-1} in Fe-Ru [28]. The similar transformation in cobalt begins at $\sim$5 J mol^{-1} in single crystals [29-30] but ΔG_c increases slightly in subsequent cycles. Measurements in which the enthalpy change during the heating transition exceeded that during cooling by $\sim$125 J mol^{-1} have been interpreted as the stored enthalpy of defects accumulated during a cycle [30], However, the result seems doubtful since at such low ΔG_c only high entropic defects could form.

Transformations from a bcc to a hcp or an orthorhombic phase in Ti, Zr and Hf alloys constitute another major group. For all Ti-Zr alloys, $\Delta G_c \simeq 220$ J mol^{-1}; M_s falls more steeply with solute content in Ti-Mn, Ti-Mo, Ti-Ta, etc., and ΔG_c is presumable larger. Many other non-ferrous transformations take place with little hysteresis and thus have small ΔG_c. Thermoelastic martensites come into this category; typical values for ΔG_c in Au-Ag-Cd alloys of varying Au:Ag ratio are 12-30 J mol^{-1}.

2.3. Thermoelastic Martensite

The concept of thermoelastic martensite, originally due to Kurdjumov and Khandros [33] has assumed increased importance in recent years because of the interest in shape-memory and related effects. In a thermoelastic transformation the assembly attains a minimum free energy at some finite volume fraction of product, so that a variation in the (thermal or mechanical) driving force produces a corresponding increase or decrease in the volume of martensite. This requires that ΔG_c, or most of it, is stored reversibly as surface, elastic and twin energies, but not as dislocation energy. I previously suggested [34] that thermoelastic martensite is characterized by a small driving force, small values of s and ξ, and a high matrix yield stress. Wayman [35] has pointed out that s is not always small.

In discussing the thermodynamics of thermoelastic martensite, Tong and Wayman [36-37] and Olsen and Cohen [38-39] have disagreed about whether A_f can be below T_o. Olsen and Cohen follow early treatments in supposing that as a plate of constant length a_1 thickens, the energy E_e per unit volume increases until a minimum in total free energy is attained. If this happens without dislocation sources operating, the plate has attained thermoelastic equilibrium with the matrix, and its thickness is given by $c = a_1\Delta g/2A$ where Δg is the net chemical and mechanical driving force per unit volume. Olsen and Cohen assume that as Δg is reduced by raising the temperature, the plate becomes unstable when it attains the dimensions of a critical nucleus, i.e., when $c^2 =$

$a_1 \sigma/A$, and that if there is no interface frictional stress it will then spontaneously contract to zero dimensions. The net driving force at this condition is $\Delta g = 2(A\sigma/a_1)^{1/2}$ so that the longest plates disappear last. In the absence of frictional stresses, this theory gives $A_f < T_o$, but it should perhaps be emphasized that for reasonably large plates $T_o - A_f$ is very small. For example, if $A = 2.10^9$ $J\,m^{-3}$ and $\sigma = 0.2$ $J\,m^{-2}$, Δg at A_f is ~ 40 MJ m^{-3} for $a_1 = 1$ μm and ~ 1 MJ m^{-3} for $a_1 = 1$ mm; $T_o - A_f$ is appreciable in the first case, but very small in the second.

A difficulty with this theory is that the shrinking plate is treated as if it had nucleated homogeneously and no allowance is made for the energy of any residual defect. Nucleation is believed to be heterogeneous and the reproducibility of the hysteresis loop and of the microstructure in successive cycles of transformation implies that the nucleation sites retain their identities. It follows that the free energy may not begin to decrease with decreasing length when the classical saddle point is reached.

Tong and Wayman neglect the coherency strain energy for the initial transformation at M_s and consider the lengthening of a plate of constant thickness; they also point out that new plates may be nucleated in any increment of Δg, It is not clear how either of these processes could result in thermoelastic equilibrium but Wayman [71] has emphasized that plate lengthening is found experimentally to be a dominant growth process in many thermoelastic alloys. In terms of the model just described, lengthwise growth and nucleation can not be separated, and both represent increments in transformed volume which are additional to those produced by thermoelastic growth. Thus, although the volume of an individual thermoelastic plate increases linearly with Δg, the overall relation between volume transformed and driving force need not be linear. There will also be a deviation from linearity during heating because of the progressive disappearance of the smaller plates.

The alloy Fe_3Pt is thermoelastic when ordered but not when disordered. Olsen and Owen [40] suggest that the lower shear modulus leads to the virtual absence of a plastic accommodation zone around a plate in the ordered matrix. In a further development, Ling and Owen [41] consider in outline the effects of an assembly of partly self-accommodating plates.

In Cu-14 Al- 2.5 Ni alloys, the transformation is normally thermoelastic but single interface transformation without elastic strain energy can be obtained in suitable single crystals held in a temperature gradient. Salzbrenner and Cohen [72] have used the single interface transformation to bracket T_o between the interface advance temperatures on cooling and heating, the hysteresis being attributed to the frictional resistance to interface motion. Multiple interface transformations in a single crystal involve elastic strain energy which depresses the transformation curves both on cooling and heating, but since the martensite apparently nucleates first at a free corner of the single crystal, there are no strain energy terms in the energy balance at M_s and at A_f, and T_o may be bracketed between these temperatures, as

postulated by Tong and Wayman. This is no longer true in polycrystalline specimens where elastic energy affects both M_s and A_f and the latter may also be below T_o.

The net heat evolution measured in a differential scanning calorimeter was 515 J mol^{-1} in the single interface transformation and some 40-90 J mol^{-1} smaller in polycrystalline specimens of various grain sizes [72]. The difference is attributed to the stored elastic enthalpy, which thus has a mean value of ∿15% of the chemical enthalpy change. There is, however, an unexplained difficulty which exactly parallels that arising from the results on cobalt mentioned above [30], namely that this estimate of the stored elastic enthalpy is much larger than would be predicted from the chemical free energy difference between the phases. From the transformation temperatures, the free energy driving force is estimated as only ∿26 J mol^{-1} for growth, 29 J mol^{-1} for corner nucleation and 39 J mol^{-1} for interior nucleation.

III. Nucleation

3.1. The Strain Spinodal

It is sometimes difficult to convince a solid state physicist that there is any difficulty in nucleating martensite, whilst a metallurgist, after substituting a few numbers into the equations of classical nucleation theory, is likely to conclude that nucleation is impossible! The truth must lie between these extremes, but the best approach to an acceptable model is by no means obvious. Pre-existing embryo theories [5] have been discarded and it is generally accepted that nucleation is probably heterogeneous. In a classical model, the interaction between a defect and an embryo may be divided, somewhat arbitrarily, into an effective addition to the driving force and an effective lowering of σ. According to Guimaraes and Alves [42], the former is negligible and the latter is estimated from experimental data [43] for steels as ∿125 mJ m^{-2} which is rather more than one-half of the assumed interfacial energy.

Various authors have speculated that the concept of a strain spinodal, which exists for example at the temperature T_u defined above, might be relevant to the nucleation of martensite. In particular, Suzuki and Wuttig [44] have proposed that a strain-gradient energy, analogous to the gradient energy of spinodal decomposition, should be introduced. If this term were positive, it would have a stabilizing effect on shorter wave-length strain fluctuations below T_u; however, Nakanishi [45] has pointed out that even in alloys which show pre-transformation anomalies, the elastic constant which softens remains finite at M_s so that simple soft mode instabilities could only arise with a negative strain gradient energy.

The present author believes that there is very strong evidence that the parent lattice as a whole does not become mechanically unstable when martensite begins to form, and this is reinforced by the morphology of the product. However, Fig. 2 suggests another possibility, namely that if some local region of the lattice at temperature T_1 is

given a finite deformation to a configuration η_1 beyond which $\partial^2 \Delta G / \partial \eta_1^2$ is negative, this region may then spontaneously transform to martensite. Clapp [46] suggested that the strains near lattice defects bring some regions close to the strain spinodal; he specifically considered the free surface and grain boundaries as likely nucleating agents, but it is perhaps more probable that a dislocation configuration is responsible. The important point about this approach, however, is that the strain field of the defect need not resemble the structure of the final product, and the critical (saddle-point) configuration for a nucleus just out- side the region of instability would be very different from the classical model of the nucleus. The theoretical treatment should then resemble Cahn and Hilliard's theory of nucleation just outside the ordinary spinodal [47]; the interface would be diffuse and the work required to form the critical configuration would tend to zero continuously as the pre-existing (defect) strain approached the value where $\partial^2 \Delta G / \partial \eta^2 = 0$. Moreover, thermally-activated nucleation would occur in the region just outside the strain spinodal, whilst if the spinodal were crossed by continued cooling, the local lattice near the defect would be mechan- ically unstable and nucleate spontaneously.

Whilst this approach appears promising, it is difficult to make it quantitative since neither the $\Delta G-\eta$ curves (which are strictly not one- dimensional curves but surfaces in six-dimensional configuration space) nor the detailed nature of the nucleating defect are known. Recent calculations of the finite strains needed to produce instabilities between the fcc and bcc structures have been made for the alkali metals by McDonald [48] using a uniaxial strain and by Ledbetter and Suzuki [49] using a general Bain strain, and represent the first stage in the construction of a theoretical curve of the type of Fig. 2. In order to deal with an inhomogeneous system, it may be necessary to use a suitable trial function for the variation of strain with distance, as proposed by Cahn and Green [50], and it will also be necessary to introduce the strain gradient energies about which almost nothing is known at present.

3.2. Specific Models of Nucleation

The traditional approach to heterogeneous nucleation is to cal- culate the energy of a nucleus forming in the vicinity of a likely defect configuration as a function of size in order to find the saddle point condition. The catalytic effect of the defect may be expressed in terms of surface or core energy which is destroyed and of elastic interaction energy between the defect and the nucleus. Another type of theory considers a nucleating defect with a highly specific strain field which either closely approximates the final structure or else is assumed to represent a critical stage in its formation. The most highly developed model of this kind is probably that of Olsen and Cohen [51], whose basic postulates are that nucleation begins with faulting on the close-packed planes of the parent lattice, the fault displace- ment being derived from existing defects, and that in the subsequent readjustments the fault plane remains unrotated.

The model is first applied to the fcc → hcp transformation and is formulated in terms of classical nucleation theory, the energy per unit

area of a fault which has n planes in hcp configuration being written as the sum of volume and interfacial free energies

$$\gamma(n) = n\rho(\Delta G + E_e) + 2\sigma(n) \qquad (4)$$

where ρ is the number of mols per unit area of the close-packed planes, E_e is the strain energy additional to that of the nucleating defect, and the interfacial energy $\sigma(n)$ is later assumed to be independent of n for faults greater than two layers thick. ΔG is negative below T_o and $\gamma(n)$ becomes negative at $T_2 < T_o$ where T_2 increases as n increases. Using parameters appropriate to Fe-Cr-Ni alloys and assuming that spontaneous dissociation occurs at $M_s = T_2$, the critical thickness is 7-10 lattice planes and thus corresponds to the dissociation of 4-5 lattice dislocations.

The most interesting part of the Olsen-Cohen theory is the proposal that the fcc → bcc, bcc → hcp, and related transformations also begin with faulting on the close-packed planes of the parent structure. The theory is partly based on the Bogers-Burgers hard-sphere model for the fcc → bcc transition [52-53] which involves two successive IPS deformations on intersecting close-packed planes. In the Olsen-Cohen theory, the first of these faulted regions is produced by dislocation dissociation, and is then supposed to change spontaneously into the bcc structure by a modified form of the Bogers-Burgers second IPS which is heterogeneous on a scale of every eight close-packed planes. This leaves the original fault planes unrotated and generates a bcc structure in the Kurdjumov-Sachs orientation but with an incorrect lattice parameter. The long-range stress field produced by this second IPS is next compensated by screw dislocations in the interface; this corresponds to the lattice invariant deformation of the phenomenological theories, and the structural model at this stage is close to Frank's model of martensite. Finally, adjustments of the lattice parameter to the equilibrium value and establishment of an IPS shape deformation to allow growth to continue require rotation away from the Kurdjumov-Sachs orientation and simultaneous rotation of the habit plane out of the close-packed plane. This last step is assumed to occur at a later time than the others, which are simultaneous with the formation of the initial fault, and it may possibly account for the different crystallography of e.g. {3,10,15} and {225} plates. Estimates of the various contributions to the energy of the fault embryo again lead to the conclusion that 4 or 5 properly spaced dislocations should dissociate spontaneously at M_s in Fe-Ni alloys.

Similar descriptions are given for crystallographic transitions between the other common metallic structures. Consideration of various possible rate-limiting steps in the formation of the nucleus leads to the tentative conclusion that the frictional resistance to the growth of the embryo in the fault plane may be the most important factor. Spontaneous growth of the fault would then take place only at some finite negative value of $\gamma(n)$; alternatively, if this growth were thermally activated, isothermal growth of the sub-critical nuclei would be expected above the temperature of athermal nucleation. In contrast to classical theories of nucleation, the activation energy would vary approximately linearly with driving force, as sometimes observed [3].

The Olsen-Cohen model is based on a very specific nucleating defect, namely a short wall of correctly spaced dislocations, which the authors consider may be present as part of a grain boundary, at a particle-matrix interface, or as a dislocation pile-up on several parallel slip planes. For the fcc → hcp transformation, the theory differs only slightly from earlier descriptions [54-55] and more recent rival models [56-57]. Experimental evidence in support of dislocation dissociation has accumulated steadily [58-60], but sometimes indicates that the hcp region develops by random accumulation of single faults. Brooks et al [60] have recently analyzed the fault contrast and shown there is a displacement normal to the fault, proportional to n and in the same sense as the deviation of the hcp structure from the ideal axial ratio of $(8/3)^{1/2}$, thus supporting the hcp model of a fault.

It is much more difficult to assess the validity of the faulting hypothesis for the formation of semi-coherent martensites where a single IPS will not produce the product structure. The basic posulate that nucleation is catalysed by a group of lattice dislocations seems very plausible and is supported by recent evidence from in situ experiments [60-61] that α martensite forms near dislocation pile-ups and also by the absence of transformation in small particles constrained by a matrix unless they are sheared [62-64]. However, it is not clear that the specific role of the dislocations is to generate the strain field of a stacking fault, and the experimental observation that the close-packed planes of the two structures remain nearly parallel, does not seem to the present author to be of great significance. Direct evidence of dislocation dissociation may be difficult to obtain, but in support of the model Olsen and Cohen [51] summarize various observations which have been made of fault-like embryos on close-packed planes. An embryo on the {110} planes of the ordered bcc structure of Au-Cd later assumed the macroscopic morphology [76]. Thus the faulting mechanism may apply to bcc structures despite the absence of metastable configurations in the calculated γ-surfaces for single layer faults [65].

There have been several other recent attempts to apply classical nucleation theory to the heterogeneous nucleation of martensite by dislocations. Easterling and Tholen [66] considered an embryo formed inside a growing dislocation loop, and concluded there would be no nucleation barrier for a twinned martensite plate. However, this result is obtained by the assumption that the interfacial free energy of twinned martensite is only ~ 20 mJ m^{-2} whereas a value similar to that calculated for the dislocation model of the interface (~ 200 mJ m^{-2}) is actually appropriate; moreover, the energy of the dislocation loop has been omitted from the free energy expression [67]. When these corrections are made, this model leads to a very large barrier. Suzuki et al [61] calculated the condition for the net free energy, including the elastic interaction with the stress field of the pile-up, to be zero, and concluded this requires ~ 22 dislocations which is consistent with their experimental observations on stainless steel. However,

their calculation appears to be invalid since the interfacial free energy is neglected, and indeed the finite number of dislocations results only from the arbitrary assumption that the oblate spheroidal nucleus has a/c ≃ 10.

In a recent calculation, Suezawa and Cook [67] treat a dislocation pile-up as a superdislocation and use Fourier methods to calculate the interaction energy with an oblate spheroidal nucleus described by the averaged strain field of two twin-related Bain strains. The dislocation stress field falls off as $1/r$ and when multiplied by the volume of an embryo, an interaction which behaves in certain respects like a negative interfacial free energy results and so facilitates nucleation. The free energy of an embryo containing q atoms is $C q + D q^{2/3}$ where C contains the chemical and coherency strain energies and D is proportional to the effective interfacial energy σ_e. For N dislocations, $\sigma_e = \sigma + N\sigma_i$ where the negative term σ_i varies with a/c and represents the interaction with a single dislocation. In order for C to be negative, which is necessary for nucleation, Suezawa and Cook estimate a/c ≃ 20 for Fe-29% Ni; this fixes σ_e as ∿ 20 mJ m^{-2} and hence N ≃ 10 if σ = 200 mJ m^{-2}. The model predicts isothermal (thermally-activated) nucleation if C < 0 and D > 0, and athermal nucleation if both C and D are negative. C contains $E_e = Ac/a$ (see eqn. 2) and thus decreases with increasing a/c, whereas D increases with increasing a/c. At temperatures where nucleation first becomes possible, C is only negative at relatively large a/c for which D is necessarily positive. However, C also decreases with increasing driving force as the temperature is lowered, whereas D is insensitive to temperature, so that a temperature may be reached where for some value of a/c, both C and D are negative. The activation barrier to nucleation has then disappeared.

Most models of nucleation predict a temperature range of isothermal nucleation above that of athermal nucleation, whereas in some steels and possibly other alloys only athermal nucleation is observed. Magee [3] pointed out that athermally nucleated steels always contain interstitials which are mobile at the M_s temperature, and he suggested that the mobility of these interstitials prevents thermally activated nucleation of martensite either by lowering the driving force or by pinning the interface. The result is a bainitic transformation in the temperature range where isothermal martensite would otherwise be formed.

IV. Kinetics of Athermal Transformation

The kinetic description given by Magee [3] in which emphasis was laid on the effects of auto-catalytic nucleation has been further extended by Guimaraes and Gomes [69] who have considered specifically the effects of prior austenitic grain size. Experimental results [68-69] show that as the grain size decreases, the burst temperature and the volume fraction of martensite formed in the initial burst both decrease. The variation is due mainly to changes in the fraction of grains which contain martensite; this fraction is small in fine-grained material where the initial transformation is thus very heterogeneous. The fraction of partly transformed austenitic grains increases with

decreasing temperature, but remains smaller in the fine-grained materials over an appreciable temperature range ($\sim$ 50K in Fe-31.9% Ni-0.02% C). The volume fraction of martensite in those grains which have partly transformed is appreciably less dependent on grain size; the increase in this fraction with decreasing temperature is referred to as "fill-in", whereas the spreading of transformation into neighboring, previously untransformed grains, is called "propagation". It follows that the influence of propagation is more pronounced in the fine-grained material.

Guimaraes and Gomes consider that their results support the concept that propagation is mainly due to autocatalytic nucleation across grain and twin boundaries, and they develop a simple equation to represent the variation of the volume fraction of partly transformed grains with temperature. In this theory, the rate of propagation is proportional to the square of the volume fraction, and the greater effectiveness of the first formed plates in the larger grained austenite is attributed to their larger sizes and hence the greater extents of their accompanying stress fields.

Acknowledgements

I should like to thank many friends and colleagues and especially Dr. J. W. Cahn, Professor M. Cohen, Dr. A. G. Khachaturyan, Professor T. Mori, Professor T. Mura, Dr. G. B. Olsen and Professor C. M. Wayman for very helpful discussion and comments. I am grateful to Dr. J. W. Brooks, Dr. H. E. Cook and Dr. H. M. Ledbetter for allowing me to mention unpublished research work.

Erratum

The very high dislocation densities assumed for lath martensites [21-2] are incorrectly quoted from [27] and if the actual measured densities [27,77] are used, the calculated stored energy due to dislocations is reduced by a factor of $\sim$20. This strongly reinforces the conclusion that any difference in stored energies of lath and plate martensites is likely to have its origin in the better elastic accommodation of the plates. I am greatly indebted to Dr Bhadeshia for bringing this mistake and reference [77] to my attention.

[77] L.A. Norstrom: Scan. J. of Met., 5(1976), 159.

References

[1] A. R. Troiano and A. B. Greninger: Metal Progress, 50(1946), 303.

[2] G. V. Kurdjumov: J. Tech. Phys. USSR, 18(1948), 999, 1004, 1011.

[3] C. L. Magee: Phase Transformations, ASM, Cleveland, (1970), 115.

[4] L. D. Landau and E. M. Lifshitz: Statistical Physics, Pergamon Press, Oxford, (1969).

[5] L. Kaufman and M. Cohen: Prog. in Met. Phys., 7(1958), 165.

[6] T. Bell and W. S. Owen: Trans. AIME, 239(1967), 1940.

[7] Y. Imai, M. Izumiyama and M. Tsuchiya: Sci. Rep. Res. Inst. Tohoku Univ., A17(1965), 173.

[8] K. Ishida: Scripta Met., 11(1977), 237.

[9] A. Gilbert and W. S. Owen: Acta Met., 10(1962), 45.

[10] W. S. Owen, E. A. Wilson and T. Bell: High Strength Materials, Ed. by V. F. Zackay and H. I. Aaronson, Interscience Publishers, New York, (1964), 167.

[11] M. J. Bibby and J. Gordon Parr: JISI, 202(1964), 100.

[12] W. D. Swanson and J. Gordon Parr: JISI, 202(1964), 104.

[13] E. A. Wilson: Scripta Met., 4(1970), 309.

[14] O. P. Morozov, D. A. Mirzayev and M. M. Shteynberg: Phys. of Metals and Metallogr., 32(1971), (6)170.

[15] O. P. Morozov, D. A. Mirzayev and M. M. Shteynberg: Ibid, 34(1972), (4) 114.

[16] R. H. Goodenow and R. F. Hehemann: Trans. AIME, 233(1965), 1777.

[17] J. S. Pascover and S. V. Radcliffe: Ibid, 242(1968), 673.

[18] K. Ishida and T. Nishizawa: Trans. Jap. Inst. Metals, 15(1974), 217.

[19] E. A. Wilson: Scripta Met., 12(1978), 961.

[20] L. Kaufman, E. V. Clougherty and R. J. Weiss: Acta Met., 11(1963), 323.

[21] B. Lee, S. Millman, I. L. MacDougall, S. R. Keown and B. B. Argent: Met. Sc., 7(1977), 261.

[22] B. B. Argent: Ibid, 10(1976), 409.

[23] O. Krisement, E. Houdrement and F. Wever: Rev. Met., 51(1954), 401.

[24] M. Hillert: Acta Met., 6(1958), 122.

[25] J. D. Eshelby: Proc. Roy. Soc., A241(1957), 376.

[26] J. W. Christian: Acta Met., 6(1958), 377.

[27] M. Kehoe and P. M. Kelly: Scripta Met., 4(1970), 473.

[28] L. Kaufman: Physical Properties of Martensite and Bainite, ISI Spec. Rep. 96(1965), 48. 93

[29] J. O. Nelson and C. Altstetter: Trans. AIME, 230(1964), 1575.

[30] R. Adams and C. Altstetter: Ibid, 242(1968), 139.

[31] L. Kaufman: Acta Met., 7(1959), 575.

[32] N. Nakanishi, M. Takano, H. Morimoto and F. Hori: Scripta Met., 12(1978), 79.

[33] G. V. Kurdjumov and L. G. Khandros: Dok. Akad. Nauk SSSR, 66 (1949), 221.

[34] J. W. Christian: The Theory of Transformations in Metals and Alloys, Pergamon Press, Oxford, (1965), 815.

[35] C. M. Wayman: New Aspects of Martensitic Transformation, Trans. JIM Suppl., 17(1976), 159.

[36] H. C. Tong and C. M. Wayman: Acta Met., 22(1974), 887.

[37] C. M. Wayman and H. C. Tong: Scripta Met., 11(1977), 341.
[38] G. B. Olsen and M. Cohen: Ibid, 9(1975), 1247.
[39] G. B. Olsen and M. Cohen: Ibid, 11(1977), 345.
[40] G. B. Olsen and W. S. Owen: New Aspects of Martensitic Trans-
      formations, Trans, JIM Suppl., 17(1976), 105.
[41] H. G. Ling and W. S. Owen: Martensitic Transformations (Kiev)
      (1977), 180.
[42] J. R. C. Guimaraes and D. L. V. Alves: Phil. Mag., 30(1974), 277.
[43] S. R. Pati and M. Cohen: Acta Met., 20(1972), 383.
[44] T. Suzuki and M. Wuttig: Acta Met., 9(1975), 1069.
[45] N. Nakanishi: New Aspects of Martensitic Transformation, Trans.
      JIM Suppl., 17(1976), 211.
[46] P. C. Clapp: Phys. Stat. Sol. (b), 53(1973), 561.
[47] J. W. Cahn and J. E. Hilliard: J. Chem. Phys., 31(1959), 688.
[48] D. E. McDonald: To be presented at ICOMAT-79.
[49] H. M. Ledbetter and T. Suzuki: Private communication (1979).
[50] J. W. Cahn and M. L. Green: unpublished work: presented at
      M.I.T. Conference on martensite, 1973.
[51] G. B. Olsen and M. Cohen: Met. Trans., 7A(1976),1897, 1905, 1915.
[52] A. J. Bogers and W. G. Burgers: Acta Met., 12(1964), 255.
[53] Olsen, G. B. and M. Cohen: J. Less-Common Metals, 28(1972), 107.
[54] J. W. Christian: Proc. Roy. Soc., A206(1951), 51.
[55] W. Bollmann: Acta Met., 9(1961), 972.
[56] H. Fujita and S. Ueda: Ibid, 20 (1972), 759.
[57] S. Mahajan, M. L. Green and D. Brasen: Met. Trans., 8A(1977), 283.
[58] L. M. Clarebrough and C. T. Forwood: Phys. Stat. Sol., 33a(1976),
      355.
[59] S. Mahajan, D. Brasen and T. Wakiyama: Met. Trans., 9A(1978), 1817.
[60] J. W. Brooks, M. H. Loretto and R. E. Smallman: Phase
      Transformations, The Institution of Metallurgists (1979); private
      communication, to be published (1979).
[61] T. Suzuki, H. Kojima, K. Suzuki, T. Hashimoto and M. Ichihara:
      Acta Met., 25(1977), 1151.
[62] K. E. Easterling and H. M. Miekk-oja: Ibid, 15(1967), 1133.
[63] C. L. Magee: Met. Trans., 2(1971), 2419.
[64] K. R. Kinsman, G. Das and R. F. Hehemann: Acta Met., 25(1977), 359.
[65] V. Vitek: Phil. Mag., 18(1968), 773.
[66] K. E. Easterling and A. R. Tholen: Acta Met., 24(1976), 333.
[67] M. Suezawa and H. E. Cook: private communication, to be published
      (1979).
[68] J. R. C. Guimaraes and J. C. Gomes: Acta Met., 26(1978), 1591.
[69] M. Umemoto and W. S. Owen: Met. Trans., 5(1974), 2041.
[70] T. Mura, T. Mori and M. Kato: J. Mech. Phys. Solids, 24(1976), 305.
[71] C. M. Wayman, private communication.
[72] R. J. Salzbrenner and M. Cohen: Acta Met., 27(1979), 739.
[73] M. Kato, T. Miyazaki and Y. Sunaga: Scripta Met., 11(1977), 915.
[74] A. G. Khachaturyan and G. A. Shatalov: Soviet Phys. JETP, 29(1969),
      557.
[75] A. G. Khachaturyan and A. F. Rumynina: Phys. Stat. Sol. 45a(1978),
      393.
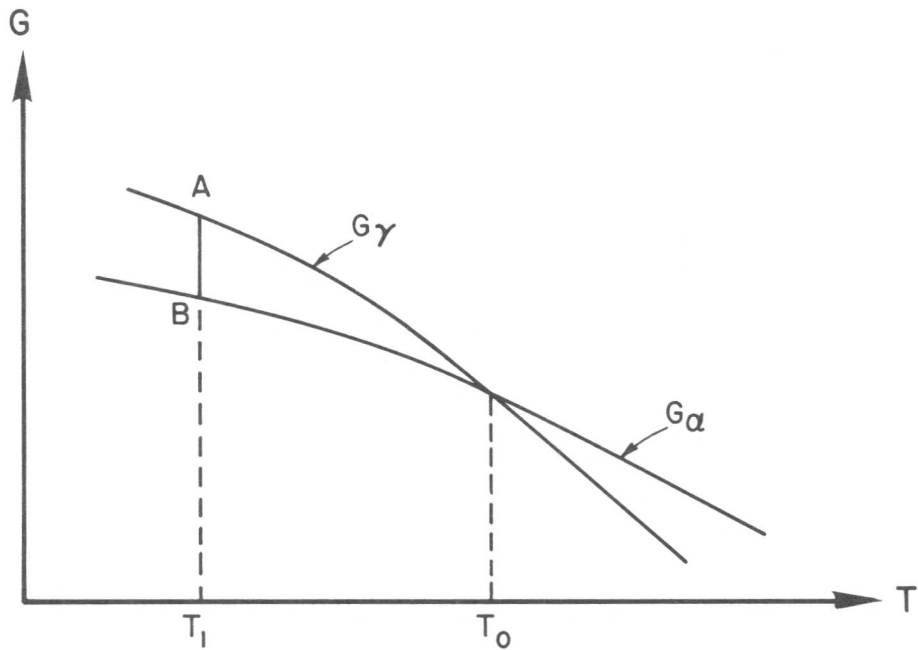[76] P. L. Ferraglio and K. Mukherjee: Acta Met., 22(1974), 835.

Fig. 1. Schematic free-energy vs temperature relations for a first order phase transformation $\alpha \overset{\rightarrow}{\leftarrow} \gamma$.
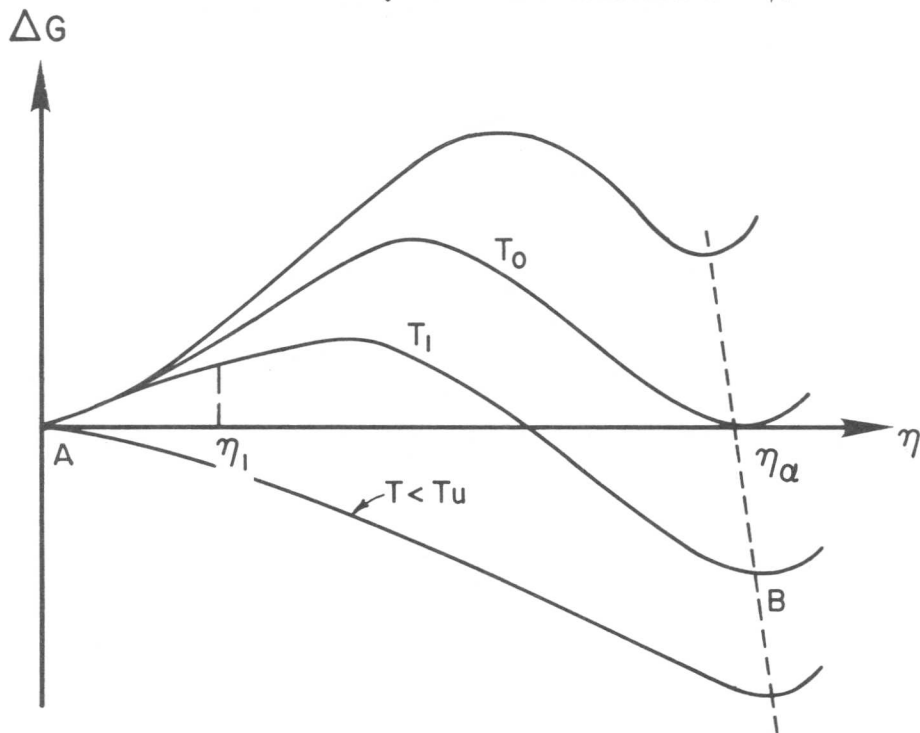

Fig. 2. Schematic free-energy vs order-parameter relations for a first order transformation. The order-parameter (η) represents continuous deformation along some path from γ to α.

Ordering and Martensite Formation in $Fe_3(Ni_xPt_{1-x})$ Alloys

D. Skinner and A.P. Miodownik*

The effect of chemical ordering on the martensite transformation of some ternary Fe-Ni-Pt alloys has been studied in order to find out how far the marked effects observed in binary Fe-Pt alloys persist when nickel is substituted for platinum. The results have been related to the effect of nickel on the chemical and magnetic ordering temperatures and the consequent changes in free energy of the FCC and BCC phases in these alloys. A new model is proposed which emphasises the magnetic component of the austenite free energy and which has been applied quantitatively to a 24.5% binary Fe-Pt alloy. An interesting consequence of the model is the possibility of a reverse $\alpha' \rightarrow \gamma$ transformation on cooling in a very specific composition range. Although nickel reduces the ordering temperature of Fe-Pt, ordering effects still persist in nickel rich alloys, and evidence will be presented to support the existence of Fe_3Ni.

I. Introduction

Although Iron-Platinum alloys have been intensively investigated, a number of unresolved questions still remain to be answered, notably the precise role of ordering in relation to the martensitic transformation in this system. The extreme sensitivity of Fe-Pt alloys to small changes in composition makes it difficult to compare results from different workers. Consequently it is of interest to consider the effect of ternary additions. Nickel presents itself as the most obvious element to add because (a) the Fe-Ni α/γ transformation range is very similar to that in the Fe-Pt system, (b) there are no compounds in the system, only ordered solutions analogous to those in Fe-Pt, and (c) although the curie temperature in the region of 25% Ni is much lower than for 25% Pt, the effect of nickel on the curie temperature of Fe_3Pt is much less drastic than the effect of iron. Finally (d) additions of nickel also provide an opportunity to explore the reported existence of Fe_3Ni by traversing the quasibinary section (Fe_3Pt - Fe_3Ni).

100 gm ingots were produced in an argon arc furnace, using Grade 1 purity Johnson Matthey Iron and Nickel, and Grade 1/2 Platinum. Each alloy was melted five times, and subsequently annealed at 1373 K for 140 hours in evacuated quartz tubes before being water quenched from this temperature. Critical temperatures were determined by DTA, electrical resistance and X-ray measurements [1].

II. Determination of Ordering Temperatures

T_o temperatures for the ordering reaction in $Fe_3Pt_xNi_{(1-x)}$ alloys

*Department of Metallurgy & Materials Technology, University of Surrey, Guildford, GU2 5XH, United Kingdom.

were calculated using the method developed by Inden [2]. These calcu-
lations provided invaluable guidance for the practical determination of
the ordering temperature and the selection of ordering treatments,
bearing in mind the best compromise between maximum rates of ordering
and the maximum possible degree of ordering [3].

The combination of experimental and theoretical results shown in
(Fig. 1) leaves little doubt that ordered Fe_3Ni does exist, although it
is difficult to prevent the competing $\gamma \to \alpha$ reaction from obscuring this
fact in binary iron-nickel alloys. Further evidence for this phase has
been reported elsewhere together with full details of the T_0 calculation
[4]. In binary iron-platinum alloys, ordering can be identified unam-
biguously by a combination of superlattice lines, a marked increase in
lattice parameter and the observation of tetragonality in any resulting
martensite. With alloys containing increasing amounts of nickel, the
observation of superlattice lines becomes more and more difficult as the
scattering power of the component atoms becomes similar, and the increase
in lattice parameter becomes a better guide. The maximum tetragonality
in martensite becomes markedly smaller as the nickel content increases
[4].

III. General Property Changes across the Quasi Binary Section

Salient property changes are shown in (Fig. 1). T_c values for dis-
ordered alloys were estimated by taking the experimental value for Fe_3Pt
[5], the extrapolated value for Fe_3Ni [6], and a calculated value for
the $12\frac{1}{2}Pt$ $12\frac{1}{2}Ni$ alloy based on the experimental evidence that $\Delta E^{\gamma 1 \gamma 2} \approx 0$
for this composition [4,7]. Although all transus lines are more tenta-
tive on the nickel rich side, there is an obvious similarity to the
analogous changes in the binary Fe-Pt system (Fig. 2).

The change in slope of the M_s curves on crossing T_c and the
associated change in the magnitude of the $(M_s - A_s)$ hysteresis is very
marked. It is difficult to evaluate the direct effect of chemical
ordering independently from associated changes in magnetic ordering.
Recourse to (Fig. 3) however shows that the direct effect of chemical
ordering is remarkably small (as soon as $T_c < M_s$). The ternary alloys show
the same features already found in Fe-Pt binary alloys, but the time
scale necessary to achieve thermoelastic behaviour is increased (Fig. 4).

IV. Proposed Thermodynamic Model

(a) G^α is taken as the reference state $G=0$ (Fig. 5), and the
    position of the G^γ curve is then fixed by the available data
    (Table I).
(b) The entropy difference $\Delta S^{\gamma \to \alpha}$ is assumed independent of tem-
    perature.
(c) The $T_0^{\gamma \to \alpha}$ temperature is assumed to be given by $(M_s + A_s)/2$.
(d) The shift is M_s directly attributable to chemical ordering is
    assumed to be 50 K (of Fig. 3).
(e) Magnetic free energy terms associated with G^α have been
    excluded as T_c^α is $\gg M_s$ so that G^α_{mag} is independent of tem-
    perature in the region of interest.

(f) The variation of G_{mag} has been calculated using the same method already used for other iron alloys [8] viz:

$$G_{mag}; [T] = [-0.9 \, RT_c \ln(\beta^o + 1)](\beta^T/\beta^o) - RT \ln[(\beta^o - \beta^T) + 1] \quad ..(1)$$

$$\text{where } \beta^T = \beta^o[1 - (T/T_c)^6] \; ; \; (T < 0.9 \, T_c) \qquad\qquad ..(2)$$

$$\text{and } \quad \beta^T = \beta^o\{(1/2)^{[2+10(T/T_c - 1)]}\} \; ; \; [T > 0.9 \, T_c] \qquad ..(3)$$

(g) Curie temperature (T_c) and saturation magnetisation data (β^o) is drawn from [5,9]. Values for the ordered alloy are taken to be slightly lower than the experimental values in order to compensate for observed deviations in the Brillouin-Langevin Curve [10]. In the vicinity of the M_s, this produces a very similar result to incorporating a more complicated formalism involving two gamma state theory [7].

(h) It is assumed that the elastic strain energy required to form martensite decreases proportionately to the shear modulus [11] and that the latter decreases linearly with temperature below T_c [12].

(Figure 5) shows the resulting <u>quantitative</u> free energy plot for both ordered and disordered 24.5%Pt <u>alloys</u>.

V. Discussion and Conclusions

1.   It can be seen that greater magnetic anomalies in the modulus lead to a <u>smaller</u> associated depression in the M_s, unless the magnetic free energy change is also taken into account. The <u>type</u> of martensite formed is not predicted by the model per se, but will depend on the elastic energy component falling below a certain critical value as already proposed by Olson and Cohen [11]. The associated changes in A_s are more dramatic because the reverse transformation is displaced into the high strain energy range on heating.

2.   The model predicts the possibility of the reversion $\alpha' \to \gamma$ <u>on cooling</u> for alloys which exhibit a critical combination of T_o and T_c. This arises because sufficient magnetic free energy can cause the G^γ curve to bend back and re-cross the G^α curve at low temperatures, creating a mirror image of the situation which is associated with γ loop forming alloys [8].

3.   The $\Delta S^{\gamma \to \alpha}$ value is seen to be highly sensitive to the precise way the elastic energy and ΔG curves intersect; the observed halving of $\Delta S^{\gamma \to \alpha}$ on ordering the 24.5%Pt alloy is thus quite understandable. A marked reduction in $\Delta S^{\gamma \to \alpha}$ on ordering is substantiated by the lower rate of formation of martensite below the M_s for ordered alloys [13,14]. The marked reduction in $\Delta S^{\gamma \to \alpha}$ cannot be explained by recourse to chemical ordering alone; the degree of chemical ordering in γ will be essentially inherited by the martensite, and cannot provide a significant change in ΔS.

4. The small direct effect of chemical ordering on the M_s can only be attributed to similar heats of ordering for both FCC and BCC structures, as the reported heat of ordering for Fe_3Pt is considerable (≈ 7500 kJ mol^{-1}) [15]. A previous analysis deduced a lower T_o for the BCC arrangement when magnetic effects are excluded [16], but it is clearly not possible to assume that the parent phase has necessarily a higher ordering temperature in every case [17,18].

5. The increase in time required to obtain thermoelastic behaviour by changing either the iron or nickel content should be attributed to the difference in the degree of chemical order required to bring the T_c above M_s, and not to any intrinsic differences in rates of chemical ordering.

References

[1] A.P. Miodownik. J. Magnetism and Magnetic Mat. 1979 (in the press).
[2] G. Inden. CNRS Colloquium No. 7, J. de Physique (Suppl.) 38 (12) (1977) 373.
[3] G.J. Dienes. Acta Met. 3 (1955) 549.
[4] A.P. Miodownik and D. Skinner. Calphad Symposium VIII Stockholm, May 1979. (To be published in Calphad Journal.)
[5] T. Mizoguchi, M. Akimitsu and S. Chikazumi. J. Phys. Soc. Japan 34 (4) (1973) 932.
[6] G.F. Bolling, A. Arrott and R.H. Richman. Phys. Stat. Solidi. 26 (1968) 743.
[7] A.P. Miodownik. Physics and Application of Invar Alloys. Honda Memorial Vol. 3 Marvsen (1978) Ch. 12 p. 228.
[8] A.P. Miodownik. Calphad J. 1 (2) (1977) 133.
[9] K. Sumiyama, M. Shiga, Y. Kobayashi, K. Nishi and Y. Nakamura. J. Phys. (F) 8 (6) (1978) 1281.
[10] K. Sumiyama, M. Shiga and Y. Nakamura. J. Phys. Soc. Japan 40 (4) (1976) 996.
[11] G.B. Olson and W.S. Owen. Trans. Jap. Inst. Metals 17 (1976) 105.
[12] G. Hausch. J. Phys. Soc. Japan 37 (3) (1974) 824.
[13] M. Foos, C. Frantz and M. Gantois. Mem. Sci. Rev. Metall. (Jan) (1977) 55.
[14] K.R. Satyanarayan, W. Eliasz and A.P. Miodownik. Acta Met. 16 (1968) 877.
[15] M. Sundaresen, Ya Gerasimov, V.A. Geiderikh and I.A. Vasileva. Russ. J. Phys. Chem. 37 (11) (1963) 1330.
[16] L. Kaufman. Private communication.
[17] D. Schofield and A.P. Miodownik. Metals Society Symposium Copper 77. (In the press).
[18] L. Chandrasekaran and A.P. Miodownik. (This symposium)
[19] H.C. Tong and C.M. Wayman. Acta Met. 22 (1974) 887.
[20] H.C. Tong and C.M. Wayman. Met. Trans. 5 (1974) 1945.
[21] M. Umemoto and C.M. Wayman. Met. Trans. 9A (1978) 891.
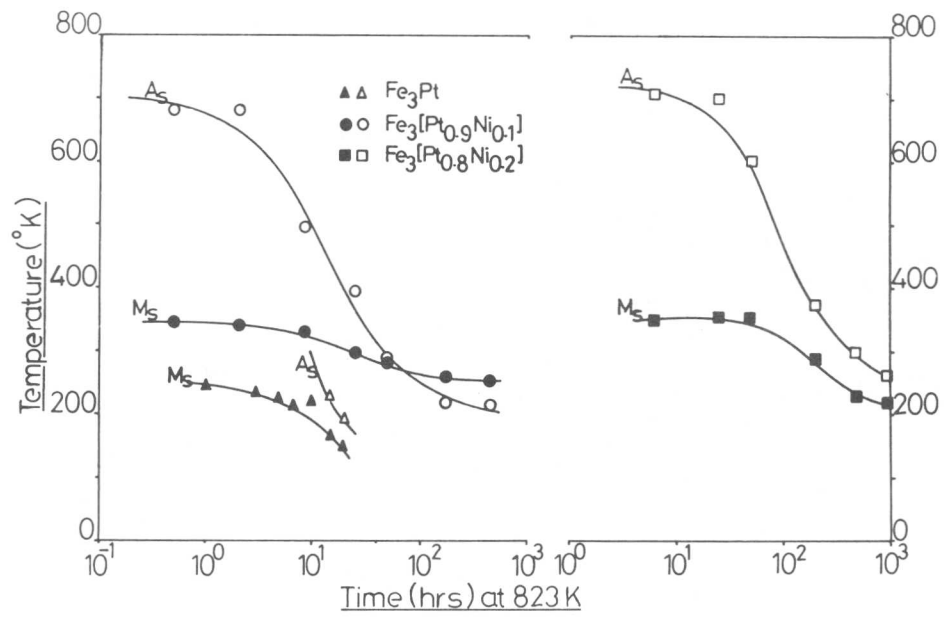[22] T. Tadaki, K. Katsuki and K. Shimizu. Trans. Jap. Inst. Metals 17 (1976) 187.
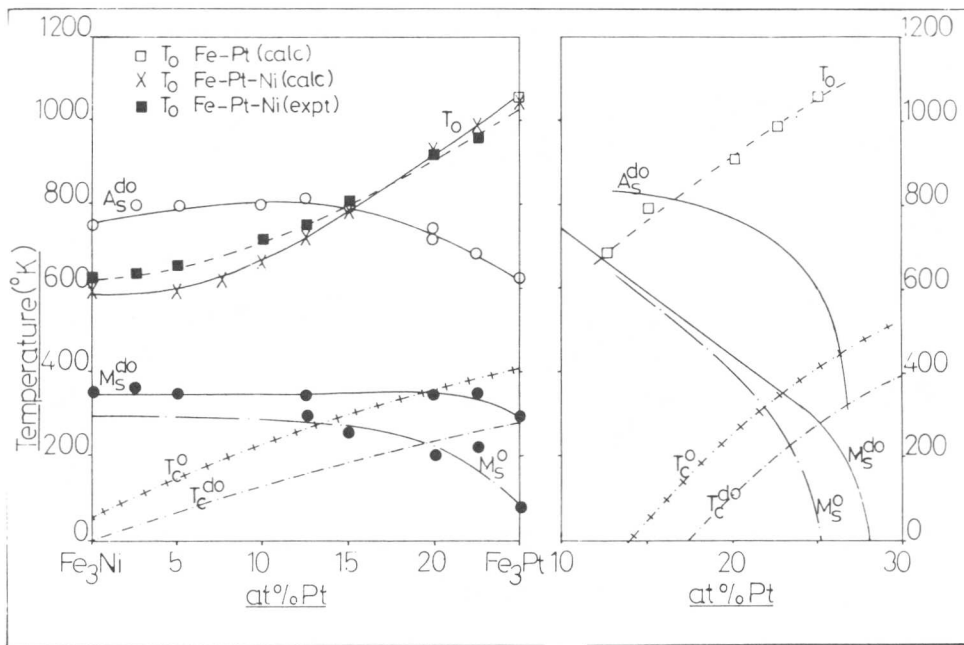
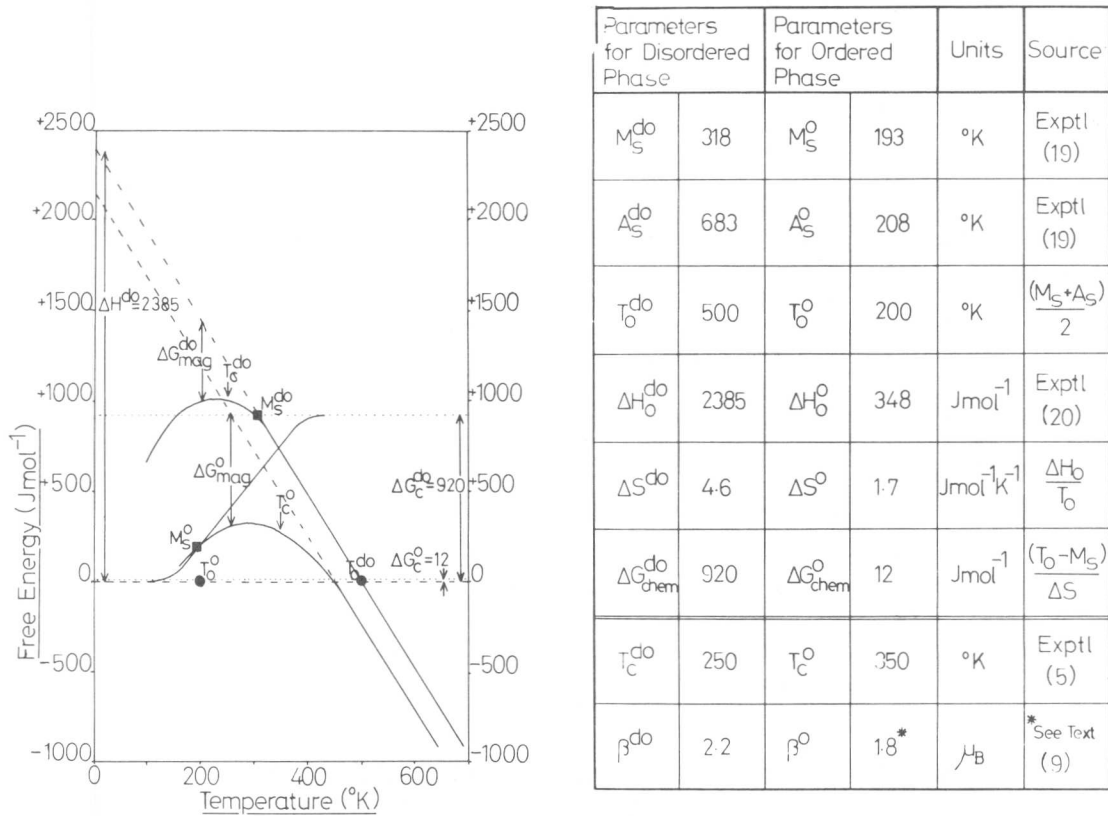Fig. 1 Critical Temperatures for the Section $Fe_3Ni_xPt_{(1-x)}$

Fig. 2 Critical Temperatures for binary Fe-Pt Alloys
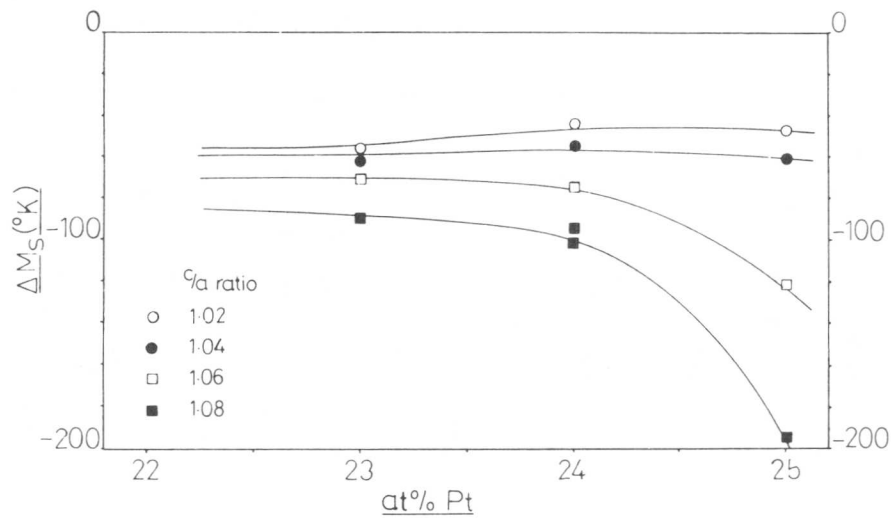
Fig. 3 Change in M_s associated with different degrees of order as evidenced by tetragonality. (Data replotted from Umemoto and Wayman [21].)

Fig. 4 Variation of M_s and A_s in $Fe_3Ni_xPt_{(1-x)}$ Alloys

Legend in Fig. 4:
▲ △ Fe_3Pt
● ○ $Fe_3[Pt_{0.9}Ni_{0.1}]$
■ □ $Fe_3[Pt_{0.8}Ni_{0.2}]$

TABLE I   Input Data for Fig. 5

Parameters for Disordered Phase		Parameters for Ordered Phase		Units	Source
M_S^{do}	318	M_S^{O}	193	°K	Exptl (19)
A_S^{do}	683	A_S^{O}	208	°K	Exptl (19)
T_O^{do}	500	T_O^{O}	200	°K	$\frac{(M_S + A_S)}{2}$
ΔH_O^{do}	2385	ΔH_O^{O}	348	Jmol^{-1}	Exptl (20)
ΔS^{do}	4·6	ΔS^{O}	1·7	Jmol^{-1}K^{-1}	$\frac{\Delta H_O}{T_O}$
ΔG_{chem}^{do}	920	ΔG_{chem}^{O}	12	Jmol^{-1}	$\frac{(T_O - M_S)}{\Delta S}$
T_C^{do}	250	T_C^{O}	350	°K	Exptl (5)
β^{do}	2·2	β^{O}	1·8*	μ_B	*See Text (9)

Fig. 5 Effect of Ordering on the Free Energy of Fe24.5Pt

THERMAL ANALYSIS ON MARTENSITIC TRANSFORMATIONS IN ZIRCONIUM BASED ALLOYS

F.D.S. Marques

Thermal analysis has been carried out in various Zr-Ti-O, Zr-Mo-O, Zr-Al-O and Zr-O alloys. The transformation temperatures (TT) T_o, α_s, α_f, M_s, M_f, β_s and β_f have been determined, CCT diagrams have been constructed and transformation mechanisms have been proposed. The TT have been found to decrease with increasing cooling rates (CR) and with additions of β stabilising elements (Mo, Ti) and to increase with small amounts of α stabilising elements (Al, O). It is proposed that for low CR (e.g. < 1000°C/s) the transformations occur by a shear mechanism in which the migration of a mobile dislocation interface is controlled by solute diffusion. For high CR (e.g. >2000°C/s) the transformations are fully martensitic. The effects of the CR and solute additions on the morphology and substructure of the martensite are discussed.

Introduction

The microstructure of zirconium based alloys can be better understood and its control can be better achieved if a time-transformation-temperature diagram is known. Two types of these diagrams can usually be constructed: the isothermal or TTT diagram and the continuous cooling or CCT diagram. In alloy development the CCT diagrams are specially useful to guide practical heat treatments which often consist in continuous cooling. They are also important to establish the transformation mechanisms. To obtain the CCT diagrams specimens were cooled continuously, from the β-phase field, at different CR. The temperatures at which the beginning and the end of the transformation occured were measured, by registering the cooling curves, and the CCT curves were drawn. These curves are shifted to lower temperatures and longer times relatively to those of the TTT diagrams for the same specimen. This results because in continuous cooling an increase in time is associated with a drop in temperature.

Experimental Procedure

Typical analyses of the materials used, details of the alloy preparation and of the thermal and mechanical treatment techniques, electron and x-ray metallography procedure have been described elsewhere [1,2,3,4]. Figure 1 shows the flow chart and specimen stage of the high speed gas-quenching thermal analysis apparatus. Small sheet specimens, which acted as the hot junction, were spot welded to a Pt/Pt-13%Rh thermocouple. They were prepared with two prepolished parallel surfaces, each with an area of about 1 cm^2. The thickness was controlled in order to achieve the required CR, being limited to about 0.5 mm. The specimens were cooled from the β-phase field either in vacuum (FC) or quenched by jetting high purity argon (ArQ) or helium (HeQ) directly on to the specimen. The CR was controlled by the nature of the gas, its pressure (5-50 psi) and its temperature. The CR achieved with He was approximately four times faster than that with Ar in the same conditions. Continuous cooling curves were recorded either

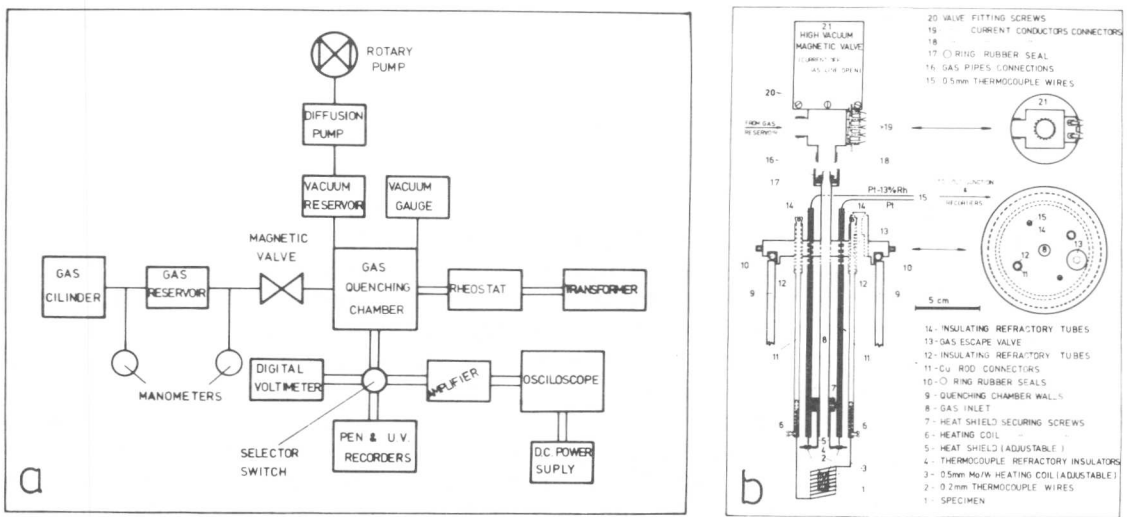Universidade do Minho, Palacio Vila Flor, Guimaraes, Portugal

Fig. 1 Thermal analysis apparatus: (a) flow chart; (b) specimen stage

on a high-speed-high-sensitivity X-Y Brians pen recorder (Fig. 2a) or from a cathode-ray oscilloscope screen using a Polaroid Land Camera (Fig. 2b), which were calibrated by feeding in measured voltages.

Results and Discussion

The following alloys have been prepared and studied (compositions are in at% and between brackets are the oxygen contents in ppm): (a) $\alpha-\beta$ iso-morphous: Zr-Ti-O: 1(1450), 2.5(1100), 5(690), 10(2050), 20(1250), 30(1050), 40(1150), 50(1000); (b) β eutectoid: Zr-Mo-O: 0.5(1200), 1(1250), 1.5(1200) and (c) α peritectoid: Zr-Al-O: 2(850), 4(560); Zr-O: 0.38, 0.91, 1.07.

(a)   The TT of all the Zr-Ti-O alloys were found to decrease with increasing CR (Figs. 2,3,5). The relationship between these TT and the CR could generally be represented by a sigmoidal curve (Fig. 3a). For a Zr-10Ti(2050) alloy and for a CR of 48°C/s the β/α transformation began at α_s=778°C and ceased at α_f=750°C. The microstructure consisted of α plates (Fig. 4a) which exhibited surface tilts. As the CR was increased from 48 to 1000°C/s α_s and α_f decreased considerably, in a linearly manner, to approximately 720 and 675°C respectively. As the CR was increased from 1000 to 3700°C/s only a small decrease was observed in α_s and α_f which at 3700°C/s were 690 and 658°C respectively. For CR exceeding 3700°C/s α_s and α_f decreased again
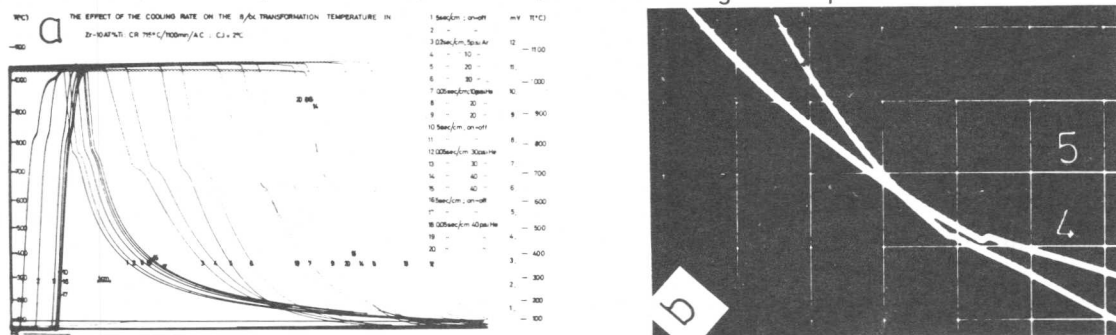
Fig. 2 Typical CR curves: (a) Zr-10Ti(2050): X-Y pen recorder; (b) Zr-40Ti (1150): oscilloscope screen: 5 and 10 psi He.
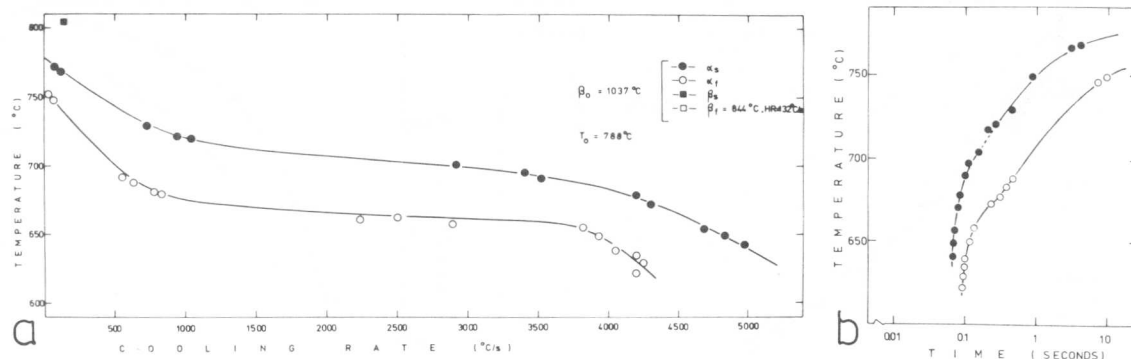
Fig. 3 Zr-10Ti(2050): (a) Effect of the CR on the TT; (b) CCT diagrams

rapidly with increasing CR, and at 4200°C/s were α_s=680 and α_f=630 C. Figure 4b shows a typical plate-like martensitic structure quenched from 1037°C by a jet of He at 40 psi (CR=4200°C/s). This alloy in the water quenched (WQ) condition exhibits a lath morphology, and the amount of internally twinned plates are higher in the HeQ condition. For CR <1000°C/s the transformation has a diffusional component, as indicated by the CCT diagram (Fig. 3b), and for CR >1000°C/s occurs by a diffusionless shear mechanism. The effect of Ti additions on the TT is shown in Fig. 5a. These results are in agreement with those of Duwez [6], Gridnev et al [7] and Huang et al [8]. For CR and HR near 100°C/s α_s=772°C and β_s=805°C, and T_0 was calculated to be 788°C.

(b)   The TT of the Zr-Mo-O alloys were observed to decrease with increasing CR in a similar manner to that described for Zr-Ti-O alloys. As the CR was increased from 50 to 2000°C/s α_s and α_f dropped by about 130°C, and for CR >2000°C/s became constant. The CCT diagrams shown in Fig. 5b indicate an intermediate or mixed mechanism. Mo strongly decreased the TT (Fig. 6a). The present α_s and M_s values are in agreement with those of Domagala et al [9,10], but the α_f and M_f values indicate a faster reaction rate. The present TT are higher than those reported by Vanderpuye and Miodownik [8]. This is attributed to the higher interstitial content of the present alloys, which was observed to raise the TT.

The microstructure of the martensite was determined by the solute concentration and the CR. A faulted and twinned substructure with lower
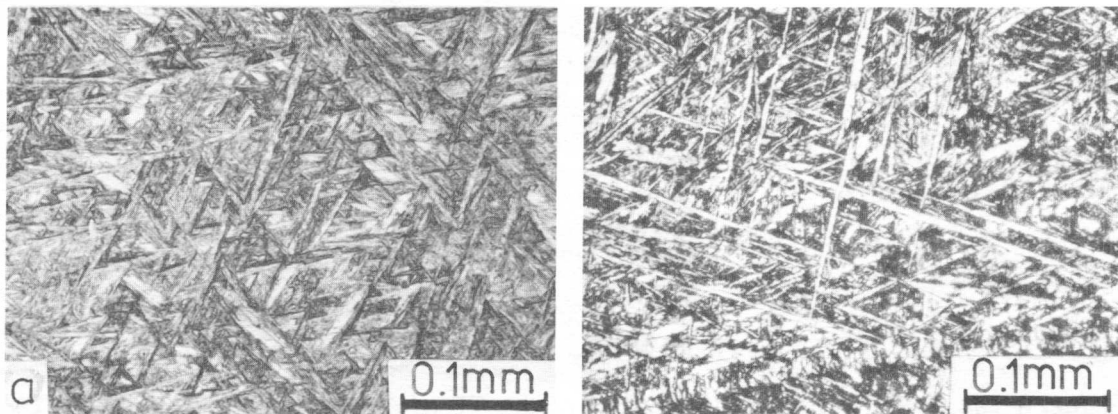
Fig. 4 Effect of the CR on the microstructure of a Zr-10Ti(2050) alloy; (a) FC (α_s=771°C, CR=48°C/s); (b) HeQ (M_s= 680°C, CR=4200°C/s).
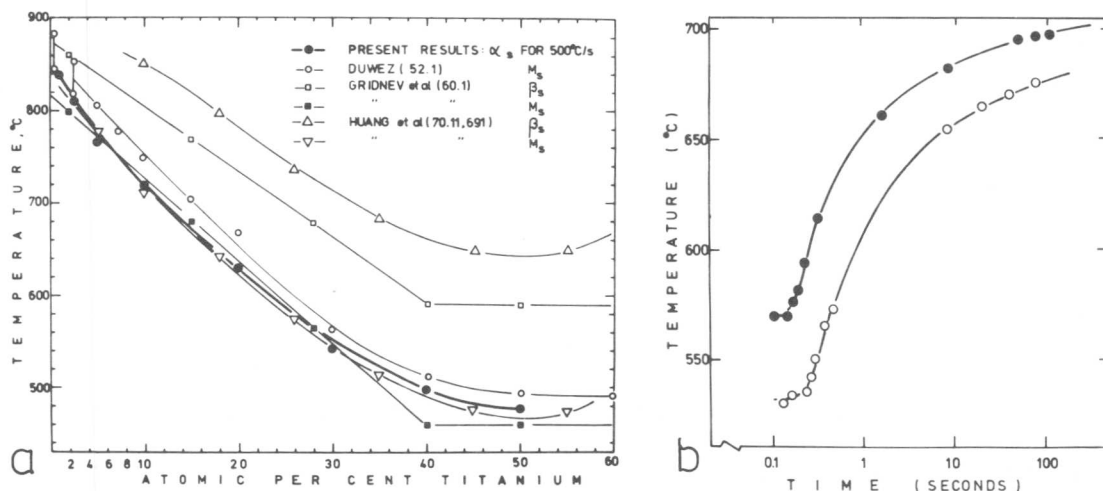
Fig. 5 (a) Effect of Ti additions on the TT of Zr-Ti-O alloys; (b) CCT diagrams for a Zr-1.5Mo(1200) alloy.

M_s was formed at very high CR (Fig. 6c) and a dislocated martensite (Fig. 6b) or a bainitic product [5] was obtained as the solute concentration and/ or the CR was reduced. Mo was also very powerfull in changing the morphology from lath (0.5) to plate-like (1.0) which was associated with the strength levels achieved.

(c) The relationship between the CR and the TT in Zr-Al-O alloys was re- presented by a sigmoidal curve (Fig. 7a). As the CR was increased from 50 to 1000°C/s α_s and α_f decreased from α_s=883°C and α_f=863°C to α_s=805°C and α_f=790°C. For CR <1000°C/s the transformation has a shear and a diffusional components, as indicated by the CCT diagrams (Fig. 7b). For CR >1000°C/s the transformation occured by a diffusionless shear mechanism. At CR and HR ≈ 100°C/s α_s=883°C and β_s=893°C, from which T_o≈888°C was calculated. Both alloys exhibited dislocated block-like crystals alternating with dislocated lath colonies, the amount of which increased with Al content.
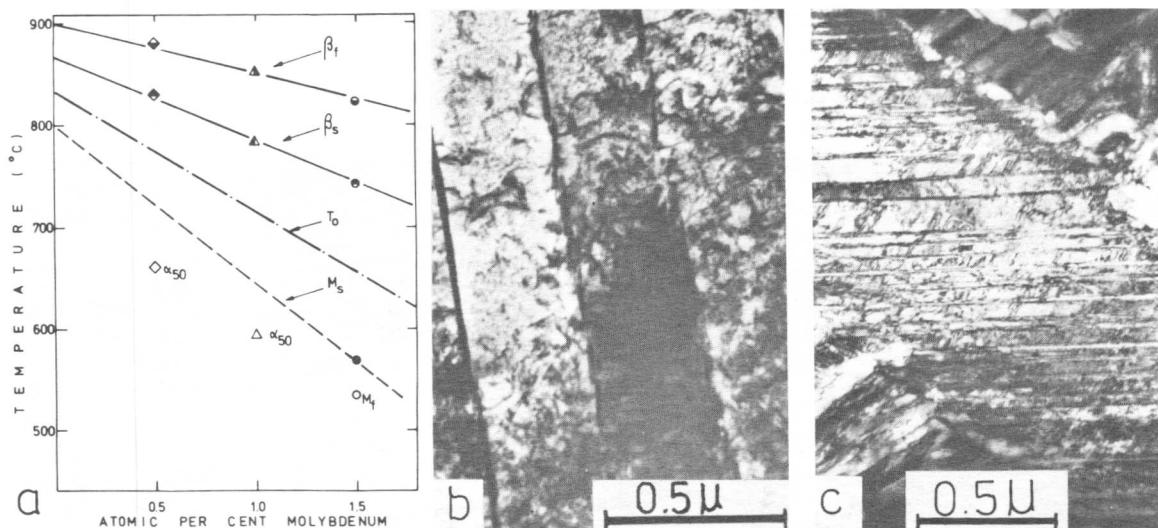
Fig. 6 (a) Effect of Mo additions on the TT of Zr-Mo-O alloys; (b) & (c) Effect of the CR on the substructure of the martensite in a Zr-0.5Mo(1200) alloy: (b) WQ: dislocated ; (c) HeQ: faulted and twinned.
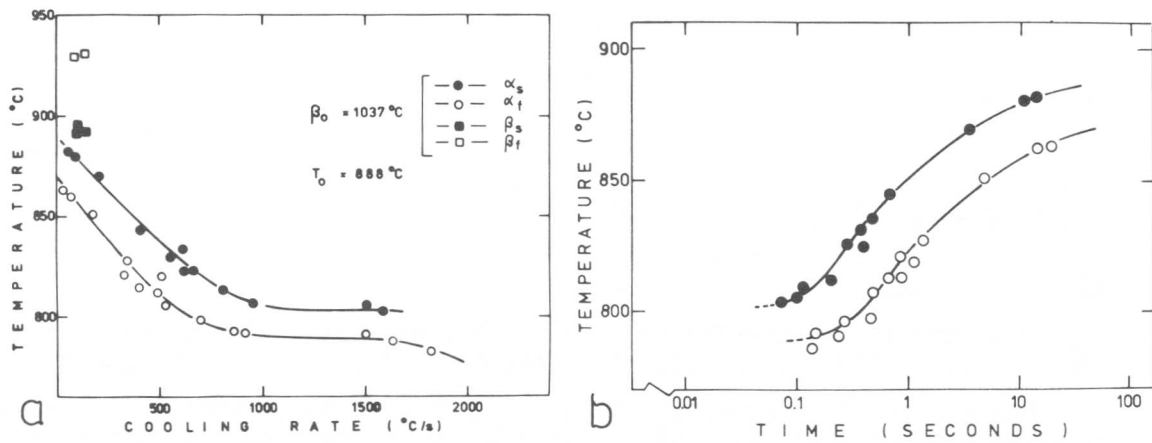
Fig. 7 Zr-4Al(560): (a) Effect of the CR on the TT; (b) CCT diagrams.

Figure 8 shows the effect of the CR on the TT of a Zr-0.380 alloy and the correspondent CCT diagrams. These results differ considerably from tho se reported by Duwez [11] which observed a depression of 15°C in α_s (from 865 to 850°C) for CR up to 10,000°C/s. However, Hayes and Kaufmann [12] al so observed a depression of 65°C in α_s for a CR≈1000°C/s; and Stewart et al [13] observed a depression of ≃ 100°C for CR≈3000°C/s. This divergence is attributed to difference in the interstitial content (H_2, N_2 and O_2). The martensite exhibited a dislocated block-like structure [5].
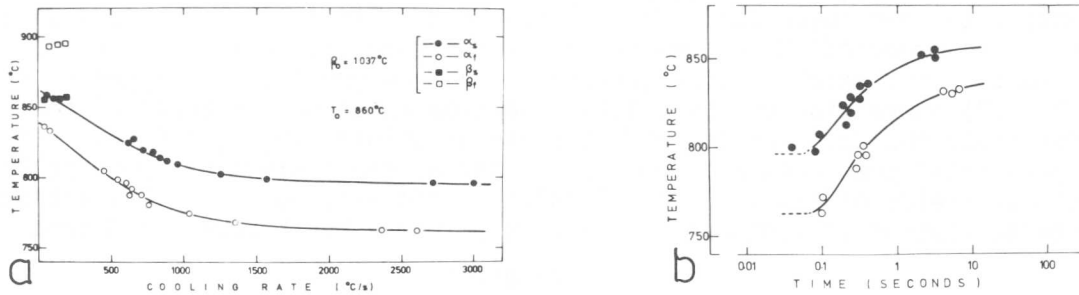
Fig. 8 Zr-0.380: (a) Effect of the CR on the TT; (b) CCT diagrams.

In the present alloys, the martensite morphological transitions: block-like → lath → lenticular plate-like →zig-zag plate-like were obser ved to occur with increasing total (substitutional + interstitial) solute content and were associated with the strengthening level achieved (Fig. 9a).

For the same alloy composition the substructure of the martensite was changed by varying the quenching rate. Increasing quenching rates were able to change the substructure from dislocated to twinned and faulted. These substructural transitions were also observed to occur with increasing β substitutional solute content, but independently of the morphological tran sitions. They were associated with the transformation temperature (Fig. 9b).

As the solute concentration increases, the lattice dist ortion beco mes more significant and the strain and surface energy increase and there fore become more effective in restraining the martensite formation (nuclea tion and growth), with a consequent decrease in M_s and M_f. In alloys con taining β-stabilising elements (Ti, Mo), not only M_s and M_f, but also T_0, decrease with increasing solute additions.
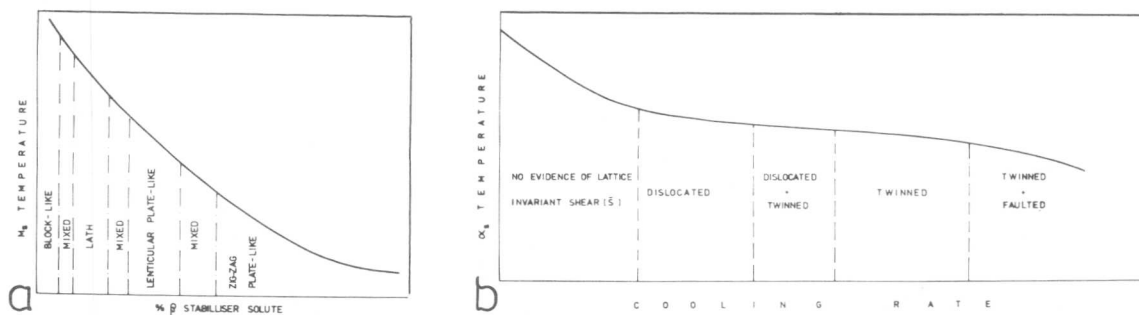
Fig. 9 Schematic representations: (a) Effect of β-stabilising additions on the morphology and M_s; (b) Effect of the CR on the substructure and M_s.

However the TT were observed to increase with small amounts of α- sta bilising elements (Al, O). This is attributed to the fact that these solutes raise T_0 by decreasing the electron-to-atom concentration. However M_s and M_f appear to decrease with higher amounts of these solutes. This is in agree ment with recent results [14] which were not explained. Since the strengthe ning effects of Zr solutes are not very strong, for small amounts the main effect is the raise in T_0 and consequently M_s also raises. However, with hi gher solute concentrations the increase in the strength overcompensates the raise of T_0 and M_s begins to decrease, while To continues to increase.

The depression of M_s and M_f with increasing CR is unconventional, although similar depressions have been observed in other Zr-based [13,15,16] and Ti-based [8,14] alloys, which have not been explained. Similar effects have also been observed in Fe [17] and Fe-Ni alloys [18]. The following rea sons are proposed: M_s and M_f depend on the type and lattice defects of the parent phase, which is strengthened by fast CR due to: (1) oxygen ordering [2]; (2) supression of the solute rejection which occurs ahead of the β/α interface and depletes the parent phase of solute[4,5]; (3) CR can act as hydrostatic pressures and depress T_0, and as shear stresses opposing the stress fields of the subcritical nuclei. It's also possible that although the nucleation is athermal the plate growth may be temperature dependent.

References

1. F.D.S. Marques: Proc. 4th Int. Conf. Strength Metals & All. 2(1966)736.
2. F.D.S. Marques: Proc. 4th Gen. Ass. CENIM, Madrid, 1(1977)59.
3. F.D.S. Marques: Zeitschrift für Metallkunde, 69, H. 3(1978)167.
4. F.D.S. Marques: Proc. 5th Int. Conf. Strength Metals & Alloys, 1979.
5. F.D.S. Marques: Proc. Rev. Course Phase Transformations, York, 1979.
6. P. Duwez: J. Inst. Met. 80(1952)525.
7. V.N. Gridnev et al: Akad. Nauk. SSSR, Doklady 134, 6(1960)1334.
8. R.I. Jaffee, N.E. Promisel: The Sci. Techn. & Appl. Ti, London (1968)691.
9. R.F. Domagala, D.J. McPherson: USAEC Rep. 2 COO-207(1955).
10. R.F. Domagala et al: Trans. AIME 209(1957)1191.
11. P. Duwez: Trans. AIME 191(1951)765.
12. E.E. Hayes, A.R. Kaufmann: ASM Sympos. Zr & Zr Alloys, Cleveland (1953)241
13. D. Stewart et al: Brit. J. Appl. Phys. 16(1965)1081.
14. M. Cormier, F. Claisse: J. Less-Common Metals 34(1974)181.
15. A.G. McMullen, J.G. Parr: Can. Metall. Quart. 4, 2(1965)117.
16. G.F. Slattery: Electrochem. Techn. 4, 7-8(1966)337.
17. M.J. Bibby, J.G. Parr: J.I.S.I. (1964)100.
18. W.D. Swanson, J.G. Parr: J.I.S.I. 202(1964)104.

The Electronic Contribution to the
Martensitic Phase Transformation in Pure Thallium

S. Ahmed*

I. Introduction

It is well known that the electronic structure and the valence elec-
tron concentration in solid solutions are important factors in determin-
ing the binary and ternary phase diagram [1-2]. It is the electrons
that bring about the bonding of positive ions. It is the concentration
of the valence electrons that determine the solid solubility limit of
the primary phases because the valence electron concentration remains
the same at different atom percents of the solubility limit. That is,
the solubility limit of the primary phases always corresponds to the
same electron/atom ratio. This correspondence implies that the free en-
ergy increases sharply when there is a certain concentration of the val-
ence electron. Any change in the concentration of the valence electron
resulting from the addition of another alloying element will result in
considerable changes in Fermi energy and of the thermodynamic parameters.
If an element with a certain valency is alloyed with elements having
higher valencies, then the Fermi energy and the partial molar free en-
ergy of the electron will increase. This increase will ultimately af-
fect the solubility of the alloying element, which will decrease. On
the other hand, if an element with a higher valency is alloyed with an
element of a lower valency, the Fermi energy and the partial molar free
energy of the electrons will decrease. This decrease will increase the
solubility. For example, if zinc is alloyed with copper, the electron
concentration will increase and the result will be an increase in the
Fermi energy and the partial molar free energy of the electron. As a
consequence, the solubility limit of zinc in copper will decrease. In
fact, the solubility limit of the alpha phase (in copper-zinc and in
copper-gallium alloys) corresponds to different atom percents but to
approximately the same electron/atom ratio. The Hume-Rothary rules
show the important effect of the variations of electron concentration
on the thermodynamic properties. However, the thermodynamic analysis of
the electronic properties have not been investigated because it is not
possible to determine the thermodynamic properties of ions and electrons.
Furthermore, in dilute solutions, the activity of the solute metal is
proportional to its concentration regardless of its ionization.

There are double polymorphic transitions in iron:

$$\alpha\text{-iron (b.c.c.)} \overset{\rightarrow}{\leftarrow} \gamma\text{-iron (f.c.c.)} \overset{\rightarrow}{\leftarrow} \delta\text{-iron (b.c.c.)}$$
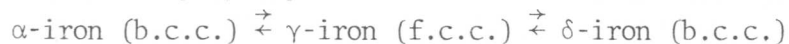
This double transition cannot be explained alone by the vibrational spe-
cific heat. Seitz [3] has explained the double transition in terms of
the Debye characteristic temperature of the γ-iron (f.c.c.) phase, whose
temperature is lower than that of α-iron. This difference in the char-
acteristic temperature is responsible for the transition. The electron-
ic specific heat of the (b.c.c) α-phase becomes greater than that of the

*Youngstown State University, Youngstown, Ohio, U.S.A.

(f.c.c.) γ-phase and is responsible for the γ→α transition.

Zener [4] discusses more completely this double transition in iron and points out that the change in the free energy with temperature is a result of the changes in the specific heat values. Zener's suggestions have been further developed by Weiss and Tauer [5]. They have separated the thermodynamic function (i.e., free energy, enthalpy, etc.) into three terms: lattice, magnetic and electronic. They have assumed the additivity of the corresponding specific heat terms. They agree with Zener (even though they criticize some of Zener's assumptions) that the (b.c.c) α-phase is stable because of the magnetic contribution to specific heat. Otherwise, the γ-phase would be the low temperature phase. Weiss and Tauer [5] and later Kaufman [6] apply their procedures to other systems. Their discussions seem to point to the fact that the electronic contribution to specific heat is substantial and should be considered.

Pure Thallium undergoes an allotropic transformation from α to β Thallium at 507°K on heating [7]. The martensitic transformations were first reported by Levin [8] in 1903, and subsequently confirmed by Werner [9] and Nishikawa and Asara [10]. The crystal structure has been determined to be hexagonal close packed (isotypic with magnesium) for the low temperature α phase and body centered cubic for the high temperature β phase [11]. The thermodynamic properties were studied by various investigators [12-19]. The average value for the heat content for the α→β transformation is 90 ±10 cal/mole [7]. The selected values of the heat content measurements of Roth, Meyer and Zeumer [15] (at temperatures ranging from 373°K to 628°K) agree within ±50 cal/mole with the results of Orr, Anderson and Hultgren [7] (at temperatures ranging from 334°K to 562°K) and of Schneider and Hilmer [17] (at temperatures ranging from 505°K to 673°K).

In the present investigation, attempts have been made to determine the effect of various alloying elements which have various valence electron concentrations on the phase transformation of pure Thallium. The enthalpies and the temperatures of phase transformation have been directly determined from the thermodynamic studies. Furthermore, x-ray studies have been conducted at various temperatures to determine the crystal structures, lattice parameters of both phases at the appropriate temperatures and ultimately the volume accompanying the phase transformation in the alloys. From these results, it has been shown that the electronic contribution to the phase transformation is significant and should be considered.

This is a partial report of research in progress. The final goals of this investigation are to evaluate the various thermodynamic parameters (i.e., free energy, specific heat of both phases in all alloys) from the measured values, then to consider and to separate various contributions to the phase transformation and, particularly, to ascertain the electronic contribution by the appropriate methods.

II. Experimental Procedure

The alloys were prepared from 99.999% pure elements. Pure Thallium was alloyed with small amounts of other elements with different valencies: it was alloyed with Au and Ag (each of which has a valency of 1),

Cd and Zn (each of which has a valency of 2), Sn (which has a valency of 4) and Sb (which has a valency of 5) (Table I). The compositions of the alloys are indicated in the tables. The amounts of Thallium and of the alloying element were first weighed and then were capsuled under vacuum (2×10^{-6} mm of Hg), then homogenized and annealed at 450°K for 24 hours and furnace cooled. The alloys were then weighed. There was no loss in weight. Two thin slices were obtained from each alloy--one for metallographic studies and the other for x-ray studies. The alloys were then electroplated with Cr and Ni to prevent oxidation. The weight of the plating was between 0.0005 and 0.0010 gm.

The metallographic samples were then mechanically polished and then electropolished in a bath of the following composition.

$$
\begin{aligned}
\text{Carbitol} &- 750 \text{ ml} \\
\text{HCl} &- 20 \text{ ml} \\
\text{HNO}_3 &- 50 \text{ ml}
\end{aligned}
$$

After etching, the sample was dipped in a solution of 90 ml H_2O and 10 ml HF. A microscopic study was conducted on each sample. It was seen that at room temperature the transformation product was finely twinned. A typical micrograph is shown in Figure 1. It was further observed that the microstructures of these alloys were uniform and homogeneous and had no secondary phases. The absence of secondary phases means that all alloying elements in pure Thallium formed primary solid solution. Thermodynamic and x-ray studies confirmed these conclusions.

The thermodynamic properties of these alloys were measured by using a modified Olsen Calorimeter (Figure 2). The calorimeter is equipped with an adiabatic jacket which is electronically controlled to maintain the jacket temperature to within ± 1°C of the media temperature. The adiabatic jacket virtually eliminated any heat loss or gain from the surroundings. The calorimeter itself contains a thermoflask containing the calorimeter media. The temperature measurement was carried out by a high-response thermopile with an electronic cold junction. The output of the thermopile was fed into a nanovolt amplifier. The amplified voltage was then fed into the y-axis of an x-y recorder with zero suppression capabilities. The x-axis of this recorder measured the temperature of the sample with the help of a thermocouple (with an electronic cold junction and an amplifier) which was inserted in the hole drilled into the sample. The thermopile measures accurately up to ± 0.001°C and it measured the temperature of the sample accurately up to ± 0.05°C.

The experimental procedure consisted of heating the sample in a furnace to a temperature of approximately 560°K and then encapsulating it in a Copper jacket (0.0005 inch thick). The Copper jacket assembly was then lowered in the calorimeter which contained a previously weighed amount of the calorimeter media. The calorimeter media was spectro-quality isopropyl alcohol. The specific heat of this alcohol in the proper temperature range was previously determined in separate experiments. The specific heat values agree closely with those of the U. S. Bureau of Standards.

The x-y recorder continuously measured the change in temperature of the calorimeter media as a function of the sample temperature.

The x-ray studies were carried out on thin samples of the pure Thallium and its alloys and were performed with a Norelco diffractometer (using a Copper target with an Ni filter) under a helium atmosphere in a high temperature MRC Camera at the indicated temperatures. The results are shown in Tables III and IV.

III. Experimental Results

The metallographic work was conducted to determine the structures of the products of the transformation and the effect of the alloying elements on the phases present. It was revealed that the transformation product is twin related (Figure 1). There are fine twins in a single grain in the pure Thallium and in all alloys. There is a "mid-rib" where the two twin boundaries merge in. The metallurgical structures further suggest that the alloying elements had formed a primary solid solution without any change in microstructure. X-ray and thermodynamic studies confirmed this observation. The experimental results of the thermodynamic studies consist of the changes in the temperature of the calorimeter media as a function of sample temperature. From the results, the enthalpy values have been calculated using the following equation.

$$\Delta H = (W)\ (C_p)\ (\Delta T) \tag{1}$$

Where W = the weight of the calorimeter media

C_p = the specific heat of isopropyl alcohol at the appropriate temperature

ΔT = the temperature change of the calorimeter media from the starting temperature

Thus, the enthalpy values can be calculated as a function of sample temperature. A typical curve is shown in Figure 3. From these results, the enthalpy of phase transformation ($\Delta H^{\alpha\beta}$) and the transformation temperature on cooling (T) have been determined (Table II).

It has been determined from the result of the x-ray studies that the crystal structure of α-Thallium is hexagonal close packed and that the crystal structure of β-Thallium (the high temperature phase) at 533°K is body centered cubic. Furthermore, the changes in the lattice parameters of α-Thallium and its alloys both at 298°K and 358°K have been determined (Table III). From these values, the lattice parameter of α-Thallium at 533°K has been obtained by extrapolation (Table III). The lattice parameters of the β-Thallium at 533°K were obtained from the results of x-ray studies. This operation enabled us to determine the volume change accompanying the phase transformation from b.c.c. to h.c.p. on cooling at 533°K (Table IV).

IV. Discussion

The purpose of the present investigation is to study: (1) the $\beta\rightarrow\alpha$ phase transformation in pure Thallium; (2) the effect of alloying elements on this phase transformation; and (3) the various contributions to the free energy of this phase transformation.

The atomic number, the electronic structure, the valencies and the

ionic radii of the alloying elements and of pure Thallium are shown in Table I.

The alloying elements were chosen with special regard to their electronic structure. Both Silver and Cadmium have smaller valencies than Thallium, which is reported to have a valency of three in solid solutions. The alloying element tin has a valency of four, which is greater than that of Thallium. All the alloying elements have atomic diameters within 15% of the atomic diameter of pure Thallium.

The results of all investigations reported here indicate that in all cases the elements alloyed with Thallium form a primary substitutional solid solution with Thallium. The occupation of the sites in the Thallium lattice will introduce some strain in the Thallium lattice. Furthermore, the alloying elements have valencies different from that of the Thallium atom. This difference in valencies will cause some differences in the electrical charge distribution. Also, the alloying elements will introduce a substitutional type of disorder in the Thallium lattice. This disordering effect will be rather small, since the concentration of the alloying element is rather small. These factors suggest that the effect of the alloying element will be to introduce: (a) a strain in lattice because of changes in size and the electrical charge distribution of pure Thallium atoms and (b) the electronic effect. The latter effect results from a change in the valence electron concentrations upon the addition of alloying elements. In the alloying elements which have higher valency that that of pure Thallium, the concentration of valence electrons per atom, and, consequently, the Fermi energy, will increase. However, in the alloying elements which have a lower valency than that of pure Thallium, the concentration of valence electrons per atom and, consequently, the Fermi energy, will decrease. The change in Fermi energy will distort the Brillouin Zone structure because of the change in the filled state in the Brillouin Zone of pure Thallium. This distortion will affect the phase transformation.

Pure Thallium exhibits a $\beta \to \alpha$ transformation on cooling at 508°K. The crystal structures of the high temperature β phase and the low temperature α phase are b.c.c. and h.c.p., respectively. The enthalpy of $\beta \to \alpha$ transformation of pure Thallium has been determined to be 100 $\pm$2 calories/mole. This experimental value agrees closely with Hultgren et al [7]. The enthalpy of phase transformation and the transformation temperature show considerable variation when different alloying elements are added. The transformation temperatures decrease monotonically with the addition of alloying elements. The enthalpies of phase transformation decrease with the addition of alloying elements for all alloying elements with the exception of Silver (Figure 4).

The minimum condition for a polymorphic phase transformation is:

$$\Delta F_{chemical} \gtreqless \Delta F_{non-chemical}$$

In order for the transformation to take place, the free energy change of the phase transformation $\Delta F^{\alpha\beta}$ represents the chemical free energy change that must be at least equal to the non-chemical free energy change. The non-chemical free energy term generally includes:

(a) the ~~strain~~ free energy change, ΔF_I, which results from the movement of an interface that accompanies a polymorphic transformation and (b) the strain free energy change, ΔF_S, which results from the change in volume of the parent and the product phases.

Thus, $\Delta F_{non-chemical} = \Delta F_I + \Delta F_S$. Of those terms, the interface free energy change, ΔF_I, in this case, will be approximately equal to the energy of a twin boundary; it will be found negligible. The strain free energy change, ΔF_S, will be dependent on the volume change associated with the phase transformation. The volume change decreases with the increase in the alloying additions of Ag, Cd and Sn. The temperatures of phase transformation also decrease with the increasing amounts of alloying additions. The decrease in transformation temperature seems to indicate that the amount of undercooling required for the phase transformation becomes smaller due to the decrease in the non-chemical free energy change. Consequently, the chemical free energy change necessary to overcome the non-chemical part also becomes smaller. This is reflected in the decrease in the enthalpy of phase transformation with increasing alloying additions, with the exception of silver.

The chemical free energy change, on the other hand, will include the lattice and the electronic terms. The lattice term is related to the vibrational mode of the crystal. The electronic term results from the change in valence electron concentration upon alloying. This contribution will be positive or negative depending upon the increase or decrease of the valence electron concentration upon alloying.

The simplest model of a metallic crystal is a lattice of positive ions held together by a "gas" of negative electrons. It is reasonable to assume that a metal dissolves in another metal in the form of its ion, contributing its valence electrons to the energy band of the solid. Therefore, the chemical potential of an element in an α phase is the sum of the chemical potential of its ions and of its valence electrons. Therefore, for an element I,

$$\mu_i = \mu_i^{ion} + Z_i \mu_e \tag{2}$$

Where μ, μ^{ion} and μ_e are the chemical potential of the neutral atom, the ions and electrons; Z_i is the atomic number of the element i.

It should be noted that any change in the chemical potential of the neutral atom will be caused directly by all the elements in the equation and also indirectly by changes in μ_i^{ion}. The effects are small and will be neglected.

The Gibb's free energy for an alloy (of pure Thallium and alloying element A) will consist of

$$F = N_{Tl}\mu_{Tl} + N_A\mu_A \tag{3}$$

Where N_{Tl} and N_A are the mole fractions of pure Thallium and of the alloying element A, respectively.

The μ_{Tl} and μ_A are the chemical potential of pure Thallium and of the

alloying element, respectively. Now a metallic binding is due to the electrostatic interaction between the positively charged ions and the negatively charged "electron gas". It follows that

$$\mu_{T1} = \mu_{T1}^{ion} + Z_{T1}\mu^{e} \qquad (4)$$

$$\mu_{A} = \mu_{A}^{ion} + Z_{A}\mu^{e} \qquad (5)$$

Where μ_{T1}^{ion} and μ_{A}^{ion} are the chemical potentials of the ions of pure Thallium and the alloying element, respectively. Z_{T1} and Z_A are the valencies of pure Thallium and of the alloying element, respectively.

If the equations (4) and (5) are substituted in equation (3), the result is:

$$F = N_{T1}(\mu_{T1}^{ion} + Z_{T1}\mu^{e}) + N_{A}(\mu_{A}^{ion} + Z_{A}\mu^{e})$$

$$= N_{T1}(\mu_{T1}^{ion} + Z_{T1}\mu^{e}) + (1 - N_{T1})(\mu_{A}^{ion} + Z_{A}\mu^{e})$$

$$= N_{T1}\mu_{T1}^{ion} + N_{T1}Z_{T1}\mu^{e} + (\mu_{A}^{ion} + Z_{A}\mu^{e}) - N_{T1}\mu_{A}^{ion} - N_{T1}Z_{A}\mu^{e}$$

The term in the bracket is equal to μ_A, so it follows that

$$F = (N_{T1}\mu_{T1}^{ion} + \mu_{A} - N_{T1}\mu_{A}^{ion}) + N_{T1}(Z_{T1} - Z_{A})\mu^{e}$$

Now, $N_{T1} \simeq 1$; therefore,

$$F = (\mu_{T1}^{ion} + \mu_{A} + \mu_{A}^{ion}) + (Z_{T1} - Z_{A})\mu^{e}.$$

It has been assumed the above factors are predominant and, therefore, the direct interaction between metal ions have been disregarded following the "Bronsted's principle" of specific interactions for electrolytes in solution. The "Bronsted's principle" only considers the interactions between ions of opposite signs; it neglects the interactions between ions of the same sign. It should be noted that the Bronsted's principle is applicable to solids, also.

Then for a phase change $\beta \rightarrow \alpha$, we have

$$\Delta F^{\beta\alpha} = F^{\beta} - F^{\alpha}$$

$$= [(\mu_{T1}^{ion} + \mu_{A} + \mu_{A}^{ion})^{\beta} - (\mu_{T1}^{ion} + \mu_{A} + \mu_{A}^{ion})^{\alpha}] + (Z_{T1} - Z_{A})(\mu_{\beta}^{e} - \mu_{\alpha}^{e})$$

$$= (A - B) + (Z_{T1} - Z_{A})\,\Delta\mu^{e}$$

Thus, the free energy change accompanying the phase transformation, $\Delta F^{\beta\alpha}$ will bear a straight line relationship with the difference in valencies, $(Z_{T1} - Z_{A})$. This observation will also be expected for $\Delta H^{\beta\alpha}$ vs. $(Z_{T1} - Z_{A})$. This is also the observed result (Figure 5) where the enthalpies of phase transformation per unit concentration have been

plotted as a function of $(Z_{T1} - Z_A)$. It is expected that $\Delta F^{\beta\alpha}$ definitely includes, among others, the electronic contribution to phase transformation.

The author wishes to acknowledge the assistance of various graduate students, particularly A. Patel and C. Sampathkumar, who helped carry out the research and made subsequent calculations.

References

[1] W. Hume-Rothary and G. V. Raynor; "Structure of Metals and Alloys", (Institute of Metals, London), 19.

[2] H. Jones; Proc. Royal Soc., London, A144(1934), 225.

[3] F. Seitz; Modern Theory of Solids, (McGraw Hill, New York) 1940.

[4] C. Zener; Trans. AIME, 203(1955), 619.

[5] R. J. Weiss and K. J. Tauer; Phy. Review, 102(1956), 1940, also J. Phys. Chem. Solids, 4(1958), 135.

[6] L. Kaufman, Acta Metallurgica, 7(1959), 575.

[7] R. Hultgren, Orr and P. Anderson; Selected Values of Thermodynamic Properties of Metals, (John Wiley & Co.), 1973.

[8] M. Levin; Zeits. Anorg. Chem., 45(1905), 31.

[9] M. Werner; Zeits. Anorg. Chem., 83(1913), 275

[10] Nishikawa and Asara; Phys. Rev., 15(1920), 38.

[11] Sinkiti Sekito, Z. Kirst, 74(1930), 189.

[12] R. Ewald, Am. Physik, 44(1914), 1213.

[13] W. Oelsen, O. Oelsen and D. Thiel; Zeib Metall Kunde, 46(1955), 555.

[14] W. Oelsen, K. H. Rieskamp and O. Oelsen; Amchiv. Eisenhuttenk, 26(1955), 253

[15] W. A. Roth, I. Meyer and H. Zeumer; Zeits. Anorg. Chemie; 216(1934), 303.

[16] S. Umino; Science Reports, Tohoku Imperial Univ. Series I, 16(1927), 775.

[17] A. Schneider and O. Hilmer; Zeits. Anorg. U. Allegem Chem., 286(1956), 97.

[18] S. Valentiner; Zeits. Metall Kunde, 32(1940), 244.

[19] T. R. Richards and C. P. Smyth; J. Am. Chem. Soc., 44(1922), 524.

TABLE I

The Electronic Structure, Valencies and
Ionic Radii of Pure Thallium and Alloying Elements

Elements	Atomic Number	Electronic Structure	Ionic Radius (R) (A)	$\dfrac{R_{T1} - R_A}{R_{T1}}$ X 100	Valency
Tl	81	$1s^2 \to 6s^2 6p^7$	1.710	0	3
Ag	47	$1s^2 \to 4d^{10} 5s'$	1.443	15.61	1
Cd	48	$1s^2 \to 4d^{10} 5s^2$	1.529	11.05	2
Sn	50	$1s^2 \to 5s^2 5p^2$	1.580	7.60	4

TABLE II

Enthalpies and Temperatures of Transformation on Cooling

Alloy Composition (atom percent A)	Transformation Temperature (°K)	Enthalpies of Phase Transformation $\Delta H^{\alpha\beta}$ cal/mole
Pure Thallium	508	100
Tl-Ag		
0.05 a% Ag	508	80
0.10 a% Ag	507	81
0.20 a% Ag	507	70
0.49 a% Ag	506	90
0.60 a% Ag	507	85
0.80 a% Ag	505	80
1.00 a% Ag	503	100
Tl-Cd		
0.05 a% Cd	508	134
0.20 a% Cd	506	130
0.44 a% Cd	503	110
0.50 a% Cd	502	100
0.60 a% Cd	500	90
0.88 a% Cd	492	78
1.00 a% Cd	488	50
Tl-Sn		
0.05 a% Sn	508	120
0.20 a% Sn	498	110
0.40 a% Sn	492	90
0.60 a% Sn	488	70
1.00 a% Sn	466	50

TABLE III

Lattice Parameter of Low Temperature Phase (h.c.p.)
at Various Temperatures for Various Alloys

Alloying Elements in Pure Thallium (atom percent A)	Lattice Parameters of Low Temperature Phase at Indicated Temperatures (Å)					
	298°K		358°K		533°K (Calculated Values)	
	a	c	a	c	a	c
Pure Thallium	3.4564	5.5320	3.4744	5.5598	3.5085	5.6390
Tl-Ag						
0.20 (atom percent Ag)	3.4531	5.5290	3.4850	5.5770	3.5589	5.7082
0.49 (atom percent Ag)	3.4494	5.5262	3.5005	5.6015	3.6323	5.8103
1.00 (atom percent Ag)	3.4462	5.5207	3.5286	5.6415	3.7619	5.9969
Tl-Cd						
0.44 (atom percent Cd)	3.4490	5.5263	3.4917	5.5860	3.5886	5.7594
0.88 (atom percent Cd)	3.4490	5.5235	3.5090	5.6130	3.6707	5.8831
1.00 (atom percent Cd)	3.4461	5.5097	3.5269	5.6399	3.7556	6.0085
Tl-Sn						
0.20 (atom percent Sn)	3.4525	5.5152	3.4850	5.5790	3.5603	5.7270
0.60 (atom percent Sn)	3.4524	5.5097	3.5075	5.6190	3.6606	5.9120
1.00 (atom percent Sn)	3.4472	5.5042	3.5300	5.6590	3.7645	5.8433

TABLE IV

Calculation of Volume Change in b.c.c. → h.c.p. Transformation at 533°K

Alloy Composition (atom percent A)	Lattice Parameter of b.c.c. phase at 533°K (Å)	Volume of h.c.p. Phase V_1 (Å³)	Volume of b.c.c. Phase V_2 (Å³)	$\dfrac{V_2 - V_1}{V_2}$ X 100
Pure Thallium	3.8297	60.114	58.5014	− 2.75
Tl-Ag				
0.20 a% Ag	3.9070	62.610	59.6847	− 4.90
0.49 a% Ag	3.9469	66.387	61.4895	− 7.96
1.00 a% Ag	4.0120	73.499	64.6060	−13.76
Tl-Cd				
0.44 a% Cd	3.9265	64.234	60.5595	− 6.06
0.88 a% Cd	3.9729	68.848	62.7127	− 9.78
1.00 a% Cd	4.0076	73.393	64.3703	−14.01
Tl-Sn				
0.20 a% Sn	3.9099	62.866	59.7764	− 5.16
0.60 a% Sn	3.9819	68.608	63.1398	− 8.66
1.00 a% Sn	4.0237	71.713	65.1491	−10.07
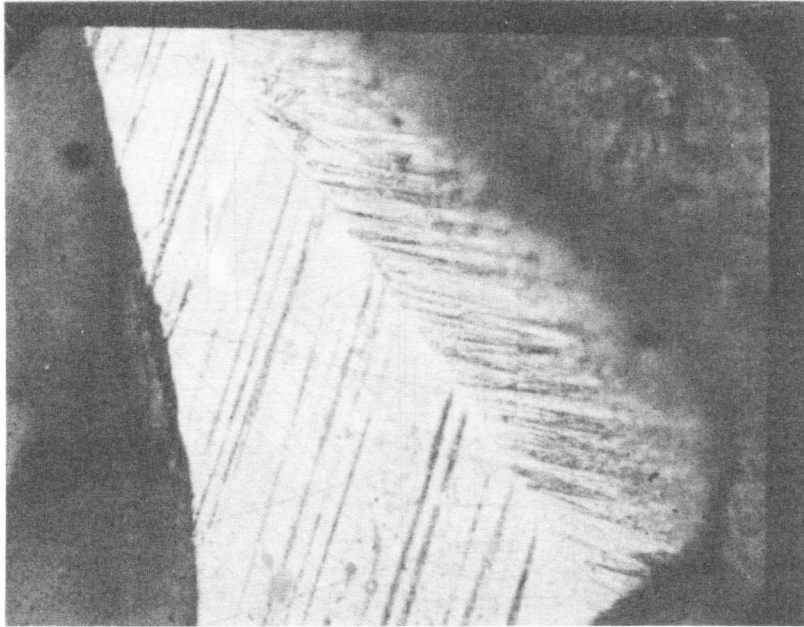
Figure 1   A Micrograph of Pure Thallium Showing the Twins

CONNECTORS FOR THERMOPILE

CAP
ASSEMBLY

CU CAN

SAMPLE

STIRRER

MAGNETIC
STIRRER
UNIT
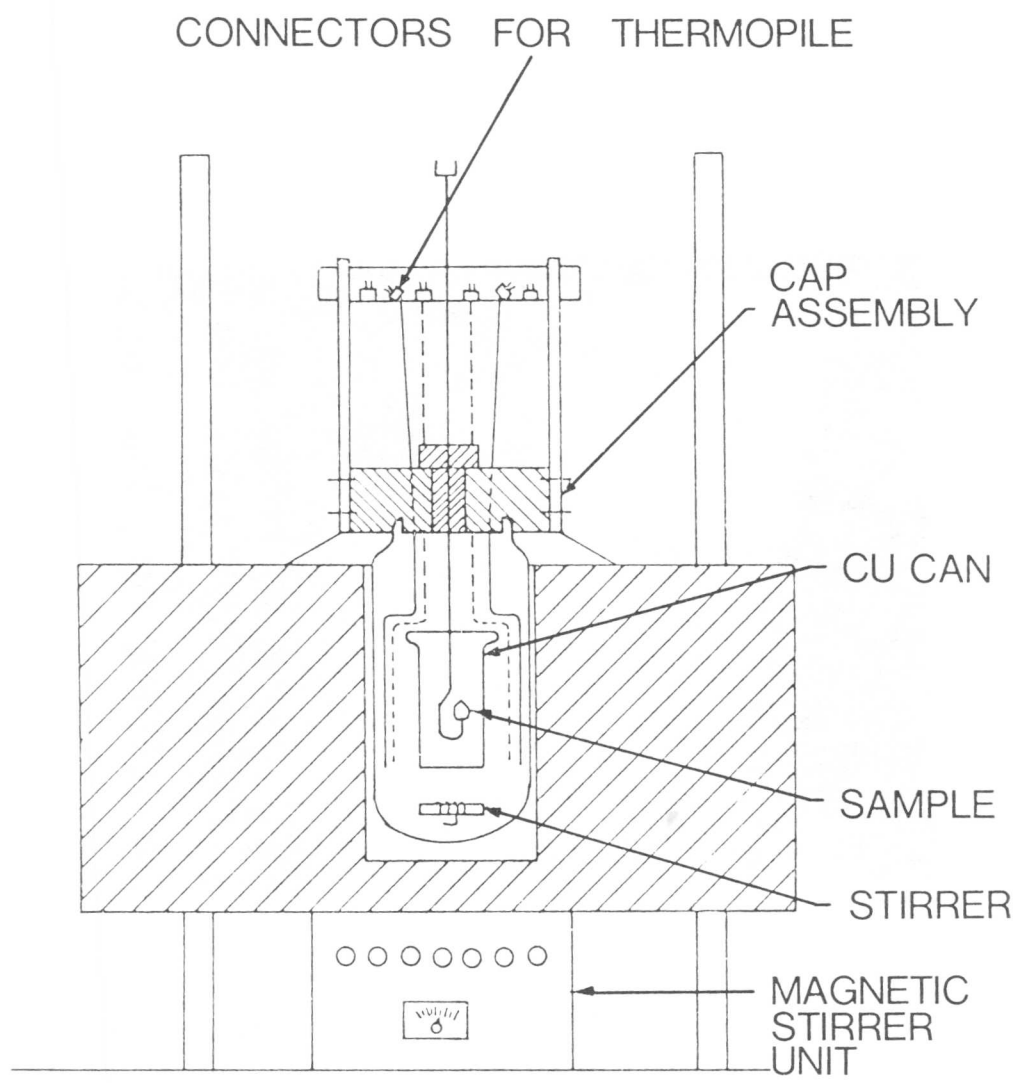
Figure 2   The Adiabatic Calorimeter
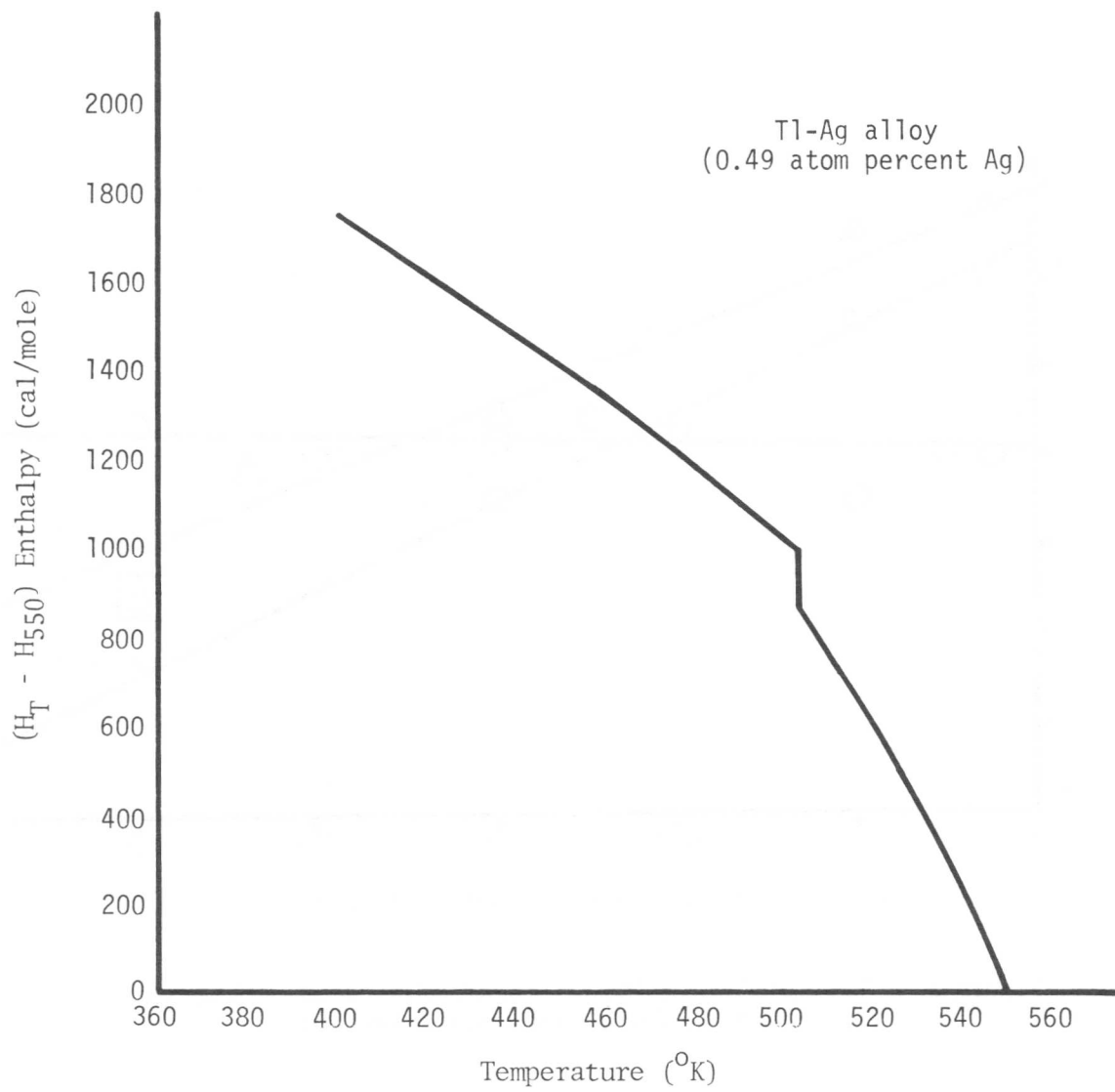
Figure 3   The Enthalpy as a Function of Temperature.
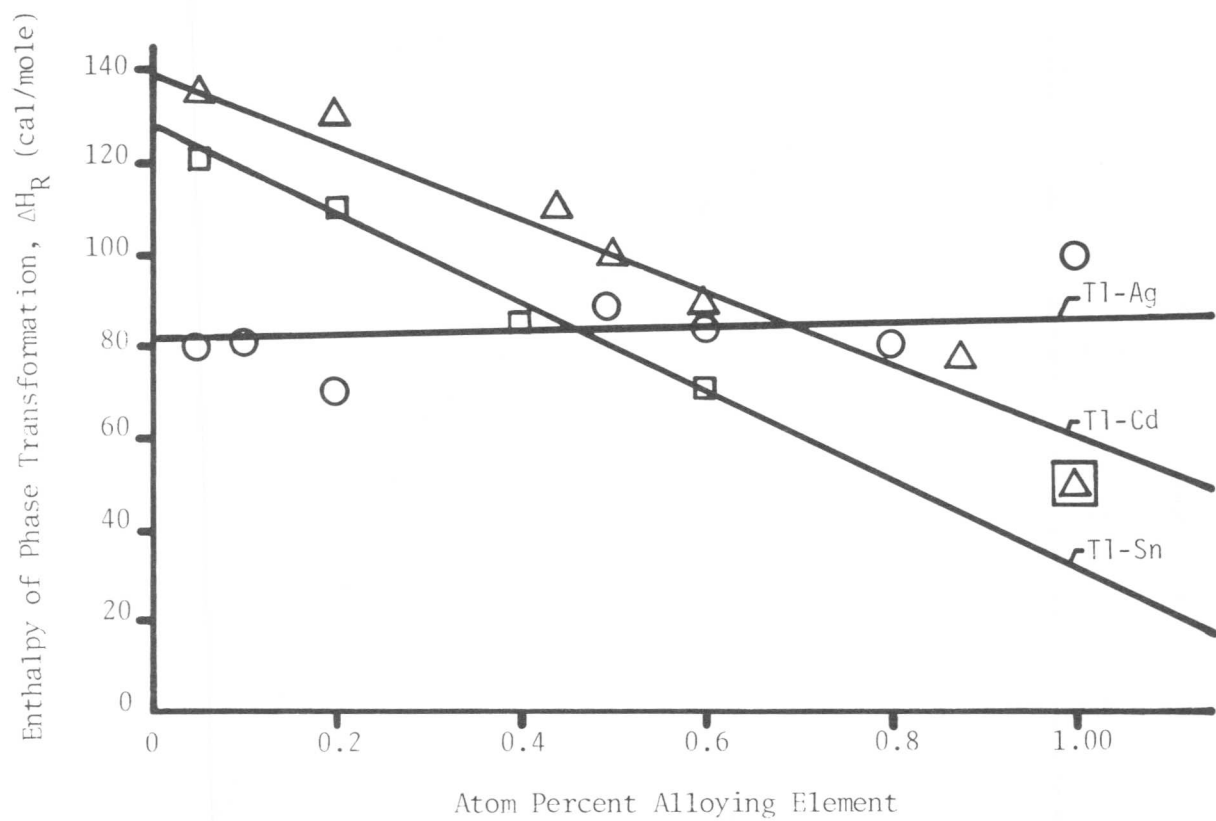
Figure 4   The Enthalpy of Phase Transformation as a Function of
Concentration for Various Alloy Systems
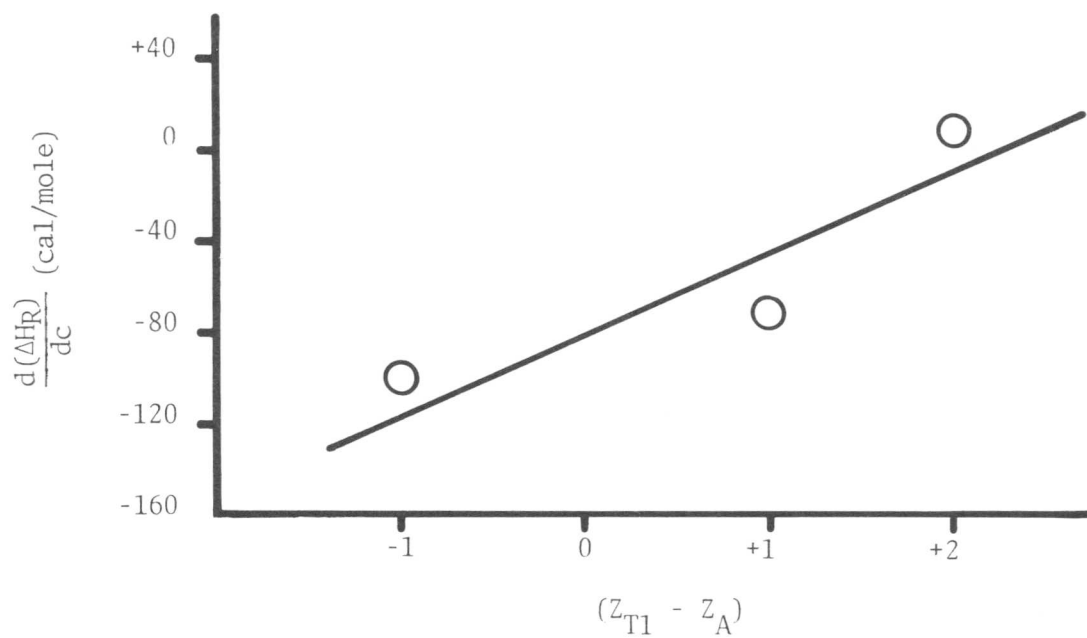
Figure 5 $\frac{d(\Delta H_R)}{dc}$ vs $Z_{T1} - Z_A$

Effects of Addition of 3d Transition Elements on the Phase Transformation in TiNi Compound

Toshio Honma, Minoru Matsumoto, Yoshiro Shugo
and Isao Yamazaki*

In order to clarify the mechanism of the transformation of TiNi compound, the physical properties of $Ti_{50}Ni_{50-x}M_x$ were studied in a wide temperature range. The transformation of $Ti_{50}Ni_{50-x}Fe_x$ during cooling and heating proceeds by two processes, namely phase I (CsCl type) $\rightleftarrows$ phase II (intermediate state) $\rightleftarrows$ phase III (monoclinic martensite). When Ni atoms are substituted by Fe atoms, the M_s (I $\rightarrow$ II) and M_s (II $\rightarrow$ III) points decrease. The decreasing rate of the M_s point is $52°C/1at\%Fe$ and that of M_s point is $21°C/1at\%Fe$, therefore the two step processes of transformation become remarkable with the increase of Fe concentration. In the case of addition of 3d transition elements to TiNi compound, M_s points change with the amount of additives (V, Cr, Mn, Fe and Co). The changing rate of M_s points is proportional to the valence electron concentration (e/a), total (3d + 4s) electron number devided by total atom number. When e/a is seven, M_s point is maximum temperature. As e/a deviates from seven, M_s points decrease linearly.

I. Introduction

TiNi exhibits thermoelestic martensite transformation. This material has the properties of "shape memory effect", and this properties have been applied to many fields, for example, nitinol heat engine, medical materials and so on. There are many unsolved problems on the phase transformation of TiNi. Authors studied various physical properties accompanied by the martensitic transformation of $Ti_{50}Ni_{47}Fe_3$ and reported the two step transformations of $Ti_{50}Ni_{47}Fe_3$ i.e. the parent phase (I: CsCl type cubic structure) $\rightleftarrows$ the intermediate state (II: CsCl type tetragonal structure) $\rightleftarrows$ the martensite phase (III: disorted B19 structure) [1].

We have studied the temperature change of the electrical resistivity, the magnetic susceptibility and the specific heat of TiNi compound which Ti or Ni atom was substituted by 3d transition element (for example V, Cr, Mn, Fe and Co).

II. Sample Preparation

$Ti_{50}Ni_{50-x}M_x$ (M: Fe or Co) and $Ti_{50-x}M_xNi_{50}$ (M: V, Cr or Mn) were

---

Research Institute of Mineral Dressing and Metallurgy, Tohoku University, Sendai, Japan. *Present address: Sumitomo Metal Industries, Ltd., Kashima, Ibaraki, Japan.

prepared. 3d transition metal element concentration, x, is less than 10 at%. Specimens were prepared by electron beam melting method and the product was remelted several times in order to homogenize it. The obtained button was forged or hot rolled and then shaped to the dimensions for measurements. These specimens were homogenized at about 900°C for 2 hrs in vacuum.

III. Experimental Methods

The temperature change of the electrical resistivity, the magnetic susceptibility and the specific heat of specimens were measured. The electrical resistivity was measured by the conventional method or A. C. method using 1kHz alternation current. The magnetic balance method was used for the measurement of the magnetic susceptibility. By the use of an adiabatic calorimeter the specific heat was measured.

IV. Experimental Results

(1) $Ti_{50}Ni_{50-x}M_x$ (M = Fe and Co)

The temperature change of the electrical resistivity, the magnetic susceptibility and the specific heat of $Ti_{50}Ni_{50-x}Fe_x$ were measured. Fig. 1 and 2 show the temperature change of the electrical resistivity and the magnetic susceptibility of $Ti_{50}Ni_{49}Fe_1$ and $Ti_{50}Ni_{48}Fe_2$. The electrical resistivity decreased linearly on cooling and increased at M'_s temperature. At M_s temperature the electrical resistivity was maximum. M_s temperature decreased linearly with the increase of Fe atom concentration. These temperature change of the electrical resistivity is the change of phase transformation accompanied by parent phase (I) → the intermediate phase (II) → martensite phase (III).

M_s, A_s, M'_s and A'_s temperature decreased linearly with the increase of Fe atom concentration. These results were shown in Fig. 3. The decreasing rate of M_s and M'_s temperature to the increase of Fe atom concentration was 52°C/1at%Fe and 21°C/1at%Fe, respectively. On the phase transformation I → II, the temperature change of the electrical resistivity increased abruptly but the magnetic susceptibility decreased slightly as shown in Fig. 1 and 2. The electrical resistivity and the magnetic susceptibility both decreased on II → III transformation. As reverse behavior of the electrical resistivity change occur on heating, so that increase of the electrical resistivity at A_s and decrease of the electrical resistivity at A'_s overlap in the specimen containing low concentration of Fe atoms, so reverse transformation temperatures did not observed clearly. Fig. 4 shows the specific heat vs. temperature curves of $Ti_{50}Ni_{47.5}Fe_{2.5}$. Two peaks of specific heat accompanied by the two step transformations, III → II → I, were observed clearly. The temperatures of the peaks decreased with the increase of Fe atom concentration.

The temperature change of the electrical resistivity and the magnetic susceptibility of $Ti_{50}Ni_{43}Co_7$ were shown in Fig. 5. The change of the electrical resistivity and the magnetic susceptibility

accompanied by two step transformations were observed in the same manner as $Ti_{50}Ni_{50-x}Fe_x$. Fig. 6 shows the decreasing rate of phase transformation temperatures to Co atom concentration. These decreasing rate were 22°C/1at%Co for M_S and 8°C/1at%Co for M_S, respectively.

(2) $Ti_{50-x}M_xNi_{50}$ (M = V, Cr and Mn)

The change of the electrical resistivity of these specimen on cooling and heating was complicated, which accompanied by two step transformations as shown in $Ti_{50}Ni_{50-x}M_x$ (M = Fe and Co). Fig. 7 shows the electrical resistivity vs. temperature curves of $Ti_{50-x}V_xNi_{50}$. In the case of $Ti_{50-x}Cr_xNi_{50}$ and $Ti_{50-x}Mn_xNi_{50}$, the electrical resistivity vs. temperature curve were similar to that of $Ti_{50-x}V_xNi_{50}$ [2]. The M_S temperatures of $Ti_{50-x}M_xNi_{50}$ were shown in Fig. 8. Ms temperatures decreased linearly with the increase of 3d transition metal element concentration. These decreasing rates of M_S temperature were 20°C/1at%V , 75°C/1at%Cr and 50°C/1at%Mn, respectively.

V. Discussion and Summary

Wang [3] reported that the transformation temperature decreased when Ni atom in TiNi were substituted by Fe or Co atom and the decreasing rate of $Ti_{50}Ni_{50-x}Fe_x$ was more than that of $Ti_{50}Ni_{50-x}Co_x$. He proposed that the transformation temperature (M_S temperature) was proportional to the valence electron concentration, e/a, ["total (3d + 4s) electron number: e" devided by "total atom number: a"] and this temperature decreased and increased with the valence electron concentration. In the present experimental results, the decreasing rate of M_S temperature with the substitution of 3d transition element are different each other. Fig. 9 shows the M_S temperature vs. e/a. M_S temperature decreased linearly in both case of e/a > 7 (M = V, Cr and Mn) and e/a < 7 (M = Fe and Co) and this temperature gave straight same lines in these case except for $Ti_{50-x}Cr_xNi_{50}$. When e/a does not change by the substitution of 3d transition element, M_S temperature will be constant. Fig. 10 shows the M_S temperature vs. Mn atom consentration in $(TiNi)_{50-x}Mn_x$. M_S temperature does not change by the addition of Mn atom in the case of constant e/a. Thus M_S temperature depends on the e/a. The decreasing rate of M_S temperature in Wang's data is almost same as present results as shown in Fig. 9. However, M_S temperature in Wang's data is about 100°C higher than that of present data. This reason is supposed to the inaccuracy of his measurements. In addition of Cr atom M_S temperature decreases exceptionally compared to other 3d transition element. This cause is not clear and this problem will be solved by the electron theory of metal.

The present experimental results are summarized as follows.

(1) Two step transformations (I ⇄ II ⇄ III) occur in $Ti_{50}Ni_{50-x}M_x$ and $Ti_{50-x}M_xNi_{50}$.

(2) The changing rate of M_S point is proportional to the valence electron concentration (e/a).

(3) When e/a is seven, M_S point is maximum temperature. As e/a deviated from seven, M_S points decrease linearly.

Acknowledgments

References

[1] M. Matsumoto and T. Honma: Proceedings of the First JIM International Symposium on "New Aspects of Martensitic Transformation", Kobe, Suppl. Trans. JIM, 17 (1976), 199.
[2] T. Honma, Y. Shugo and M. Matsumoto: Bulletin Res. Inst. Min. Dress. Met., Tohoku Univ., 28 (1972), 209 (in Japanese).
[3] F. E. Wang: Proceedings of the First International Conference on Fracture, 2 (1965), 899.
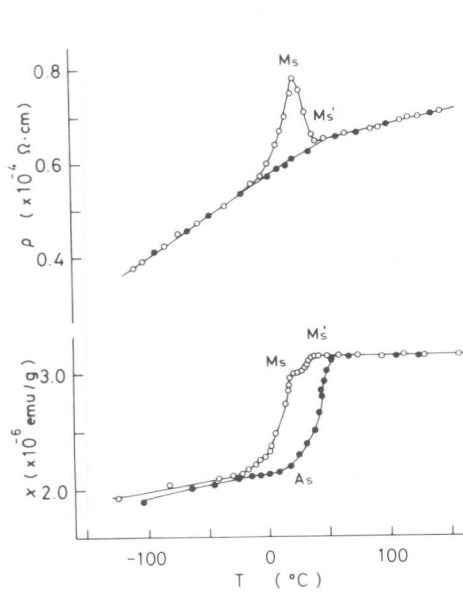
Fig. 1 The electrical resistivity and the magnetic suscepti-bility vs. temperature curves of $Ti_{50}Ni_{49}Fe_1$. o cooling, ● heating
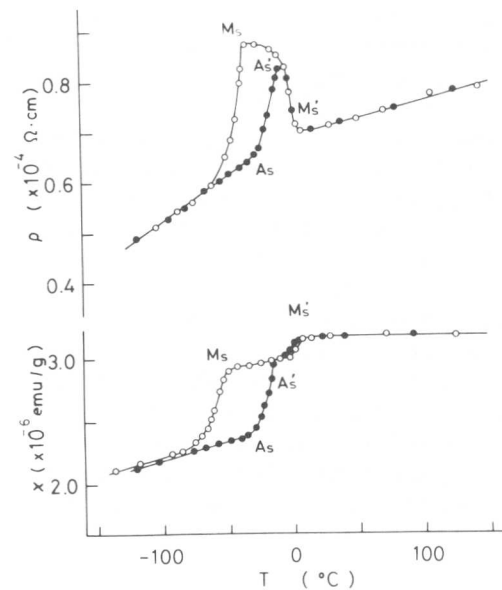
Fig. 2 The electrical resistivity and the magnetic suscepti-bility vs. temperature curves of $Ti_{50}Ni_{48}Fe_2$. o cooling, ● heating

-262-
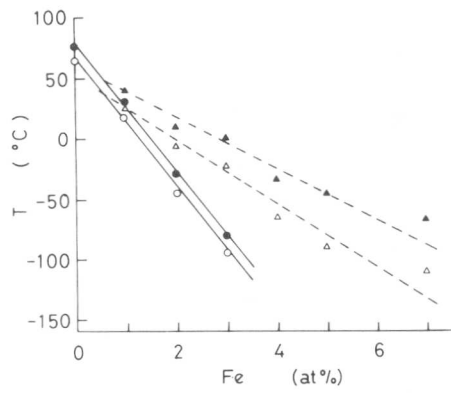
Fig. 3 M_S', M_S, A_S and A_S' tempera-
tures vs. Fe atom concent-
ration in $Ti_{50}Ni_{50-x}Fe_x$.
o M_S, ● A_S, △ M_S', ▲ A_S'
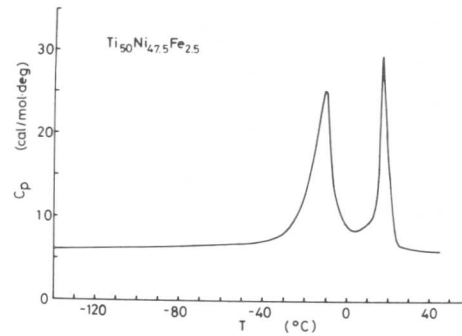
Fig. 4 The specific heat vs.
temperature curve of
$Ti_{50}Ni_{47.5}Fe_{2.5}$.
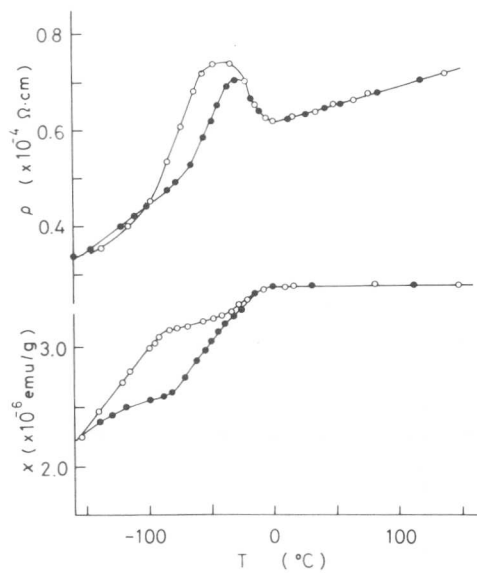
Fig. 5 The electrical resistivity
and the magnetic suscepti-
bility vs. temperature
curves of $Ti_{50}Ni_{43}Co_7$.
o cooling, ● heating
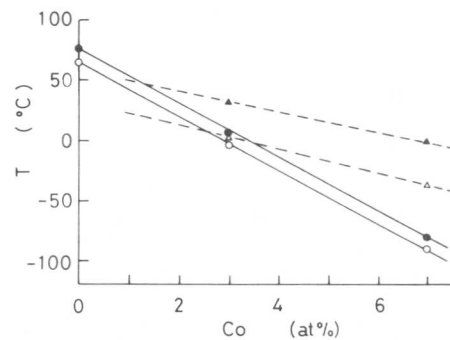
Fig. 6 M_S', M_S, A_S and A_S' tempera-
ture vs. Co atom concent-
ration.
o M_S, ● A_S, △ M_S', ▲ A_S'

-263-
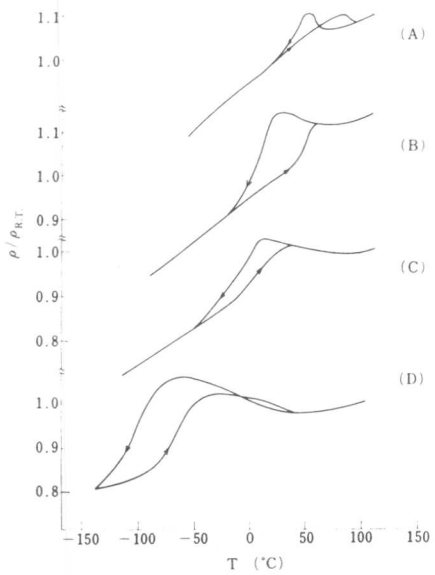
Fig. 7 The electrical resistivity
vs. temperature curve of
$Ti_{50-x}V_xNi_{50}$.
(A) x = 0.5, (B) x = 2,
(C) x = 3, (D) x = 5
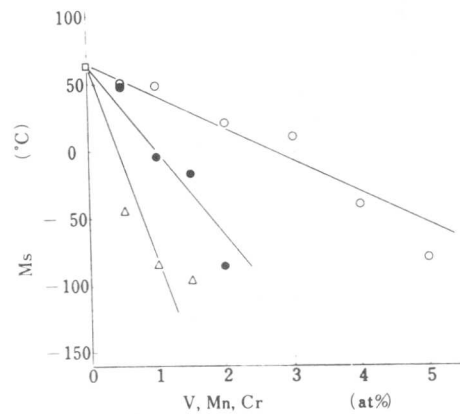
Fig. 8 M_S temperature vs. V, Cr
and Mn atom concentration.
o V, △ Cr, ● Mn, □ TiNi
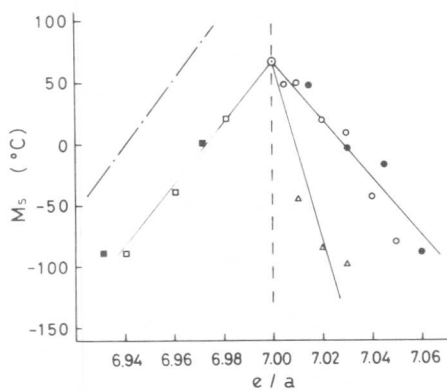
Fig. 9 M_S temperature vs. e/a.
o V, △ Cr, ● Mn,
□ Fe, ■ Co, ⊙ TiNi
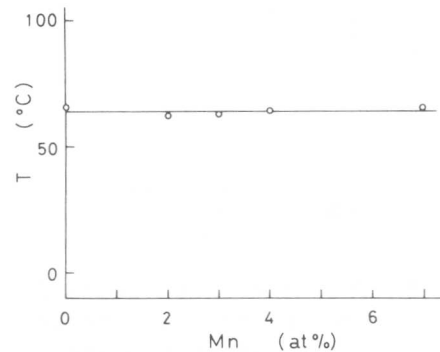
Fig. 10 M_S temperature vs. Mn
atom concentration in
$(TiNi)_{50-x}Mn_x$.

Martensitic Transformation in the Beta AuZn-CuZn System

R. C. Bowe* and L. Muldawer

.

The martensitic transformation temperature To of the $Au_xCu_{50-x}Zn_{50}$ and $Au_xCu_{52-x}Zn_{48}$ systems for $20 \leq x \leq 50$ were measured using resistivity and x-ray diffraction. In the Heusler region, $\Delta\rho$ at To was positive on cooling except near $x = 25$ where it was zero. The Heusler region curves of To vs x for our alloys are consistent with those of other studies of the Au-Cu-Zn system. In the gold-rich ($x > 33$) beta region we have found the To is relatively insensitive to composition. This was interpreted in terms of the strengths and number of Au-Zn and Cu-Zn bonds and the repulsive ion-core overlap energy. Other investigators have found sharp decreases in To starting at the end points of this region. Near $x = 33$ we find a sharp change in the slope of To vs x, indicating an expected relationship between parent structure and martensite To. Our lattice constant measurements will be used in the discussion of ion core separation.

I. Introduction

In this study the martensitic transformation temperatures, T_o, of alloys in the $Au_xCu_{50-x}Zn_{50}$ and $Au_xCu_{52-x}Zn_{48}$ systems were measured using resistivity and x-ray techniques. An attempt was made to determine stability factors operative in these systems by examining curves of T_o vs. composition (such as the anisotropy factor A).

Data of T_o vs composition are usually interpreted in terms of factors to which A is related, i.e. e/a (electron/atom ratio) and ionic radii. In most cases T_o decreases, indicating increased stability, with increasing e/a. Such is the case in the noble metal alloy systems $\beta'-Cu_xZn_{1-x}$[1], $\beta'-Au_xCd_{1-x}$[2], and $\beta'Ag_xCd_{1-x}$[2], with the $\beta'-Au_xZn_{1-x}$[3] system being the exception. The decrease in T_o observed when the smaller copper atom [4] or silver atom [2] is substituted for the large gold atom in $\beta'-Au_{52.5}Cd_{47.5}$ has been attributed to a reduction in exchange repulsion. The stability of the $\beta'-Au_{50}Cd_{50}$ type alloy has also been related to quenched-in vacancies and order. Differences in electronegativity are considered an important stability factor in the various ternary systems produced by divalent substitutions for Cd in $\beta'Au_{50}Cd_{50}$.[5]

Unlike other Au-Cu-Zn systems which have been reported [6,7], transformation occurs throughout the Au rich region of the $Au_xCu_{50-x}Zn_{50}$ system. In these other Au-Cu-Zn systems, transformations occurring in their β' and Heusler regions are separated by a region either in which no transformation was observed or in which none was investigated.

Physics Department, Temple University, Philadelphia, PA 19122, USA.
*Regularly at St. Joseph's College, Philadelphia, PA 19131, USA.

II. Experimental Methods

Resistivity measurements were made using the standard four termi-
nal technique on annealed specimens. Temperature control was
accomplished by raising or lowering the sample chamber in the neck
of a liquid helium storage dewar. The temperature was very stable
and the temperature difference between the potential contacts was
believed to be less than $1^{\circ}K$.

CuK_{α} radiation was used in all x-ray work. Precision room tempera-
ture lattice constants and crystal structures were determined from
powder patterans obtained using a 114 mm diameter Debye-Sherrer camera.
Low temperature x-ray diffraction studies were made using an MRC model
X-86GC low temperature attachment mounted on a GE XRD5 diffractometer.

The martensitic transformation temperatures were determining using
resistivity and x-ray techniques. Determination of transformation
temperature from resistivity data is illustrated in Fig. 1. The
resistivity method was applied to alloys in the β' region of the
$Au_x Cu_{50-x} Zn_{50}$ system (x = 50, 49, 45, 40, 37½ and 34), and to certain
alloys in the Heusler region of this system (x = 32, 30, 29). The
x-ray technique was applied to alloys (x = 28, 25, 23, 20) whose
transformation could not be well determined by the resistivity method.

The x-ray technique consisted of monitoring the intensity of a
strong Heusler line as a function of temperature. M_s, M_f, A_s and A_f
of $Au_{30} Cu_{20} Zn_{50}$ were determined by both techniques. It was found that
$T_o = \frac{1}{2}(M_s + A_s)$, obtained by each of the two techniques were within a
few degrees of one another.

III. Results

1. X-ray Diffraction Studies

The x-ray diffraction patterns produced by all the Au-Cu-Zn
samples contained lines which indexed to either a CsCl (β') or Heusler
(β'') structure. Room temperature crystal structures and lattice con-
stants of the Au-Cu-Zn ternaries were obtained. The precision lattice
constants and ionic radii were used to calculate average ion core
separations. The ionic radii used were those given by Pauling [8]:
Cu^+ 0.96A, Au^+ 1.37A, and Zn^{++} 0.74A. The calculated separations
show a linear reduction as the gold concentration is increased. The
values become smaller for the lower zinc alloys; the separation for
$Au_{25} Cu_{25} Zn_{50}$ is 0.75A while that for $Au_{25} Cu_{27} Zn_{48}$ is 0.74A. Murakami
et al [9] also obtained a linear variation with their values somewhat
larger presumably because their ionic radii were different.

Low temperature x-ray diffraction studies were carried out on
$Au_{25} Cu_{27} Zn_{48}$ and on certain alloys of the $Au_x Cu_{50-x} Zn_{50}$ system
(x = 20, 23, 25, 28, 32, 34, and 50). All transformed martensitically
and no evidence was found to indicate that these transformations were
incomplete. The low temperature structure (θ'') of alloys with com-
positions near $Au_{25} Cu_{25} Zn_{50}$ have been studied by a number of investi-
gations [10,11]. On the

basis of their studies and the findings of the present investigation, the low temperature phase of $Au_{25}Cu_{25}Zn_{50}$, $Au_{25}Cu_{27}Zn_{48}$, and $Au_{32}Cu_{18}Zn_{50}$, all of which possess the Heusler structure at room temperature is thought to be monoclinic. More recent studies by Murakami et al have interpreted this martensitic structure as being a combination of two martensites, both of them orthorhombic [12].

The similarity of the low temperature x-ray patterns of $Au_{34}Cu_{16}Zn_{50}$ and $Au_{50}Zn_{50}$, both of which possess the CsCl structure at room temperature, indicate they probably possess the same martensitic structure (θ'). These patterns are different from those produced by the martensite of the Heusler alloys. β'-$Au_{50}Zn_{50}$ was studied extensively and the structure of its martensite appears to deviate only slightly from a cubic structure. Indexing on the assumption of a cubic structure gives a lattice constant of 9.43 Å. The actual lattice, whatever it is, is thus seen to have roughly three times the dimensions of the room temperature β' unit cell.

Breedis [13] suggests a rhombohedral unit cell for the martensite of β'-$Au_{50.9}Cd_{49.1}$ with a_o = 9.936 Å and a rhombohedral angle of 89.55°. This unit cell is seen to be nearly cubic. Comparing the Breedis diffraction lines from β'-$Au_{50.9}Cd_{49.1}$ with those of the present study on β'-Au Zn, we conclude that both possess similar martensitic structures.

2. Resistivity Studies

Resistivity as a function of temperature over a range around T_o was obtained for our alloys. An interesting feature of the transformation was the percent change in resistivity. This is plotted as a function of gold concentration in Fig. 2. The zero values of $\Delta\rho/\rho$ in the range around 24% Au are noteworthy; it is not clear how the curve should be drawn in this region. Values of 4.1% for annealed $Au_{28}Cu_{27}Zn_{45}$[9] and 2.3% for $Au_{26}Cu_{27}Zn_{45}$[14] were obtained; no other values were reported by these researchers.

3. T_o vs composition

Transformations occurring in $Au_xCu_{50-x}Zn_{50}$ and $Au_xCu_{52-x}Zn_{48}$ as observed by us are compared with those of the $Au_xCu_{51-x}Zn_{49}$ and $Au_xCu_{55-x}Zn_{45}$ systems as observed by Nakanishi et al [6] in Fig. 3. Inasmuch as the thermocouple was on the sample in our resistivity measurements, we expect that these resistivity method data would be more accurate. The T_o from resistivity measurement for $Au_{30}Cu_{20}Zn_{50}$ is 133.5°K, that from x-ray measurement is 126°K. Thus, we should expect that the tops of our curves (mainly x-ray measurements) should be somewhat higher improving agreement with the data of Nakanishi et al. in the Heusler region.

It should be noted that the T_o peaks line up for x=25 independent of the zinc concentration. Thus, the gold concentration is more important than the copper concentration; to this extent, copper and zinc are close in effect.

-267-

Our data are taken throughout the entire region of composition while there is a large missing section in that of Nakanishi et al. Fig. 3 shows that our transformation curve for the $Au_xCu_{50-x}Zn_{50}$ system is continuous; however, there is a sharp break in the slope of the T_o vs. composition curve with the break occurring near the β'-Heusler boundary. For this reason we shall treat separately the two regions, that near stoichiometry and that near AuZn. Furthermore, as we have indicated, the Heusler phase undergoes a transformation to one structure, the β' phase to another.

IV. Discussion

1. The Heusler Region

Figure 3 shows that T_o for the Heusler region is parabolic in nature with peaks occurring near stoichiometry. The shape of the transformation curve indicates a strong relationship to deviations from the stoichiometric composition. However, the peak maxima observed in the transformation curves of the Au-Cu-Zn systems near stoichio-metry are unexpected. The noble metal order that exists in the Heusler region would be expected to enhance stability and thus result in a dip rather than a peak near stoichiometry. Such a dip is observed in the transformation curve of the Au-Ag-Cd(47.5%Cd) system [2]. However, a good correlation between T_o and elastic anisotropy A for the Au-Cu-Zn alloys was obtained by Nakanishi et al [6]. Another study by Nakanishi et al [14] of the Debye temperatures of these alloys shows a minimum in the stoichiometric region indicating that these alloys are softer.

Murakami et al [9] have examined the stability problem in these alloys. They attribute the decrease in T_o with increasing Au concentration on the Au rich side of stoichiometry to the increase in the number of Au-Zn bonds, and attribute the decrease in T_o with decreasing Au concentration on the Cu rich side of stoichiometry to the decrease in exchange repulsion. One of us (L.M.) has suggested that the ternary $AuCuZn_2$ is "expanded" relative to the average of CuZn and AuZn because of the large size of the gold atom [15]. This may be taken as an indication that exchange repulsion is significant. The observation concerning the correlation of the peak in T_o with x = 25 is evidence for this speculation.

In the Heusler region the curve of T_o vs. composition for $Au_xCu_{50-x}Zn_{50}$ is below that of $Au_xCu_{52-x}Zn_{48}$. This is generally con-sistant with the studies performed on the Au-Cu-Zn systems of 45%, 47%, 49%, and 50% Zn [7], and with the observation that, in the structurally similar β' phase alloys, T_o decreases with increasing e/a except for the very important case of β'-AuZn [3].

2. The Gold Rich β' Region

According to our results as seen in Fig. 3, substituting copper for gold in this region has little effect on T_o for $Au_xCu_{50-x}Zn_{50}$. This is in serious disagreement with the data of Nakanishi et al. as

reported by them for $Au_xCu_{51-x}Zn_{49}$; here A_s decreases sharply with increasing copper concentration. It is highly unlikely that the 1% Zn difference can produce such divergent results. Their alloys were quenched; however, Ref. 9 shows that quenching produces a change of only two or three degrees. Our data for this region is excellent as is obvious from Fig. 1.

These results may also be interpreted in terms of exchange repulsion and atomic bonding. Nakanishi et al. [6], in a study which correlated elastic anisotropy with A_s of the $Au_xCu_{53-x}Zn_{47}$ system, interpreted their results in terms of exchange repulsion and strong Au-Zn bonding. Brookes and Smith [5], in studying the effect on stability of ternary divalent substitutions for Cd in $\beta'-Au_{50}Cd_{50}$, concluded that strong ordering forces (related to large electronegativity differences) between Au and the divalent substitute enhance stability.

The electronegativity difference between Au and Zn is larger than that between Cu and Zn. Following the reasoning of Brookes and Smith it would then be expected, on the basis of electronegativity effects, that substituting Cu for Au in $\beta'Au_{50}Zn_{50}$ would reduce stability by virtue of the resulting decrease in the number of stronger Au-Zn bonds.

The explanation of the insensitivity of T_o to noble metal interchange in the Au rich β' region may be as follows. As Au is replaced by Cu in the $\beta'-Au_xCu_{50-x}Zn_{50}$ system there is a decrease in the number of Au-Zn bonds, which would tend to increase T_o, and a decrease in the exchange repulsion, which would tend to decrease T_o. The net result of these effects might then account for the relative insensitivity to T_o to noble metal interchange. Obviously, such an explanation should also hold for the 49% Zn alloys for compositions containing more than just a few percent copper.

The assumption that substituting the smaller Cu for Au reduces exchange repulsion is supported by our calculated ion core separations. Exchange repulsion should decrease with increasing ionic separation. In the $Au_xCu_{50-x}Zn_{50}$ system the average ion core separation increases with increasing Cu concentration. Thus, we expect that the exchange repulsion in this system decreases with increasing Cu concentration. However, it is clear that we do not have a good understanding of the behavior of T_o in the Heusler region.

V. References

[1] H. Pops and T. B. Massalski, Trans. AIME 230, 1662 (1964).
[2] F. Rothwarf and L. Muldawer, J. Appl. Phys. 33, 2531 (1962).
[3] H. Pops and T. B. Massalski, Trans. AIME 233, 728 (1965).
[4] N. Nakanishi and C. M. Wayman, Trans. AIME 227, 500 (1963).
[5] M. E. Brookes and R. W. Smith, Metal Sci. J. 2, 181 (1968).
[6] N. Nakanishi, Y. Murakami, and S. Kachi, Scripta Met. 2, 673 (1968).
[7] N. Nakanishi, Y. Murakami, H. Takehara, Y. Senda, H. Sugiyama, and S. Kachi, Japan. J. Appl. Phys. 7, 302 (1968).

[8] L. Pauling, The Nature of the Chemical Bond, 3rd ed., p. 514, Cornell U. Press (1960).

[9] Y. Murakami, H. Asano, N. Nakanishi, and S. Kachi, Japan J. Appl. Phys. 6, 1265 (1967).

[10] M. Duggin, Japan. J. Appl. Phys. 7, 296 (1968).

[11] Y. Murakami, N. Nakanishi, and S. Kachi, Japan J. Appl. Phys. 5, 820 (1967).

[12] Y. Murakami, N. Nakanishi, and S. Kachi, Japan J. Appl. Phys. 11, 1591 (1972).

[13] J. F. Breedis, Univ. of Ill. Progress Report, contract no. AT(11-1)-1076 (1962).

[14] N. Nakanishi, Y. Murakami, and S. Kachi, Scripta Met. 5, 433 (1971).

[15] L. Muldawer, Acta Cryst. 20, 594 (1966).
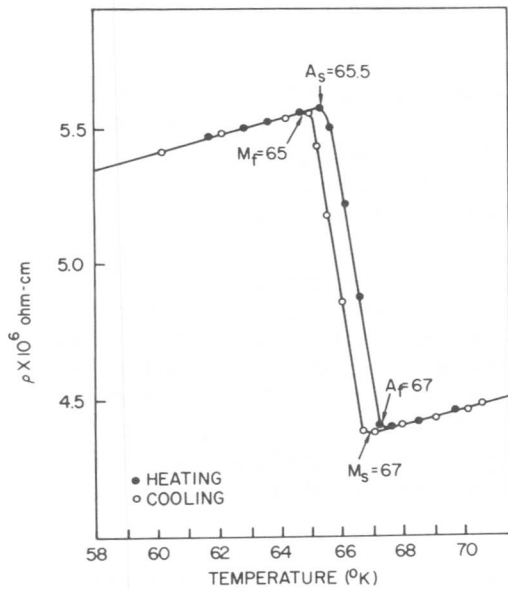
Fig. 1 Resistivity vs temperature for $Au_{45}Cu_5Zn_{50}$.
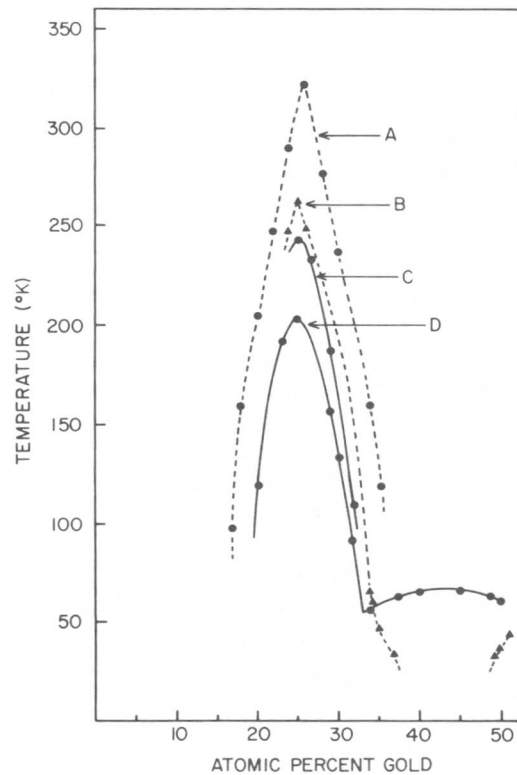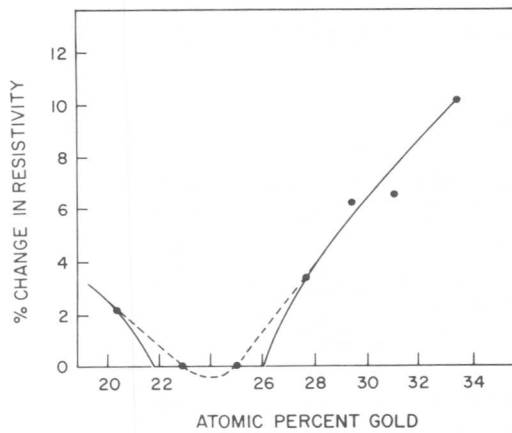
Fig. 3 T_o for various alloys: A, 45% Zn; B, 49% Zn; C, 48% Zn; D, 50% Zn. Alloys A and B are those of Nakanishi et al, C and D are ours.

Fig. 2 Changes in resistivity at T_o for alloys in the Heusler region.

The Stability of Martensite in Binary Cu-Zn Alloys.

M. Ahlers*

Abstract: The stability of the metastable martensite is compared to the bcc β' phase, which is stable at higher temperatures. The enthalpy difference between the phases is separated into a term that depends on the atom configuration (order), and a term that is independent of it. It is shown that the configuration part can be described essentially by interactions between fourth nearest neighbor atom pairs in the marten-site, and that the concentration dependence of the enthalpy difference (and also of M_S) is mostly determined by this term. The hypothetical enthalpy change for pure copper,which is derived from the configuration independent enthalpy term is in good agreement with theoretical values. The entropy difference between β' and martensite has been found to be quite insensitive to long range order, and is believed to be nearly the same as that between β' and the α phase, which is stable at lower con-centrations.

The martensitic transformation in the Cu-Zn system has three impor-tant characteristics, which facilitate considerably the evaluation of the stability of the phases involved: 1) The transformation between the high temperature long range ordered β' phase and the martensite is nearly reversible, which makes it possible to determine experimentally the enthalpy and entropy of transformation by neglecting hysteresis effects [1]. 2) The transformation occurs with a negligible volume change ($\Delta V/V \lesssim 2.10^{-3}$ [2]). Therefore all those contributions to the free energy that depend on volume do not enter into the discussion. 3) The transformation is diffusionless, i.e. the distribution of the atoms in the martensite is completely determined by that in the β' phase. There-fore the configuration is not a variable, and it is not necessary to minimize the free energy in both phases separately with respect to the atom configuration.

---

*Centro Atómico Bariloche, Comisión Nacional de Energía Atómica. (8400) S.C. de Bariloche, Argentina

It has become customary to describe the stability of phases by pairwise interaction energies between atoms, as long as volume changes are not involved. This procedure has been justified for simple metals by the pseudopotential method using up to second order perturbation theory [3]. In this approximation central force pair interaction energies can be derived which are independent of the type of lattice and its atom distributions. Although it is not clear whether the CuZn system can be analyzed quantitatively in this way, nevertheless this approach can serve as a useful starting point, which will be adopted in this paper. Thus the basic assumption that will be made here is, that the volume independent part of the energies of the two phases can be calculated using central force type interaction energies which depend only on the distance of the atoms but not on the lattice structure.

The long range order in β brass has been described successfully by pairwise interaction energies [4]. It has been shown that it is sufficient to take into account first (i=1) and second (i=2) neighbor "chemical interaction energies" $w_{CuZn}^{(i)}$, where $w_{CuZn}^{(i)} \equiv -2W_{CuZn}^{(i)} + W_{CuCu}^{(1)} + W_{ZnZn}^{(i)}$ is the difference between interaction energies of CuZn and CuCu, ZnZn pairs. While nearest neighbor (nn) distances are approximately the same in the martensite as in the β' phase, the second neighbor (nnn) distances are considerably larger in the martensite than in β'. An evaluation of the order energy in the martensite with the assumption that higher than nn interactions can be neglected leads to a value approximately the same as the order energy in the β' phase. Thus the predicted change in order energy remains much smaller than the observed enthalpy change during the transformation. However, this is not to be taken to conclude that order is not important since strong evidence exists for a relationship between order and the transformation enthalpy [5,6].

In order to interpret the observed enthalpy difference between β' and martensite, it is therefore insufficient to assume that changes in order energy only due to first nearest neighbors in the martensite are significant. It is shown from theory as well as from experiment that the pair interaction energy is an oscillating function whose amplitude decreases relatively slowly with pair distance. Therefore higher neighbor interaction energies may contribute to the stability of the phases. Indeed in a detailed analysis of the enthalpy of transformation in CuZn it has been shown that fourth nearest neighbors in the martensite (corresponding to $\frac{a}{2}$ <112> in fcc) can satisfactorily account for the observed enthalpy differences [6].

Recently investigations of the ordered fcc phase which is induced by stressing a 3R martensitic single crystal has lent further support to this analysis [7]. The martensite has a lattice that is close to an orthorhombic ordered structure with the stacking sequence ABCBCACAB and which transforms on stressing to the fcc phase with stacking ABCABC without involving changes in the number of first neighbour pairs. It has been shown that indeed chemical interaction energies from higher than first and second neighbor pairs in the martensite are necessarily important and a numerical value of $m_{CuZn}^{(4)}$=-110K has been derived, compared to a first and second neighbour chemical energy in the β' phase

of $w_{CuZn}^{(1)}=955K$, $w_{CuZn}^{(2)}=535K$ [1] (in units of k, the Boltzmann constant, $m_{CuZn}^{(4)}$ the chemical interaction energy in the martensite and $w_{CuZn}^{(i)}$ that in the β' phase).

Using the three values $w_{CuZn}^{(1)}$, $w_{CuZn}^{(2)}$ and $m_{CuZn}^{(4)}$ a curve has been drawn as seen in the lower part of figure 1. The r/a_{fcc} is the pair distance normalised with respect to the fcc lattice parameter (considering the martensite as a faulted fcc lattice with the same atomic volume as in the β' phase). Consecutive r/a_{fcc} values for which the curve
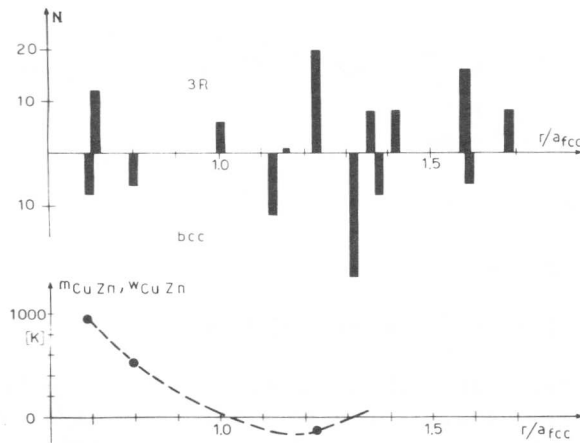
Fig.1.:Above:Number N of pairs versus pair distance r/a_{fcc} for 3R martensite (positive direction)and for bcc (negative direction) (a_{fcc} lattice parameter for fcc with the same atomic volume as 3R and bcc).Below:chemical pair interaction energies for β'(w_{CuZn}) and 3R (m_{CuZn})versus r/a_{fcc}.Circles denote measured values.

passes through zero can be obtained from the wavelength $\Delta r/a_{fcc}$ of the Friedel oscillations for free electrons which are supposed to be a good approximation for large r; Δr is given by $2k_F\Delta r=\pi$ [8]. In the upper part of the same curve are drawn the pair distances and their number in the 3R martensite (positive direction) and in the bcc lattice (negative direction). Comparing the pair positions with the continuous curve, which is thought to be qualititatively correct, some conclusions can be drawn concerning contributions of the different pairs to the enthalpies. In the β' phase first, second and third neighbors are expected to contribute to the stability, but not fourth neighbors, in spite of their large number, since $w_{CuZn}^{(4)}$ is close to zero. In the 3R lattice second neighbors do not contribute, since $m_{CuZn}^{(2)} \approx 0$. Fifth and higher order neighbors in β' and 3R contribute considerably less, because m_{CuZn} decreases according to Friedel as r^{-3}, apart from the oscillating factor. Also, $m_{CuZn}^{(3)} \approx m_{CuZn}^{(4)} \approx w_{CuZn}^{(3)}$ is approximately valid, and will be used (see also [7]). The chemical interaction energies for first neighbors which have nearly the same distance in β' and 3R will be set equal.

With these simplifications the change in order energy during the transformation has been calculated, and from the measured enthalpy change a value of $m_{CuZn}^{(4)}=-125$ [K] was deduced [6], that is in good agreement with $m_{CuZn}^{(4)} = -110$ K , which was derived from the stress induced transformation from 3R to fcc [7].

In order to show in more detail how the approximations enter into the calculated enthalpy differences, the relationship is written here, assuming that the β' phase has reached its maximum degree of order at the low transformation temperatures. As derived earlier [6]:

$$E^{\beta} - E^{M} = \Delta E_{Cu}^{\circ} C_{Cu} + \Delta E_{Zn}^{\circ} C_{Zn} + \Delta E_{CuZn}^{(1)} (C_{Cu} - C_{Zn}) C_{Zn} + \Delta E_{CuZn}^{(2)} C_{Zn}$$

with

$$\Delta E_{CuZn}^{(1)} = -3w_{CuZn}^{(2)} - 6w_{CuZn}^{(3)} + 2m_{CuZn}^{(1)} + 3m_{CuZn}^{(2)} + \frac{2}{3}m_{CuZn}^{(3)} + \frac{10}{3}m_{CuZn}^{(4)}$$

$$\Delta E_{CuZn}^{(2)} = -4w_{CuZn}^{(1)} + 4m_{CuZn}^{(1)} + \frac{20}{3}m_{CuZn}^{(4)}$$

using the approximation this reduces to

$$\Delta E^{(1)} = 2w_{CuZn}^{(1)} - 3w_{CuZn}^{(2)} = 305 \text{ K}$$

$$\Delta E^{(2)} = \frac{20}{3}m_{CuZn}^{(4)} = -730K \text{ (using } m_{CuZn}^{(4)} = -110 \text{ K from } [7])$$

In $\Delta E_{CuZn}^{(1)}$ all contributions from higher than second neighbors in bcc cancel within the approximations used. If the approximation $w_{CuZn}^{(3)} = m_{CuZn}^{(3)} = m_{CuZn}^{(4)}$ is not justified, one would expect in the extreme case an additional term of $6w_{CuZn}^{(3)}$, which however has little influence on $E^{\beta} - E^M$ since the $\Delta E_{CuZn}^{(2)}$ term has a larger value. In $\Delta E_{CuZn}^{(2)}$, apart from first neighbor contributions which cancel, only the fourth neighbor pairs appear. All contributions, which are independent of the chemical interaction energy terms enter through the terms ΔE_{Cu}° and ΔE_{Zn}°. If they were independent of composition they would represent the transformation enthalpies between the hypothetical β' and 3R for the pure metals.

Evaluating $E^{\beta} - E^M$ from the relationship $(E^{\beta} - E^M) = M_S \Delta S$, with $\Delta S = 0.15k$ [1] and M_S from [9] and taking $m_{CuZn}^{(4)} = -110$ [K] from [7], the ΔE_{Cu}° and ΔE_{Zn}° around $C_{Zn} = 0.4$ can be derived, in order to compare with theoretical estimates. In figure 2 are shown the $E^{\beta} - E^M$ estimated from M_S in the composition range $C_{Zn} = 0.378$ to 0.408. The upper curve presents the data for $\Delta E_{Cu}^{\circ} C_{Cu} + E_{Zn}^{\circ} C_{Zn}$ for the same composition range. Extrapolation to $C = 0$ gives $E_{Cu}^{\circ} = 380K$ and $E_{Zn}^{\circ} = 80K$. These values are to be compared with the theoretical estimates for Cu and Zn reported by Kaufman in their bcc, fcc and hex structures [10]. Considering the 3R martensite as a mixture of 2/3 hexagonal and 1/3 fcc according to [7], we deduce for Cu a $\Delta E_{Cu}^{\circ} = 373K$, and for Zn $\Delta E_{Zn}^{\circ} = 280$ according to the theoretical data of Kaufman. The ΔE_{Cu}° is in excellent agreement with our values, whereas the ΔE_{Zn}° differ considerably. This need not
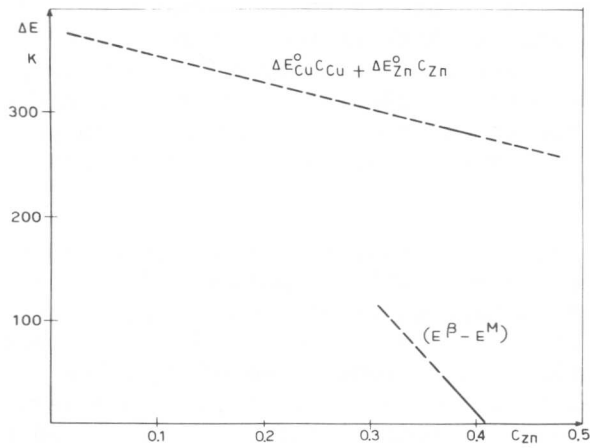
Fig.2:Upper curve:calcula-
ted configuration indepen-
dent enthalpy difference
$\Delta E^{\circ}_{Cu} C_{Cu} + \Delta E^{\circ}_{Zn} C_{Zn}$. Lower Curve:
measured enthalpy difference
$E^{\beta} - E^{M}$ between β' and marten-
site versus zinc concentra-
tion

be surprising since the hexagonal zinc has a different atomic volume
than that obtained from extrapolating of the β' phase, and also has a
non ideal axial ratio [11]. Furthermore a small uncertainty in $m^{(4)}_{CuZn}$
affects ΔE°_{Zn} much more strongly than it affects ΔE°_{Cu}. The good agree-
ment in ΔE°_{Cu} however is a further support to the vadility of the
approach described in this paper to determine the transformation enthal-
pies between β' and martensite in CuZn.

In an evaluation of the phase stability of β' and martensite a
discussion on the entropy change has to be included. Only a few remarks
will be made here, for lack of space and since a more complete discu-
ssion has been published elsewhere [6]. The entropy difference between
β' and martensite can be decomposed into: $S^{\beta'} - S^{M} = (S^{\beta'} - S^{\alpha}_{dis}) - (S^{M}_{dis} - S^{\alpha}_{dis}) -$
$- (S^{M} - S^{M}_{dis})$ where $(S^{\beta'} - S^{\alpha}_{dis})$ is the entropy difference between the or-
dered β phase and the disordered fcc α phase extrapolated from lower
zinc concentrations where α is stable, $S^{M}_{dis} - S^{\alpha}_{dis}$ the change when a
regular array of stacking faults on each third plane is introduced in
the disordered phase and $S^{M} - S^{M}_{dis}$ constitutes the influence of order
in the martensite. $(S^{M}_{dis} - S^{\alpha}_{dis})$ can be estimated from the temperature
dependence of the stacking fault energy in α phase CuZn alloys. In Cu-
30% Zn thin foils Gallagher [12] observed a decrease in dislocation node
radius with increasing temperature. If the temperature dependence is
due to an intrinsic variation of the stacking fault energy with tempe-
rature [13], then from the measured $d_{\gamma}/dT \approx 2.10^{-2} m$ J/m^{2}K a $S^{M}_{dis} - S^{\alpha}_{dis} =$
$= 3.10^{-2}$k is obtained for Cu-30 at% Zn. The contribution of $S^{M}_{ord} - S^{M}_{dis}$ has
been evaluated in [6] and is also found to be small, $S^{M} - S^{M}_{dis} \approx -2.10^{-2}$k
compared to the measured $(S^{\beta} - S^{M}) \equiv \Delta S = 15.5.10^{-2}$k [1]. The conclusion drawn
from these results is that order has a negligible influence on the
entropy in the martensite, in agreement with the observation that ΔS
is quite composition intensitive.

The entropy difference between β' and the martensite should be
approximately the same as that between the equilibrium phases β' and
(extrapolated) α. In order to check this,Debye temperatures from low
temperature specific heat measurements in α [14] and β' [15] have been

-275-

used to calculate the entropy change according to the Debye model. The resulting value of $\Delta S=0.36k$ is twice as high as the measured $\Delta S=0.155k$. The reason may be that Debye temperatures θ_D estimated from low temperature measurements are not adequate to calculate entropies at higher temperatures, especially since the difference in θ_D between both phases at 0.4 at % Zn amounts to only 35K. More experimental data are clearly needed.

In this paper it is shown, in conclusion, that long range order has a strong influence on the difference in stability between β' and martensite, mainly through interaction between fourth nearest neighbors. This order contribution is essentially responsable for the strong concentration dependence of the enthalpy difference (and of M_S). The entropy difference, on the other hand, depends very little on order, and is believed to be approximately the same as that between β' and the α phase which is stable at lower concentrations.

REFERENCES

[1]   W.Arneodo,M.Ahlers,Acta Met 22 (1974) 1475
[2]   H.Warlimont,L.Delaey,Progr.Mat.Sci. 18 (1974)
[3]   V.Heine,D.Weaire,Solid State Phys 24 (1970)
[4]   G.Inden,Z.Metallkde, 66 (1975) 648
[5]   M.Ahlers,Scripta Met 8 (1974) 213
[6]   M.Ahlers,Z.Metallkde (1979), to be published
[7]   G.Barcelo,M.Ahlers,R.Rapacioli,Z.Metallkde(1979) to be published
[8]   J.Friedel,Nuovo Cim (Suppl) 7 (1958) 287
[9]   H.Pops,Trans AIME 236 (1966) 1532
[10] L.Kaufman,Progr.Mat.Sci. 14 (1969) 57
[11] T.B.Massalski,H.W.King,J.Phys.Rad. 23 (1962) 607
[12] P.C.J.Gallagher,Met.Trans. 1 (1970) 2429
[13] L.Remy,A.Pineau,B.Thomas,Mat.Sci.Engg. 36 (1978) 47
[14] L.Isaacs,T.B.Massalski,Phys.Rev. 138A (1965) 134
[15] B.W.Veal,J.A.Rayne,Phys.Rev. 128 (1962) 551

The Stress Induced Transformation Between Orthorhombic and Face Centered Martensite in CuZn Alloys

M. Ahlers[*], G. Barceló[*] and R. Rapacioli[*]

Abstract: Single crystals of CuZnAl martensite transform to a fcc long range ordered phase at a critical stress τ_B which has been measured for two sets of ternary CuZnAl alloys, one of constant electron concentration e/a=1.48 but varying M_S temperatures and the other of a constant M_S=-50°C and varying e/a. It is shown that τ_B depends not only on e/a but also on order. The influence of order can be described by chemical interaction energies between fourth neighbors in the orthorhombic 3R lattice. The second contribution to τ_B is determined by the stacking fault energy (SFE) of the disordered α phase solid solution which is stable at lower e/a. The analysis shows that 3R martensite can be considered as a faulted fcc lattice, and that the regularity in the stacking fault array does not introduce a significant additional stability. It is concluded that the reason for the frequent formation of the 3R martensite during the transformation is not one of higher stability compared to other close packed structures, but that it must be related to the transformation mechanism which requires an undistorted habit plane.

The deformation behavior of martensitic CuZn single crystals depends on the orientation of the deformation axis with respect to the crystal lattice [1]. If the martensitic single crystal is obtained by stressing in tension a β'phase single crystal with orientation near $[100]_\beta$ above its spontaneous M_S temperature then by further tensioning it is possible to induce a new ordered face centered phase [1-3]. This phase forms by a shear on the $(001)_o$ plane in the $[100]_o$ direction of the orthorhombic 3R lattice (corresponding to a $\{1\bar{1}1\}_{fcc}$ $\langle 1\bar{1}2\rangle_{fcc}$ shear system in the disordered fcc lattice). The transformation can be described as a movement of partial dislocations on every third close packed plane, which during their movement eliminate stacking faults and thus produce a fcc lattice. This concept does not imply that the partials move independently of each other, since in the 3R martensite the faults constitute a structural element due to their regular array. This regularity can be responsible for an additional phase stabilisation, and the movement of partial dislocations can become highly correlated.

---

*Centro Atómico Bariloche,Comisión Nacional de Energía Atómica, (8400) S.C. de Bariloche - Argentina

For an evaluation of the martensitic structures it is important to know the stabilizing influence of the regular faulting: If, on one extreme, the lattice energy is proportional only to the stacking fault density and is not affected by the regularity of the faults then a structure with less faults or more faults compared to 3R would be more stable, depending on the sign of the stacking fault energy. Consequently it would not be possible to attribute the frequently observed 3R structure as due to a high phase stability. Instead it would be necessary to invoke some other factors connected with the mechanisms of the martensite transformations to explain their frequent occurrence [4]. Stability arguments, on the other hand are valid if the regularity in stacking sequence lowers the energy sufficiently. This question is considered in the present paper, on the basis of measurements [2] from which the stress τ_B is determined that is necessary to induce the fcc phase in the martensitic single crystals of CuZn and CuZnAl alloys. It will be shown in the analysis that in fact the occurrence of the 3R structure cannot be justified in terms of stability.

A second point of interest in the evaluation of the different martensitic structures is their relationship to the stable phases, i.e. to the ordered β' which is stable at higher temperatures, and to the disordered fcc α solid solution, which is stable at lower alloy concentrations. The stability of the martensite with respect to β' in CuZn and CuZnAl is given by the enthalpy and entropy of transformation, which have been measured [4-6], and analysed [7,8]. Of similar interest is the relationship between martensite and the α phase. Here the transformation can be formally considered to proceed in two steps, first by the transformation of the ordered to the disordered 3R and in a second step from the disordered 3R to the disordered fcc α phase solid solution. For both steps the enthalpy and entropy of transformation can be evaluated from the measured critical transformation stresses τ_B.

The experimental methods to deform the martensitic single crystals, and the results obtained for the relevant shear stresses are reported elsewhere [2]. Therefore the following remarks may suffice: The critical resolved shear stress τ_B at which fcc started to form, and the stress τ_{retr} at which fcc started to retransform to the 3R were determined for two sets of CuZnAl samples, one with constant electron concentration $e/a=1.48$ and varying M_S, the other with constant M_S temperature, $M_S \approx$ $\approx -50°C$, but of different e/a ratios. Some of the results are shown in figure 1 to 3. As seen in figure 1 τ_B is independent of deformation temperature for CuZn (data from ref 1), and feebly dependent on temperature for ternary alloy. This T dependence is sufficiently small compared to the composition dependence of τ_B and therefore is neglected in the evaluation of the enthalpies. In figure 2 is shown the dependence of τ_B on electron concentration e/a for the binary CuZn (inclined crosses) and for the ternary CuZnAl with a constant $M_S=-50°C$ (closed circles). Also shown is the retransformation stress (crosses) for some of the CuZnAl alloys. In figure 3 τ_B is plotted versus Al concentration at a constant $e/a=1.48$ for CuZnAl alloys in the composition range between 10 and 18 at % Al (the open circle is a point from a slightly different e/a, corrected by using figure 2).
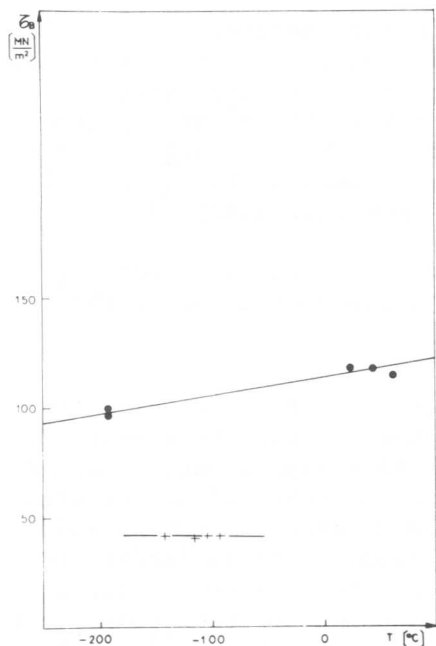
Fig.1: τ_B versus T
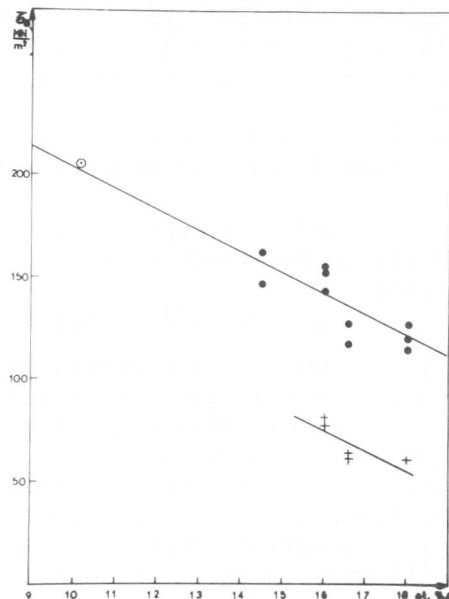for Cu-14.4 at% Zn-16.6 at% Al
(○) and Cu-39.6 at% Zn (+)
from ref.1.

Fig.2: τ_B(circles) and the
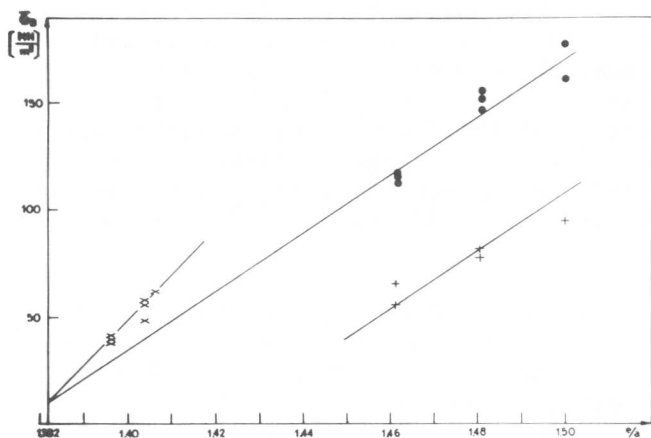retransformation stress (+)
versus C_{Al} for e/a=1.48.

Fig.3: τ_B and retransfor-
mation stress versus e/a
for CuZnAl with $M_S=-50°C$
(○and +) and for CuZn (x)
from ref.1.

Figures 2 and 3 show clearly that τ_B is not solely a function of
e/a, but that some other factor must be involved. It is known that in
many noble metal alloys in addition to electron concentration, short
and long range order plays an important role in phase stability. Order
generally is described in terms of chemical interaction energies
$m_{AB}^{(i)} \equiv -2M_{AB}^{(i)}+M_{AA}^{(i)}+M_{BB}^{(i)}$ between A-B atom pairs in i-th neighbor position.

-279-

(the $M_{AB}^{(i)}$, $M_{AA}^{(i)}$, $M_{BB}^{(i)}$ are the usual interaction energies between AB,AA and BB pairs). According to pseudopotential theory [9] for simple metals the $m_{AB}^{(i)}$ depend only on the pair distance but not on the lattice structure at constant volume. An explicit dependence of $m_{AB}^{(i)}$ on electron concentration may also be present according to Friedel [10]. On this basis the phase stabilities between β' and 3R martensites [7,8] and between 3R and fcc ordered martensite [2] have been analysed.

Using this approach it is assumed that the critical stress τ_B which is necessary to induce fcc can be written as the sum of three terms:

$$\tau_B = \tau_{fr} + \tau^{(1)}(e/a) + \tau^{(2)}(m_{AB}^{(i)})$$

τ_{fr} is the friction stress during the movement of the partials. Its upper limit is given by the difference between τ_B and the stress τ_{retr} for retransformation on unloading (which within experimental scatter is composition independent) that defines the hysteresis. If the friction stress is independent of the direction of dislocation movement and if an elastic stress field due to the dislocations develops during the transformation, then τ_{fr} is smaller than half the hysteresis stress. $\tau^{(1)}(e/a)$ is the contribution which is independent of the atomic configuration, and remains constant for constant e/a. Lastly $\tau^{(2)}(m_{AB}^{(i)})$, describes the influence of the order, and through $m_{AB}^{(i)}$ may also depend on electron concentration.

The stress τ which is necessary to move a partial dislocation $\tau = \tau_B - \tau_{fr}$ is related to the stacking fault energy (SFE) by $\tau b_p = \Gamma$, where b_p is the Burgers vector of the partial. The SFE corresponding to $\tau^{(2)}$ can be evaluated by counting the change in number of A-A, B-B and A-B bonds in i-th neighbor configuration per stacking fault and multiplying them with the corresponding pair interaction energies. During the transformation from 3R to ordered fcc by a shear on the $(001)_o [100]_o$ orthorhombic system, the number of first and second neighbors is not changed. The observation that τ_B is not solely a function of e/a implies therefore that third and higher neighbor pairs contribute to the SFE. The role of third and higher neighbor pair contributions to phase stability had already been deduced from the analysis of the transformation enthalpy between β' and 3R [8], and the present results confirm this.

For the numerical calculations the simplifying assumptions have been made that $m_{AB}^{(3)} = m_{AB}^{(4)}$, $m_{AB}^{(i)} = 0$ for i⩾5. The former is supported by the observation that DO$_3$ order does not shift τ_B compared to B2 order, since as seen in figure 2, the extrapolated τ_B at e/a=1.382 (i.e. M_S=-50°C) is the same for B2 (in CuZn) as for DO$_3$ (in CuZnAl). The DO$_3$ order manifests itself in the difference terms $m_{AB}^{(3)} - m_{AB}^{(4)}$, [2], which therefore must be small. Neglecting $m_{AB}^{(i)}$ for i⩾5 can be justified, since apart from an oscillating factor the $m_{AB}^{(i)}$ decreases in an inverse proportion of the third power in pair distance (see also figure 1 of ref 7, this conference). The only unknown factors that enter in $\tau_{AB}^{(2)}$ therefore are the $m_{AB}^{(4)}$. The lattice occupation probabilities are known from the β' phase, since the martensitic transformation is diffusionless one. Of the three chemical interaction energies in the CuZnAl

ternary system $m_{AlZn}^{(4)} \approx 0$, since also $m_{AlZn}^{(1)}$ and $m_{AlZn}^{(2)}$ are small [11], and $m_{CuAl}^{(4)} = fm_{CuZn}^{(4)}$, where the proportionality factor f=1.375 has been derived from the concentration dependence of M_S in the ternary system (2). The only parameter that remains unknown in (2) thus is $m_{CuZn}^{(4)}$, which can be calculated from the slope of the line in figure 3 for e/a=1.48, and from the curves in figure 2 for e/a=1.40, resulting in $m_{CuZn}^{(4)}$=-260 K for e/a=1.48 and $m_{CuZn}^{(4)}$=-110 K for e/a=1.40 ($m_{CuZn}^{(4)}$ in units of the Boltzmann constant, and with dimension degree Kelvin). It is apparent that $m_{CuZn}^{(4)}$ depends on electron concentration, which however has not yet been studied. Furthermore the value for e/a=1.40 agrees closely with that obtained from the transformation enthalpy between β' and 3R [8], $m_{CuZn}^{(4)}$=-125 K.

Let us now restrict our attention to the binary CuZn alloys with e/a around 1.40, and let us analyse the enthalpy of transformation from the ordered to the disordered 3R structure, and from the disordered 3R to the fcc phase: The transformation enthalpy (or its value per stacking fault, i.e. the SFE) for the order-disorder transformation in the 3R lattice is calculated with the known $m_{CuZn}^{(4)}$=-110k. By subtracting the order contribution from the total SFE, the SFE of the stacking faults in the disordered 3R are obtained. These SFE can then be compared with the values that have been obtained for SFE in α phase CuZn solid solution from transmission electron microscopy studies. Both values should differ if the regular stacking fault sequence in 3R presents an additional stabilising factor. In figure 4 are shown the results.
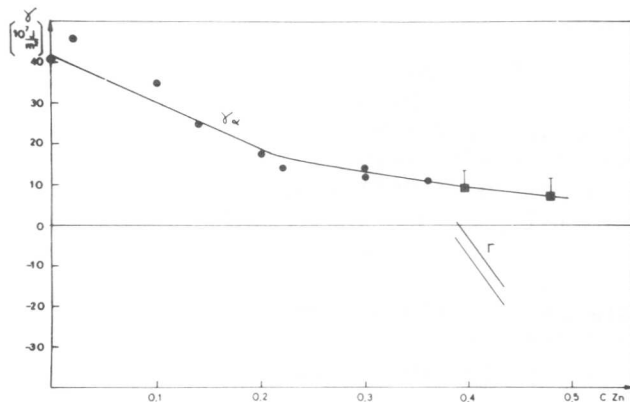

Fig.4: SFE γ versus C_{Zn} for α phase CuZn(○), for ordered 3R martensite (Γ) and the calculated values for disordered 3R(T).

Γ denotes the SFE of the ordered 3R, with the two lines denoting the upper and the lower limits, corresponding to a friction stress of one half the hysteresis stress and to a zero friction stress, respectively. The SFE contribution in the disordered 3R is marked by a filled square at e/a=1.40, with the error bar covering the uncertainty due to the friction stress. Filled circles denote stacking fault energy values for the α phase, and the continuous line is the best fit to it [7,8], which, as can be seen, passes through the filled square. The second

-281-

square at e/a=1.48 has been obtained from extrapolating the curve of figure 3 to zero Al-concentration. The SFE for the disordered 3R agrees closely with those extrapolated from the α phase, which implies that the regularity of the stacking order in 3R, has only a small effect on the phase stability, if it has any. Consequently, the ordered 3R martensite can be considered simply as a face centered α phase with stacking faults of density 1/3 in it and whose energy Γ is determined by the α phase value γ and by $m_{CuZn}^{(4)}$. Both γ and the order contribution per stacking fault are independent of the stacking fault density [2] and thus by adding stacking faults to the 3R structure, a more stable phase can be obtained, which implies that 3R is not the most stable phase formed during the martensitic transformation, and therefore its frequent formation must be due to constraints during the transformation mechanisms [4].

In summary then, two conclusions can be drawn from the measurement of the critical transformation stress from 3R martensite to fcc: (a) The relationship between the ordered 3R martensite and the disordered α phase which is stable at lower zinc concentrations is determined by the α phase stacking fault energy and the chemical interaction energy $m_{CuZn}^{(4)}$ between fourth (which are equal to third) neighbor pairs. (b) The 3R martensite does not form for stability reasons, during the martensitic transformation, but is related constraints during the transformation mechanism [4].

References

[1] W.Arneodo,M.Ahlers,Scripta Met. 7 (1973) 1287
[2] G.Barceló,M.Ahlers,R.Rapacioli,to be published
[3] E.Hornbogen,G.Wassermann,Z.Metallkde 7 (1957) 379
[4] W.Arneodo,M.Ahlers,Acta Met. 22 (1974) 1475
[5] H.Pops,T.B.Massalski,Trans AI E 230 (1964) 1662
[6] H.Pops,N.Ridley,Met.Trans 1 (1970) 2653
[7] M.Ahlers, this conference
[8] M.Ahlers,Z.Metallkde, to be published
[9] V.Heine,D.Weaire,Solid State Phys 24 (1970) 249
[10] J.Friedel,N.Cim. (Suppl) 7 (1958) 287
[11] R.Rapacioli,M.Ahlers,Scripta Met. 11 (1977) 1147.

A Thermodynamic Analysis of the Stress-Induced Martensitic Transformation : The Clapeyron-like equation and Efficiency of the SME-Engines

P. Wollants, M. De Bonte, L. Delaey and J.R. Roos

A rigourous thermodynamic analysis of the stress-induced martensitic transformation shows that the latent heat of transformation accompanying the stress-induced transformation (at $T_o(\sigma)$) is not equal to the latent heat of the stress-free transformation (at $T_o(o)$). The difference between these latent heats is the work performed by displacing the external load during the reverse transformation. At the same time the relationship between transformation temperature and applied stress (the modified Clausius-Clapeyron relationship) is calculated. Based on this analysis a correct formula for the theoretical attainable efficiency "η" of a given work performing cycle is deduced. This cycle is represented in a TS-diagram. Assuming some justified approximations both the efficiency formula and the TS-diagram are converted into a convenient form. Using experimental data for a CuZnAl alloy efficiency and output power are estimated. The results are compared with those published by other authors. It appears that many efficiency values reported in the literature are highly overestimated due to the selection of wrong thermodynamic data and to the violation of some basic thermodynamic principles.

I Thermodynamics of the Stress-induced Martensitic Transformations

A rigourous thermodynamical treatment of the stress-induced martensitic transformation in a single crystal has been published by P.Wollants et al. [1]. The results of this analysis are very important for any calculation concerning efficiency or power capacity of a solid state engine. Therefore the most important conclusions of this analysis will be summarized in this paper.

(1) Basic relations

Based on the first and the second law of thermodynamics the following important state functions are defined for the crystal under stress :

$$H^* = U + PV - FL \qquad (1)$$

$$G^* = H^* - TS \qquad (2)$$

G^* is the characteristic function and it can easily be shown that the fundamental equation for the stressed crystal is written as :

$$dG^* = VdP - LdF - SdT \qquad (3)$$

Departement Metaalkunde, Katholieke Universiteit Leuven, Belgium

and consequently

$$\left(\frac{\partial G^*}{\partial T}\right)_{P,F} = -S \qquad (4) \qquad\qquad \left(\frac{\partial G^*}{\partial F}\right)_{P,T} = -L \qquad (4)'$$

From the fundamental equation (3) we obtain the condition for thermodynamic equilibrium :

$$dG^*_{T,P,F} = o \qquad (5)$$

(2) The relation between work and heat

For an isobaric change of state of a stress-free crystal, the heat exchange $\Delta Q(o)$ equals the enthalpy change ΔH; and in the same way for an isoforce-isobaric change of state of a crystal under stress the heat exchange $\Delta Q(F)$ equals ΔH^* (the change of the state function H^*)

$$\Delta H^* = \Delta Q(F) \qquad (6)$$

Between ΔH and ΔH^* there exists the relation

$$\Delta H^* = \Delta H - F \, \Delta L \qquad (7)$$

which explains the work performing capacity associated with the martensitic transformation in a crystal under stressed conditions.

(3) The Clausius-Clapeyron-like relation

From the equilibrium criterium (5) the most important Clausius-Clapeyron-like relation can be deduced :

$$\frac{dF}{dT} = -\frac{\Delta H^*}{To(F).\Delta L} \qquad (8)$$

which relates the values of F and T at thermodynamic equilibrium between a martensitic and a parent phase. In fig. (2) the Clapeyron-like relation is illustrated schematically, approaching the G^*-T curves by straight lines.

Let us assume that we have at our disposal a rod shaped single crystal showing the shape memory effects, and trained under compression and tension, such that the shorter shape can be associated with the martensitic phase and the longer one with the parent phase. The thermodynamic cycle is presented in Fig. (3) in a TS-diagram.

In "state 1" the crystal is stress-free at a temperature $M_f(o)$, which is the temperature at which the P→M transformation of the unstressed crystal is completed. At this temperature the crystal is reversibly stressed until a compressive stress level σ is reached. This is "state 2" of the crystal. From the temperature $M_f(o)$ the crystal is now reversibly heated at constant external stress until at the temperature $A_s(\sigma)$ "state 3" is reached. $A_s(\sigma)$ is the temperature at which

the M→P transformation starts when the crystal is under stress σ. The transformation is completed at $A_f(\sigma)$, reaching "state 4". Next the crystal is reversibly unloaded at constant temperature and so "state 5" is realised. The stress-free crystal is then cooled reversibly from $A_f(\sigma)$ to $M_s(o)$ ("state 6"), and finally at the temperature $M_s(o)$ the stress-free P→M transformation starts, and is completed at $M_f(o)$. The crystal is now back in its initial "state 1". The cycle is closed and may be repeated.

II Calculation of the Characteristics of the Work Performing Cycle of a CuZnAl-single Crystal

For a CuZnAl-single crystal the cycle described above can be simplified substantially, taking into account some justified approximations. For a single crystal in which only one martensitic variant is stress-induced, $M_f(o)$ and $M_s(o)$ are nearly identical. The same holds for $A_s(o)$ and $A_f(o)$. This is confirmed by experiments of Salzbrenner and Cohen [4] on a CuAlNi-single crystal and by tensile tests of Van Humbeeck [5] on a Cu -25,33 at % Zn - 9,11 at % Al-single crystal. Since the hysteresis between A_s and M_s is also very small it is justified in this case to describe the martensitic transformation by the chemical equilibrium temperatures $T_o(o)$ and $T_o(\sigma)$ alone. Further, concerning the closed cycle, there is no netto work performance due to the elastic loading and unloading of the crystal. The entropy effects involved with elastic loading and unloading of the crystal are also negligibly small [3].

Based on this "simplified thermodynamic cycle" and on formulae (6) and (9) we arrive at the following expression for the efficiency of the cycle :

$$\eta = \frac{\Delta H_{T_o(o)} \cdot \Delta T_o}{T_o(o) \left[\overline{C}p \cdot \Delta T_o + \Delta H^*_{T_o(\sigma)} \right]} \times 100 \qquad (9)$$

With $T_o(o) = 206K$, $\Delta H_{T_o(o)}$ as calculated from the Clapeyron relation $= 289$ J.mole^{-1}, $\frac{d\sigma_s}{dT}^{P \to M} = 2,5$ MPa . K^{-1}, $\rho = 7,007$ kg . dm^{-3} and $\varepsilon_{tr} = 0,065$ %, we have calculated work, power and efficiency of the work performing cycle. Efficiencies have also been calculated for $T_o(o)$ values of 100, 300 and 400K (for the lower values corrections for Cp have been made). The results are summarized in Figs. 4 and 5. The TS-diagram of this cycle is presented in Fig. 6.

Based on formula (9) and Fig. 5 we conclude that the theoretical maximum efficiency of this work performing cycle of this CuZnAl-single crystal with the low temperature reservoir at about room temperature is 2,5 ... 3%.

III Discussion and Conclusions

Many authors [6] and [15] have reported different efficiency values, some of them as high as 20%. A thorough thermodynamic investigation of

their results [3] revealed:
- that ΔH has always been used instead of ΔH^*,
- that many times uncorrect thermodynamic data have been selected,
- and that sometimes basic thermodynamic principles have been violated.

Recalculation of their results proved that for the low temperature heat reservoir at about room temperature efficiencies higher than 3 ... 5% are never obtained [3]. Therefore we may conclude that theoretical efficiencies of the SME-engine are restricted to maximum values of 2 ... 5%, depending on the type of alloy used. For $T_o(o)$ values larger than 50K the influence of ΔT_o on the efficiency becomes negligibly small, as can be seen from Fig. 5. The main reasons herefore are the heat losses due to the warming up and cooling down of the working material. Power generation however increases linearly with ΔT_o, as can be seen from Fig. 4. For $\Delta T_o = $ 50K and for a rotation speed of 1 cycle sec^{-1} a theoretical power generation of about 1 kW kg^{-1} is calculated. Reported values of true existing machines however are much lower. (only a few watts per kg for very small rotating engines).

We think that if one wants to use the concept of a solid state engine for direct conversion of heat into mechanical energy, values of at least 1 kW kg^{-1} should be realised. Today this seems not possible. Therefore direct applications of these remarkable memory materials could rather be found there where power generation is not the principal aim. One might think of special devices such as regulation devices, tube fittings where a small but controllable work output is needed or generation of T-controlled stresses is required.

REFERENCES

[1] P. Wollants, M. De Bonte and J.R. Roos : Zeitschr. Metallkde, 70 (1979), 113.
[2] P. Wollants, M. De Bonte, L. Delaey and J.R. Roos : Zeitschr. Metallkde, to be published April 1979.
[3] P. Wollants, M. De Bonte, L. Delaey and J.R. Roos : Zeitschr. Metallkde, to be published May 1979.
[4] R.J. Salzbrenner and M. Cohen : submitted to Acta Met.
[5] J. Van Humbeeck, L. Delaey and A. Deruyttere : Zeitschr. Metallkde, 69 (1978), 575.
[6] H.C. Tong and C.M. Wayman : Met. Trans., 6A (1975), 29.
[7] M. Ahlers : Scripta Met., 9 (1975), 71.
[8] C.M. Wayman and H.C. Tong : Scripta Met., 9 (1975), 757.
[9] L. Delaey and G. Delepeleire : Scripta Met., 10 (1976), 959.
[10] H.C. Tong and C.M. Wayman : Scripta Met., 10 (1976), 1129.
[11] A.D. Johnson : IECEC '75 Record, 759082.
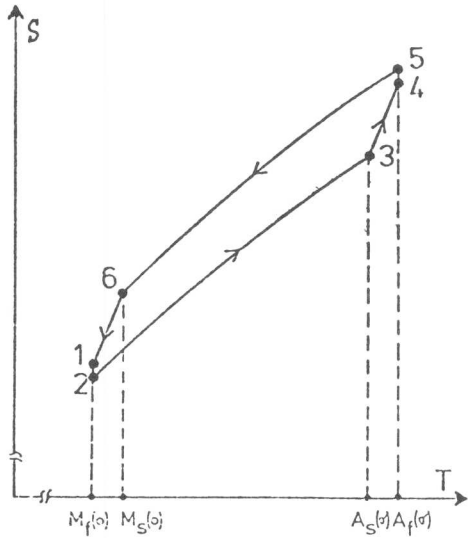[12] B. Cunningham and K.H.G. Ashbee : Acta Met., 25 (1977), 1315.

[13] A.A. Golestaneh : J. Appl. Phys., 49,(3), (1978).

[14] R.D. Kopa : Presented at the American Section of the International Solar Energy Society, Inc., Aug. 28-29, 1978, Denver, Co.

[15] J.S. Cory and J.L. McNichols : IECEC '78 Record.

[16] F. Baumgart, J. Jorde and H.G. Reiss : Techn. Mitt. Krupp, 34 (1976), 1.

Fig. 1 Schematic representation of the partial derivatives of the characteristic function G^*

Fig. 2 Three-dimensional schematic representation of the Clapeyron-like relation : $dF/dT = - (\Delta S/\Delta L)^{P \to M}$

Fig. 3 Schematic representation in a TS-diagram of the work performing cycle of a single crystal
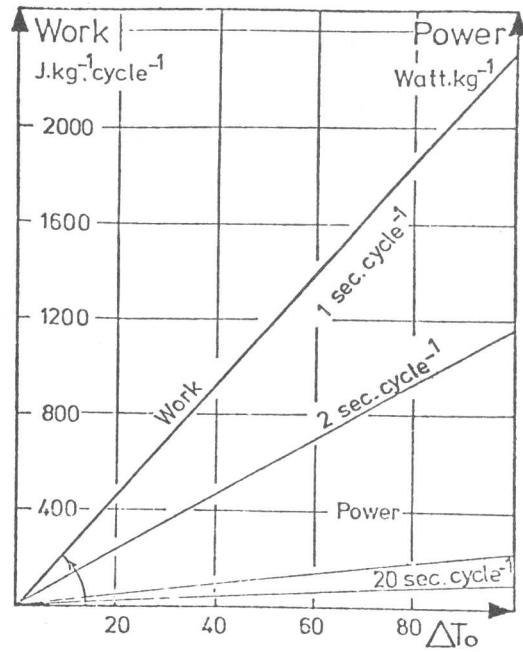
Fig. 4 Work per cycle and power of the CuZnAl-single crystal as a function of ΔT_o ($T_o(o) = 206K$)
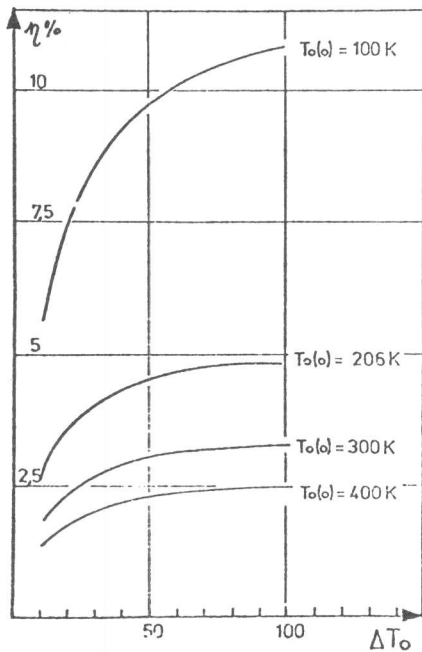
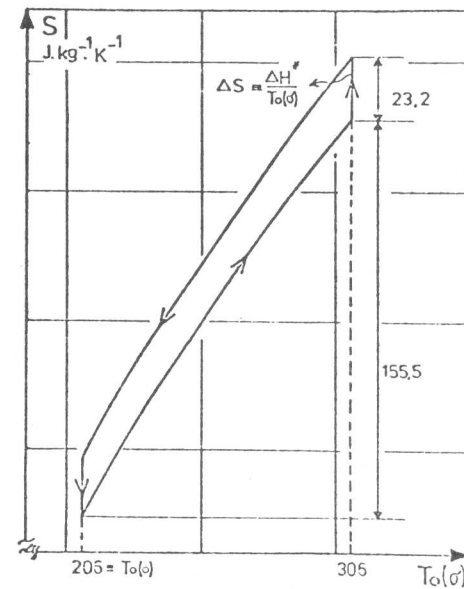Fig. 5 Efficiency vs. ΔT_o diagram for $T_o(o)$ temperatures of 100, 206, 300 and 400K

Fig. 6 Simplified quantitative TS-diagram for the work performing cycle as described in this paper

Kinetics and Thermodynamics of the Shape Memory Effect in NiTi and $(Ni_{1-x}Cu_x)Ti$ Alloys

O. Mercier   and   K.N. Melton

By rapid pulse heating of NiTi based shape memory wires, the details of the recovery process have been studied, i.e. the enthalpy of transformation was measured and the resistance change, resulting from motion arising from the shape memory effect with or without applied load was recorded on an oscilloscope. For different loads, the thermodynamic data associated with the transformation were measured as a function of copper. The enthalpy of transformation decreases in two stages, one between 0 and 5% and the other between 10 and 15% copper; whereas the transformation temperatures stay about constant.

Without the load, the reverse phase transformation is measured to occur within 3 ms, and motion under load is shown to be largely governed by the mechanical time needed to move the weight. An equation relating the speed of transformation to the thermodynamic data is proposed.

I. Introduction

It is known that a shape memory (SM) effect can be obtained in alloys showing a thermoelastic martensitic phase transformation. There are however no published experimental data for the thermodynamics and kinetics of a specimen undergoing the SM effect. In the present paper, measurements of the enthalpy and speed of transformation are reported for binary NiTi and the NiCuTi system [1] in which SM wires were rapidly heated, both with and without an applied opposing stress.

II. Experimental

The rapid heating technique developed by Parker [2] was used since it enables simultaneous measurement of both the enthalpy and speed of transformation. The method consists of pulse-heating a wire specimen and then measuring the electrical resistance change and temperature rise in the wire, see Fig. 1. Temperature measurements were made using thin nickel/nickel chromium thermocouple wires spot welded to the centre of the wire specimen with the points of contact a few millimetres apart. This intrinsic arrangement gives a faster response to temperature change than a bead thermocouple spot welded to the wire. Resistance was measured by monitoring the voltage drop across two Ni wires spot welded near the top and bottom of the specimen. Both resistance and temperature signals were

---

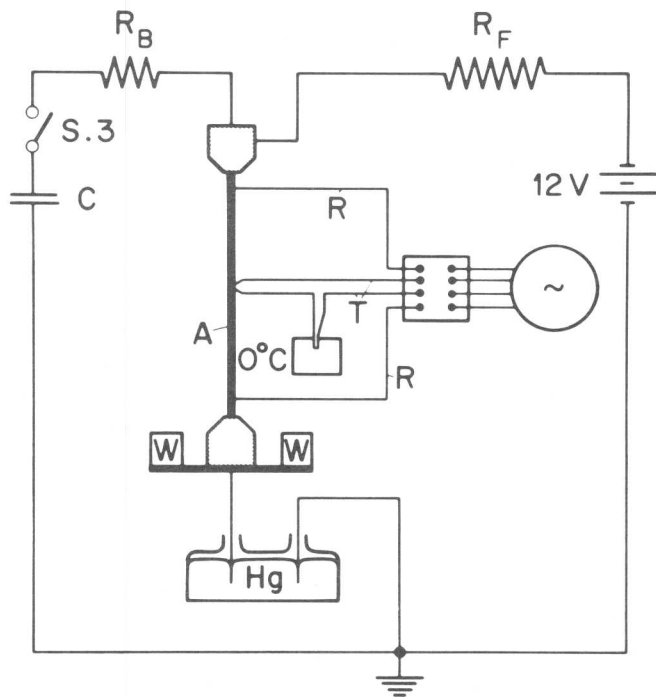Brown Boveri Research Center, CH-5401 Baden, Switzerland

Fig. 1: Schematic diagram of the rapid heating apparatus. A is the wire specimen, R the resistance measurement wires, T the temperature measurement wires, C the capacitor bank, S.3 the rapid switch, R_B and R_F resistances, W the weight hung on the specimen.
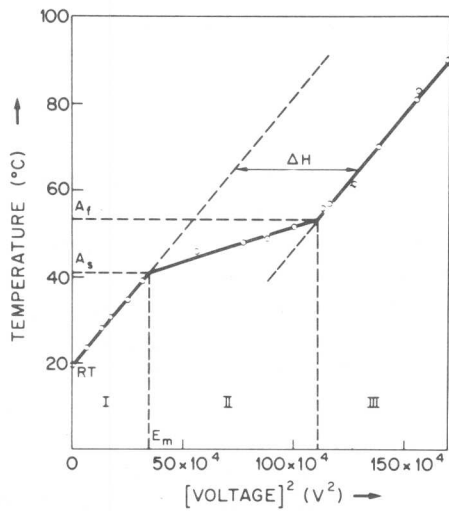

Fig. 2: Example of maximum heating temperature as a function of the square of the capacitor bank voltage, measured on the wire 5.
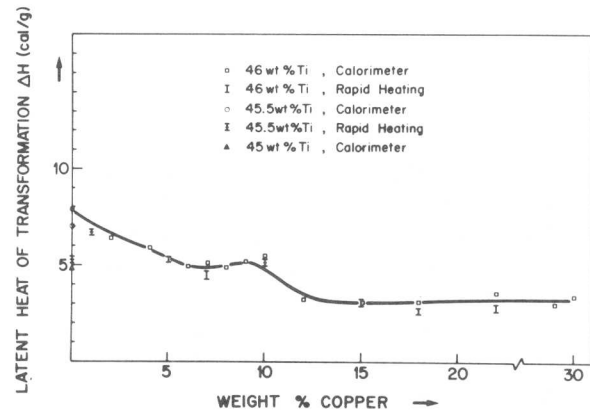

Fig. 3: Latent heat of transformation as a function of copper content for $(Ni_{1-x}Cu_x)_{1-\varepsilon}Ti_{1+\varepsilon}$ alloys.

recorded on a storage oscilloscope.

Measurements were made on a number of binary NiTi and ternary NiCuTi alloys with Ti contents between 45 and 46 wt% and Cu contents of up to 22 wt%. Material preparation has been described previously [3]. Wires of diameters between 0.39 mm and 0.85 mm were cold swaged with intermediate anneals from hot swaged 3 mm rod.

III. Results and Discussion

(1) Thermodynamics

By heating the wire to increasing temperatures using pulses of increased voltage with constant capacitance, the temperature increase can be plotted as a function of the Joule energy deposited in the specimen, energy which is proportional to the square of the pulse voltage. A typical result is shown in Fig. 2. In region I of the figure, an almost straight line is observed which corresponds to heating of the specimen in its martensitic phase. The slope of the line is given by the inverse of the heat capacity. During the phase transformation a change in slope is observed, corresponding to the supplementary energy needed to be supplied for the endothermic transition, region II. Then in region III, a line of almost identical slope to that in region I is found, corresponding to the heating of the wire in its high temperature β phase. Provided the Joule energy deposited in the wire can be calculated exactly, a value for the enthalpy of transformation can be obtained by measuring the distance between the lines of region I and III. Unfortunately, it was found that values obtained for binary NiTi were approximately 30% too high. This means that the power loss in the cables, connectors etc. of the circuit is not negligible. A possible solution is then to calibrate the energy scale from the known heat capacity of the β phase. The remaining problem is then that the martensite to austenite transformation does not begin and end abruptly which makes difficult the precise determination of A_f, the finish of the reverse transformation, to be sure to be in the β phase. Nevertheless it was found that a satisfactory solution was to take values at high enough temperatures, and the results were confirmed using standard measurements of heat capacity and enthalpy obtained from a conventional calorimeter. The heat capacity and enthalpy measurements were made on a series of alloys with Ti content between 45 and 46 wt% and Cu content between 0 and 30%. Within the range of experimental error, calorimetric measurements showed no variation of the heat capacity of the alloys as a function of either titanium or copper content and a value for Cp between 293 K and 393 K of 0.112 $\pm$ 0.005 cal/g.K was obtained for both phases. Measurements of the enthalpy of transformation obtained both from pulse heating and from calorimetry are shown in Fig. 3, where it can be seen that good agreement is obtained between the two techniques. The values obtained for binary NiTi vary from 4.8 cal/g for the 45 wt% Ti alloy to 7.9 cal/g for that with 46 wt%. This shows the strong dependence of ΔH on Ti content and can explain some of the difference previously reported. (for a review of the calorimetric data on NiTi see ref.4) The present results are in good agreement with the higher values previously measured.

As can clearly be seen in Fig.3, the effect of increasing copper additions, maintaining a constant titanium content, is to decrease ΔH. A first plateau is obtained between 7 and 10 wt% Cu, with a value of 5 cal/g, and a second plateau for copper contents between 15 and 30 wt%, ΔH~ 3 cal/g.

Within the range of experimental errors, no differences in ΔH were observed when wires of a given composition showed a one- or two way SM effect of ca. 1 % or when the SM effect involved lifting an applied weight.

(2) Kinetics

It is known that the martensitic phase transformation in NiTi [5] and $(Ni_{1-x}Cu_x)Ti$ [1,6] is associated with a relatively large change in electrical resistivity and its measurement on pulse heating enables the start and finish of the transformation to be measured.

It was found that on heating wires with no applied weight, the resistance corresponding to the high temperature phase had already been reached after 3 ms. The variation of resistance within the initial 3 ms was not possible to measure because of the recovery time of the oscilloscope amplifier after the effects of the heating pulse. A lower limit for the speed of transformation can thus be put at 3 ms (Fig. 4).

For wires displaying the one- or two-way SM effect with a weight hung on them, an interesting effect is observed when the wire is heated into or above the transition range (Fig.5). The resistance of the wire does not reach directly a constant value but shows damped oscillations. These oscillations can be characterised by a period τ and an attenuation δ (defined as the logarithmic ratio of 2 successive amplitudes) which can be considered as characteristic of the motion. Small temperature oscillations antiphase to those of resistance were also observed.

The oscillations were observed on all the specimens stressed by a weight, the composition of the alloys used and the dimensions of the wires are shown in Table I. The wires 1, 3 and 4 had a one-way effect of about 1%, whereas the wire 2 had been predeformed 10% in tension to produce a two-way effect of about 1%. From the equation

$$K' = ml/S \times (2\pi/\tau)^2 \qquad (1)$$

where m is the mass hung on the wire of length l and cross section S, a spring constant K' can be calculated, normalised to obtain a parameter independant of the geometry of the specimen. The result is shown in Fig. 6. as a function of temperature T* for different specimens. T* is the temperature obtained in supposing that no transformation has taken place, i.e. in extrapolating the temperature vs V^2 curve of the martensite phase to higher temperatures, and reading T* from the input energy V^2. Fig. 7 shows the variation of the logarithmic decrement δ as a function of temperature T (measured on the specimen) for wires 1 and 3 and as a function of stress for wire 4. Due to the limited number of measu-
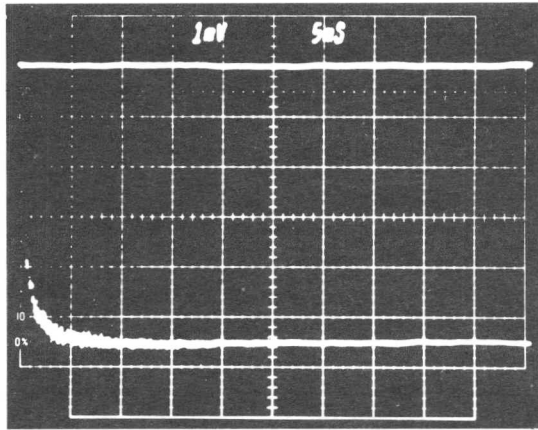
Fig. 4: Resistance measurement (vertical, 1mV/div.) as a function of time (5ms./div.).The upper curve was measured before heating and the lower curve afterwards (wire 5).
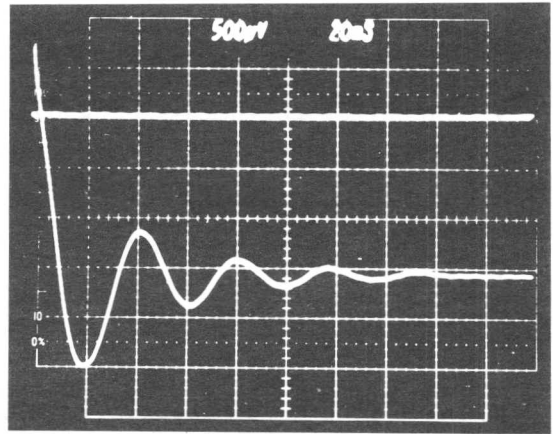

Fig. 5: Resistance measurement (vertical, 500µV/div.) before (upper curve) and after heating (lower curve) as a function of time (horizontal, 20ms./div.). The wire (no. 4 of Table I) was loaded with a 1.91 kg weight.
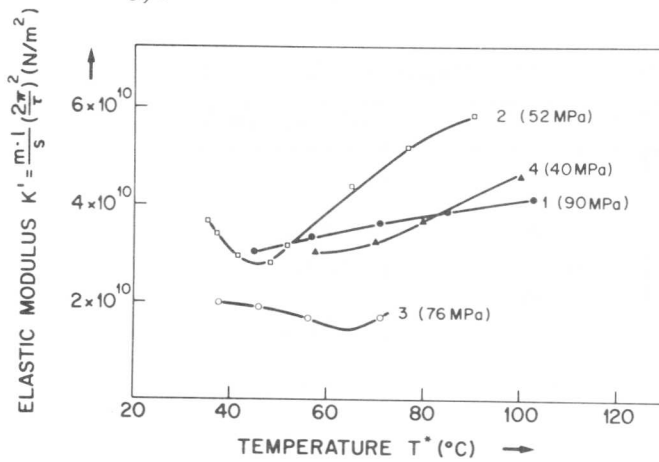

Fig. 6: Elastic modulus K', calculated from the experimental values of the period τ of the oscillations as a function of the theoretical temperature T* (see text) (wires 1 to 4 of Table I).

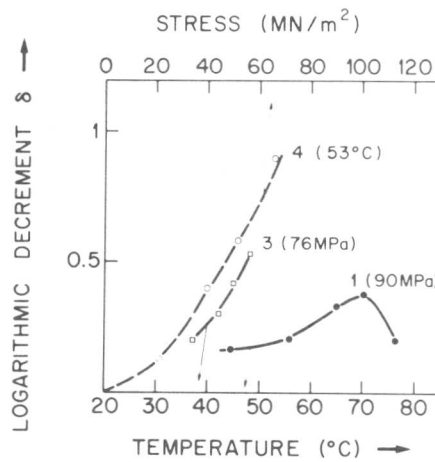Fig. 7: Experimental logarithmic decrement δ as a function of temperature T* (wires 1 and 3) and as a function of applied external stress (wire 4).

-293-

rements, general conclusions cannot be made. However it seems that the alloy composition or type of SM effect (one way or two way) does not affect K', whereas there is a tendency for increasing the Cu content of the alloy to increase the damping. Also the high value of δ is in agreement with the usual damping value observed during the phase transformation.

Further details of this model will be published elsewhere.

References

[1] O. Mercier and K.N. Melton: Met. Trans. in press.
[2] R. Parker, Trans: AIME 233 (1965), 1545.
[3] K.N. Melton and O. Mercier: Acta Met 27 (1979), 137.
[4] C.M. Jackson, H.J. Wagner and R.J. Wasilewski: NASA report SP 5110, (1972).
[5] J.H. Hanlon, S.R. Butler and R.J. Wasilewski: Trans. AIME 239 (1967), 1323.
[6] K.N. Melton and O. Mercier: Scripta Met. 12 (1978), 5.

Table I: The composition, diameter and length of the 5 wires

Wire No	Composition (wt%)			Diameter (mm)	Length (mm)
	Ni	Ti	Cu		
1	54.5	45.5	0	0.38	78.2
2	50	45	5	0.5	120.5
3	49	46	5	0.46	70.7
4	39	46	15	0.60	132.1
5	45.5	45.5	10	0.59	115.0

The High Pressure Induced Omega Phase Transformation in Ti-Mo and Ti-V Alloys

Ch. Leibovitch, A. Rabinkin and M. Talianker

The crystal structure obtained as a result of high pressure soaking (hps) at 300K of quenched alloys were studied by X-ray analysis and electron microscopy. The choice of the alloys' concentration was done in such a way that all the main as-quenched structures in Ti alloys, i.e. α', $\alpha'+\omega+\beta$, and β could be investigated. It was observed that after hps up to $P > P_S$ ω phase appears or its quantity increases in all these crystal structures (here P_S is the critical pressure of either starting or further promoting of the transition to ω phase). This process was never completed after the application of hps 9.5 GPa (95 kbar) even when ω phase was present in its initial state. The values of critical pressure of phase equilibria P_O at 300K were calculated using regular solution approach and Kaufman semiempirical parameters [1] and compared with the P_S experimentally observed. The details of structure reconstruction process and the influence of solute content on it were presented. In addition, the comparison with ω phase structure, obtained by aging of the same as-quenched samples are done. The analysis of relative stability of various structure regarding to hps is performed using detailed data on basic physical properties: Debye temperature θ_D, temperature of superconductive transition T_c, density of electronic states on Fermi level $n(E_F)$.

I. Introduction

The present study has the following goals. First, to establish the kind of structure changes induced by the high pressure soaking (hps) in Ti-based alloys with different initial crystal structures. Second, to compare the influence of high pressure and alloying on the stability of various phases. Third, to try to explain the observed regularity using data on basis physical properties: Debye temperature θ_D, Fermi density of stated $n(E_F)$, etc. The Ti-V and Ti-Mo systems were chosen for the following reasons: 1) In both systems, upon quenching from the β (bcc) field, a sequence of metastable phases easily appears: martensitic hcp α', $\alpha'+\alpha''$ orthorhombic, α' + hexagonal ω phase, $\beta + \omega$ and pure β. The appearance of any particular structures depends on Mo or V content. 2) V and Mo represent opposite examples of solute elements. V is next to Ti: therefore the "rigid band" model of electronic structure can be successfully applied to Ti-V alloys. While Mo is located far away from Ti in the Periodic Table, and the model is not applicable in this case. 3) In alloys of both elements hps would result in substantial changes in crystal structures, the extent to which would depend on the solute atom's nature and its concentration.

II. Experimental Procedure

15 alloys Ti containing up to 35 at.% Mo and 20 at.% V were heated at 1350 K and quenched to 300 K. After quenching the samples were subjected

Department of Materials Engineering, Technion, Israel Institute of Technology, Haifa, Israel.

to hps at 300 K using a single stage apparatus with a solid-medium cell insuring minimal deviation (1-2%) from uniformity. The disk-shaped samples were soaked during several hours and then subjected to structure analysis : X-ray diffractography and transition electron microscopy. The volume fractions of the phases were determined from the relative intensities of α, β and ω reflections. In some cases also resistivity changes under pressure were traced.

Results and Short Discussion

In alloys with α' + α'' structure in as-quenched state (fig.1a) the first very small particles of the ω phase together with a high density dislocation network are observed in α'-martensite plates after hps 7.5 GPa (Ti-3% Mo). A moderate but definite change in the resistivity of this specimen takes place at $P \simeq 7.0$ GPa that can certainly be attributed to the start of ω phase appearance. After hps 9.2 GPa its quantity increases as ensured from X-ray analysis and its volume fraction approaches 0.23. The contrast of the ω particles appears only under certain diffraction conditions and their morphology is difficult to distinguish (fig.1b). In alloys with (α') + β + ω structure (fig.2a), the quantity of α' and ω phases increases upon hps (fig.2b). One can see the large α'-plates containing the ω + β mixture as a result of possible partial reverse transformation $\alpha' \rightarrow \omega + \beta$ during unloading of the specimens. A diffuse scattering effect appears on the diffraction patterns as two long side streaks. The orientation relationships between phases are as follows: $(110)_\beta || (0001)_{\alpha'}$, $[\bar{1}11]_\beta || [11\bar{2}1]_{\alpha'}$ and $(11\bar{2}0)_\omega || (110)_\beta$, $[0001]_\omega || [111]_\beta$. In contrast with hps, annealing results only increase the ω phase amount at the expense of the β phase. The size and morphology of the ω phase in both structures are very different (compare figs.2b and 2c). In alloys with higher content of the alloying element having the $\beta + \omega$ or β phase in the as-quenched state, as is known, there is a prominent effect of diffuse scattering. It has a maximum in alloys located near the border of the $\beta + \omega / \beta$ phase regions at 300K. In the Ti-Mo system, that is the alloy with 15% Mo (figs. 3 a,b). Application of hps 9.0 GPa to the alloys located inside the $\beta + \omega$ or in the β regions leads to increase of the amount of ω phase, and simultaneously to increase of diffuse scattering. However, in the "border" alloys, appearance of clear ω reflections is accompanied by a decrease in diffuse scattering.

The higher the concentration of the alloying element, the higher the pressure to be applied to the alloys with the β phase in as-quenched state in order to create the ω phase. The amount of ω phase after hps 9.5 GPa is very small in alloys with 18-25% Mo. X-ray diffractograms do not reveal its presence. The ω phase might be seen as ellipsoidal particles with diffraction patterns indicative of substantial distortion in its lattice. These distortions can be caused by its elastic interaction with the β-matrix, possessing significantly more rigidity in comparison with low Mo concentration alloys [2].

As is known, the diffuse scattering effect is ascribed to a short range order in displacement of short atomic rows [3,4]. As a result of such a displacement, a short-ordered state or zone is created [3]. These zones serve as the sites where the ω phase forms in its final shape when the change from short to long-range ordered displacement takes place under an increasing driving force such as cooling or pressure. In the same sequence, the diffuse streaking changes into sharp ω reflections. It

should be pointed out that our experiments displaying such a sequence were done under "pure conditions". In contrast with an annealing process there was no change in the phase content. In the alloys located far away from the β+ω/β phase region border at 300K, for example with Mo<12-13 or Mo>18%, the amount of short ordered regions is very small, or they are absent altogether. In these alloys, pressure brings about not only formation of the ω phase, i.e. completely ordered regions, but also a partially ordered ones that give the appearance of diffraction scattering.

Using the regular solution approach and the Kaufman semiempirical parameters for Ti-Mo and Ti-V systems [1] and our experimental data, the P_o-x sections at 300K of T-P-x metastable phase diagram were constructed (for details see [5,6]). The use of hps creating α' and ω in a large amount enabled us to obtain concentration dependencies of phase specific volumes U^α $^\beta$ $^\omega$ more rigorously and in wide concentration range and to use it for $\Delta U^{i \to j}$ data. Thus the following are yielded. $U_{Ti_{1-x}Mo_x}^{\omega} = 10,46$ $(1-0,146x)$, $U_{Ti_{1-x}Mo_x}^{\alpha'} = 10,67$ $(1-0,312x)$, $U_{Ti_{1-x}V_x}^{\omega} = 10,46$ $(1-0,131x)$, $U_{Ti_{1-x}V_x}^{\alpha'} = 10,67$ $(1-0,214x)$ cm^3/mole. According to calculations the critical pressure of α⇄ω transition in Ti-Mo or -V alloys $P_o^{\alpha \to \omega}$ linearly decreases with Mo and V concentration and approaches zero at 9% Mo and 12.5%V. There are the ranges of concentration where the ω phase has to exist in a mixture with the β phase in the as-quenched state at P=1 atm since $P_o^{\beta \to \omega}<0$. $P_o^{\beta \to \omega}$ at 300K linearly increases with Mo or V. It is worth noting that TEM reveals the presence of small ω particles in Ti with ~20-25 Mo alloys after hps at pressures less than the calculated one. The possible reason for it can be an increased value of $n(E_f)$ of the β phase in this region [7] resulting in reduced β stability and even displacement of the miscibility gap on the stable phase diagram in this region [8]. The same reason could be for anomalous behaviour under pressure T_c that was observed on the same samples [9].

The qualitative analysis of phase stability under pressure was done [5,6] using detailed data obtained by Collings et al [2,10]. It was shown that Mo effects on phase stability more substantially than V. The influence of Mo and, in a less degree, V alloying and uniform compression on the sequence in phase stability in Ti-Mo and Ti-V alloys is different and specific for various concentrations, despite their similarly diminishing the alloy's interatomic distance and increasing the electronic concentration.

Acknowledgement

References

1. L. Kaufman, H. Bernstein, Computer Calculation of Phase Diagrams, Acad. Press, 1970.

2. E.W. Collings, J.C. Ho and R.I. Jaffe, Phys. Rev. B, 5, 4435 (1972).

3. D. de Fontain, N. Paton and J. Williams, Acta Met., 19, 1153 (1971).

4. I.V. Lyasotskiy, Yu. D. Tyapkin, Fiz. Met. Metalloved., 36, N6, 1260 (1973).

5. H. Leibovitch, E. Gartstein, A. Rabinkin (in publication).

6. H. Leibovitch, A. Rabinkin (in publication).

7. J. Waber, in "Physics of Solid Solution Strengthening", ed. E. Collings and H. Gegel, Plenum Press, N.Y., 1975.

8. S. Terauchi, H. Matsumoto, T. Sigimoto, K. Kame (preprint).

9. D. Kohnlein, A. Rabinkin, H. Scherer, W. Buckel (in publication).

10. E.W. Collings, J.C. Ho, Phys. Rev., B, 1, 4289 (1970).

Figures
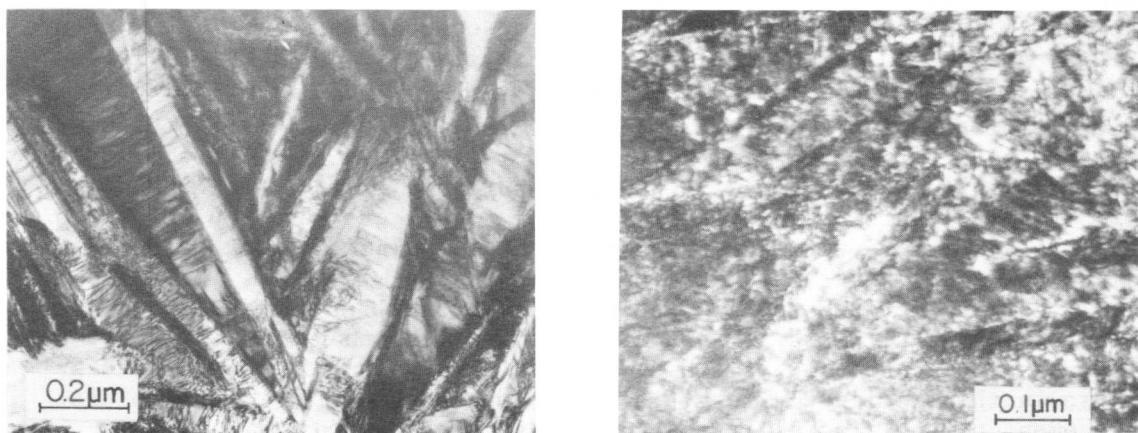
a

b

Fig.1. The structure of the Ti-3% Mo alloy. a) TEM bright-field micrograph showing the complex martensitic structure in the as-quenched state: fine plates of the α' martensite together with large plates of the α'' martensite. z.a.$[010]_{\alpha''}$. b) TEM dark-field micrograph after 9.2 GPa showing the small ω phase particles together with α' and α'' phase.
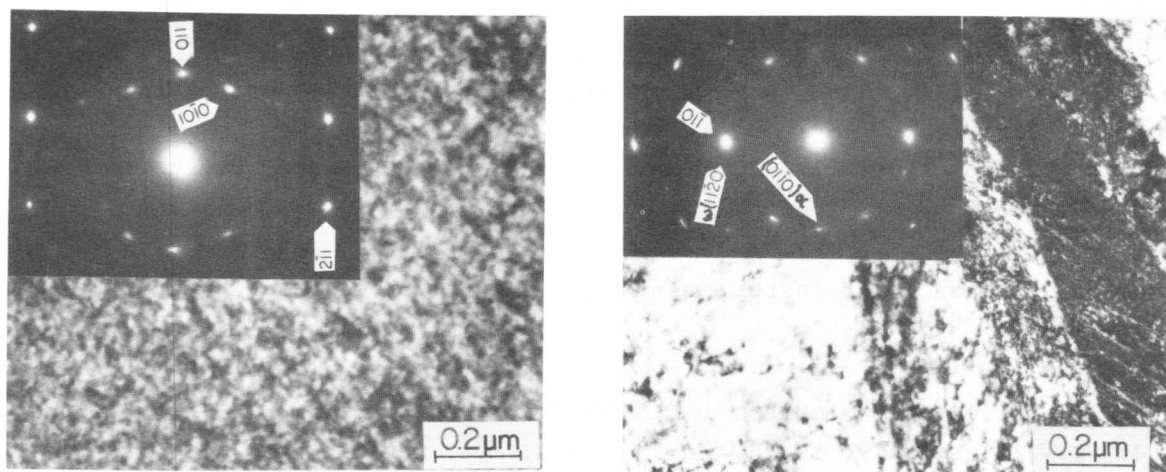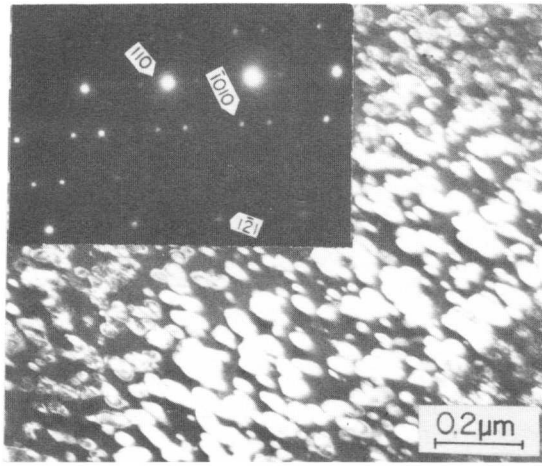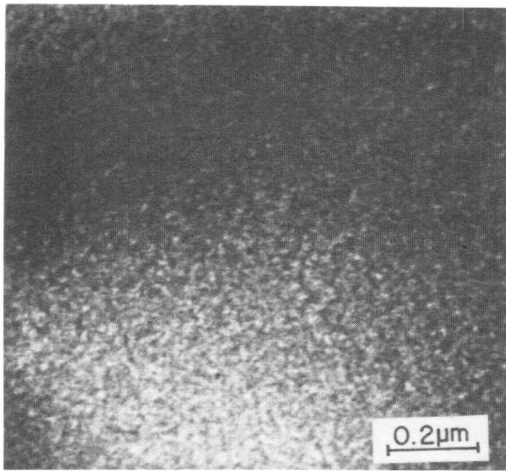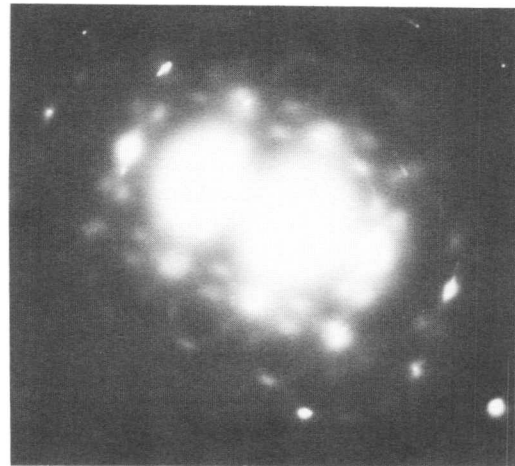
Fig.2. The structure of Ti-7% Mo alloy. a) TEM micrograph and electron diffraction pattern of the as-quench state. The fine ω particles are present in the β matrix. b) TEM dark-field micrograph and the corresponding diffraction pattern after hps 9.0 GPa showing the pressure induced α' and ω phase in the β-matrix. z.a.$[111]_\beta$.
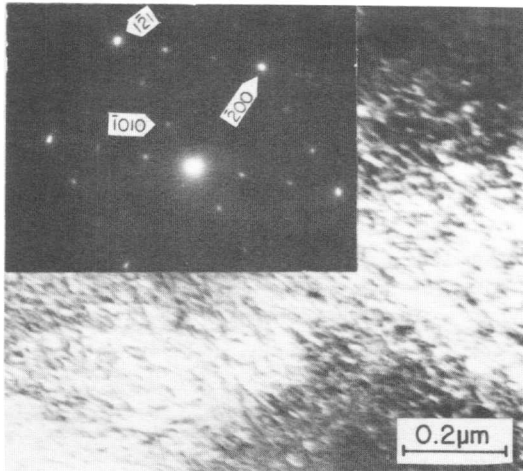
c) TEM dark-field micrograph of the same sample after ageing at 380°C for 72 h. The large ellipsoidal particles of the ω phase are clearly seen. z.a.$[131]_\beta$. There are three variants of the ω phase: ω_1 with z.a.$[10\bar{1}5]$, ω_2 with z.a.$[\bar{1}2\bar{1}3]$ and ω_3 with z.a.$[1\bar{2}13]$.

Fig.3. The structure of the Ti-15% Mo alloy. a) TEM micrograph and b) the corresponding electron diffraction pattern of the as-quenched state showing a complex network of diffuse intensity. z.a.~$[100]_\beta$. c) TEM dark-field micrograph and electron diffraction pattern after hps 9.0 GPa. The ω phase reflections are clearly visible, while the diffuse scattering has practically disappeared.z.a.$[012]_\beta$.

On the $\gamma \to \varepsilon$ Phase Transformation in Fe-Mn Alloys Induced by High Pressure and Plastic Deformation

A. Rabinkin, M. Ron, F. Trichter and E. Gartstein

In Fe alloys with 25.6 - 37.2 at.% Mn, the $\gamma \to \varepsilon$ transformation induced by three driving forces: temperature change, high pressure soaking (hps) and cold work (cw), was studied by means of Mössbauer spectroscopy, electron microscopy and X-ray analysis. In contrast to well-established data, presence of small ε phase particles was observed after quenching even in Fe-37.2 at.% Mn. The quantity and sizes of ε phase are stongly increased when hps and cw are applied. The details of this process were traced on all its stages including complete transformation to pure ε phase after hps 9.0 GPa (90 kbar). The well-known orientation relationships between γ and ε phases, i.e. $(\bar{1}11)_\gamma 11 (0001)_\varepsilon$ and $[10\bar{1}]_\gamma 11 [11\bar{2}0]_\varepsilon$ were observed in all obtained structures whatever driving force was applied. It is proposed to explain the unusual behavior of Fe-Mn alloys (limited growth of ε martensitic phase upon cooling in vicinity of $M_S^{\gamma \to \varepsilon}$, very small sizes of ε phase in high Mn alloys, etc.) by taking into account the antiferromagnetic ordering in both phases.

I. Introduction

It is now well known that in the Fe-Mn systems, the denser ε phase is stabilized on cooling [1] or on application of high pressure and/or cold deformation [2-5]. The phase diagram for metastable equilibria in Fe-Mn alloys is regarded as well-established. The $M_S^{\gamma \to \varepsilon}$ line of $\gamma \to \varepsilon$ martensitic transition was determined by magnetic and dilatometric methods [6] as well as X-ray analysis [7]. According to these data, the limit concentration for the transition at T>300K is 27-28 at.% Mn, and alloys exceeding that limit contain no ε phase in the quenched state. A strong concentration-dependence of $M_S^{\gamma \to \varepsilon}$ was also observed. At the same time, the calculated phase diagram [8], constructed by using the regular solution approach, has a much wider region of ε phase stability: $T_0^{\gamma \rightleftarrows \varepsilon} \approx 300K$ at Mn$\approx$50 at.%. The $\gamma \to \varepsilon$ transformation is associated with a moderate free-energy change ($\Delta F^{\gamma \to \varepsilon} \sim 210 - 420$ J.mole); in these circumstances, the γ matrix contains numerous stacking faults, which act as martensitic nuclei as the temperature drops to the M_S level. However, in substantial contrast to many other alloy systems, ε martensite develops on cooling (Mn $\sim$ 20 - 25 at.%. Here and later on Mn content is given in at.%) only in a narrow temperature range $T_N^\gamma < T < T_0^\gamma$ where T_N^γ is the Néel temperature of the γ phase [7]. Earlier, it was found that cooling even down to 4.2K does not change the amount of primary martensitic ε phase [4]. Plastic deformation contributes to onset of the $\gamma \to \varepsilon$ transition as a thermodynamic factor and a "generator" of new nucleation sites [9]. In thermodynamic terms, pressure is analogous to cooling as a driving force.

It was thought worthwhile to study the $\gamma \to \varepsilon$ transformation induced by three driving forces: cooling, high pressure soaking (hps), and cold

Department of Materials Engineering, Technion, Israel Institute of Technology, Haifa, Israel.

work (cw). The highly sensitive and differentiable Mössbauer spectro-
scopy, X-ray analysis and in some cases electron microscopy, were chosen
as the methods for tracing this transformation from its very beginning
up to the final stage. Fe-alloys with 25.6 - 37.2% Mn were chosen, there-
by making it possible to study only the $\gamma \rightarrow \varepsilon$ transformation and to check
to what extent the region of ε phase stability can be enlarged by high
pressure.

II. Experimental Procedure

Alloy ingots were cut into plates and cold-rolled to the assigned
thickness. Afterwards, plates and foils were held at $850^{\circ}C$ for 2 hours
and finally quenched to $0^{\circ}C$ in oil, under vacuum. Part of the specimens
so prepared were cold-worked to different degrees of thickness reduction,
$\psi = h_0-h/h_0$ where h_0 and h are, respectively, the initial and final
thickness. The as-quenched specimens were soaked under pressure up to
3.0GPa (30 kbar) for 1h in a hydrostatic liquid-medium cell. For soaking
at pressures of up to 9.2 GPa, the solid-medium cell ensuring minimal
deviation ($1\div2\%$) from uniformity was employed. The structural changes
were traced with the aid of a standard Philips diffractometer and a
JOEL 100B transition electron microscope. The Mössbauer spectrometer and
details of measurements have been described elsewhere [4]. The Mössbauer
spectra were analyzed as a superposition of one or two doublets or a
sextuplet and a single line attributed to the γ_1, γ_2, γ and ε phases
respectively. The relative amounts of the ε, γ_1, γ_2 and γ phases were
taken as proportional to the relative area attributed to a particular
phase: A_ε/A, A_{γ_1}/A, A_{γ_2}/A and A_γ/A.

III. Results and Discussion

Fig. 1a is a characteristic example of spectra taken at 300K after
hps, and fig. 1b - after cw. Figs. 2a,b show the changes in Mössbauer
parameters of the ε phase, i.e. $I.S._\varepsilon$, Γ_ε and relative spectral area,
A_ε/A, as a function of ψ and P for two alloys. Here $I.S._\varepsilon$ designates the
isomeric shift, Γ_ε - the experimental line width. The change in the iso-
meric shift is proportional to the electronic charge density and there-
fore is inverse proportional to the change in the specific volume of a
phase. The line width usually correlates with the static distortions of
the lattice. As follows from the data obtained, the maximal pressure
applied by us (~10.0GPa) suffices to complete $\gamma \rightarrow \varepsilon$ transformation only
in the alloy with 25.6% Mn. In alloys with higher Mn content (see fig.
2b) this level of hps is already inadequate: the amount of ε phase for-
med under P = 9.2GPa decreases with % Mn. Approximately the same tend-
ency is observed regarding the influence of cw: minimal cw of $\psi = 45\%$
is needed to obtain only ε phase for a 25.6% Mn-alloy, but even cold
work with $\psi = 90\%$ creates only ~5 vol.% ε phase in the alloy with 37.2%
Mn. In contrast with our X-ray data, Mossbauer spectra indicate the
presence of considerably more ε phase in the quenched state (~20 vol.%)
in alloys with 25.6 - 33.8% Mn. However there is good agreement with the
amount found by others [7]. The presence of very small amounts of ε
phase (<0.5 vol.%) can be seen in the spectrum for the as-quenched alloy
with 37.2% Mn. Application of pressure definitely increases the amount
up to ~2 vol.% and not before P has exceeded 8.0GPa.

It is significant that the changes in the Mössbauer parameters of the ε phase are the same on all stages of the $\gamma \to \varepsilon$ transformation induced both by hps and by cw. There is a steep change in $I.S._\varepsilon$ and narrowness of Γ_ε during the first stages of this process, and afterwards they approach a constant value. At the same time, the line widths of the γ phase spectra increase with decrease of its amount. In the as-quenched state, the coherent ε phase is subjected to high tensile stresses, since its density is higher than that of the γ phase. Subsequent growth of the ε phase on application of either hps or cw leads to release of the coherency stresses, which in turn results in line narrowing. The reverse picture is observed in the γ phase. It is of interest that severe plastic deformation of the "newly formed" ε phase does not cause "secondary" increase of Γ_ε, as is usually observed in metals and alloys where plastic deformation is not accompanied by phase transition [10].

The electron microscopy study of the alloys with 29.8 and 37.2% Mn was intended to verify the Mössbauer results and check the morphology and peculiarities of the crystal structure as affected by three driving forces in question (for details see [11]). Without doubt, the ε phase is present in small amounts after cooling to 300K, even in the alloy with 37.2% Mn, and has the shape of small elongated needles with dimensions <200 - 300 Å; many dissociated dislocations are also present. Application of hps and cw leads to a substantial increase in the amount of ε phase due both to growth of already present ε particles and to simultaneous appearance of new ones. Twinning of the γ phase also takes place. Fig. 3b is a good illustration of successive stages of formation of the ε phase under high pressure, proceeding in a well-defined course of development of stacking faults during the $\gamma \to \varepsilon$ martensitic process induced by temperature change [12].

Analysis of the diffraction pattern showed that the crystallographic relationships of the $\gamma \to \varepsilon$ transformation in Fe-Mn alloys induced by hps and cw are exactly the same as in the most other steels in which it is induced by cooling and/or cold deformation, i.e. $(\bar{1}11)_\gamma 11 (0001)_\varepsilon$ and $[10\bar{1}]_\gamma 11 [11\bar{2}0]_\varepsilon$. The similarity between all features of the crystal structure as a result of quenching, hps and cw explain why there is also no difference between the changes of Mössbauer parameters after various treatments. Detailed thermodynamic analysis of phase equilibria was done by one of us [13], taking into account the magnetic entropy terms due to the antiferromagnetic ordering in both phases. In alloys with $T_N^\gamma < T_0$, the chemical driving force according to the Kaufman model [8] moderately decreases, and the $\gamma \to \varepsilon$ transition proceeds normally until T_N^γ is reached. Below this temperature the γ phase again becomes increasingly stable because of magnetic contributions which may eventually reduce the driving force below the potential barrier. Magnetic ordering in the ε phase at low temperatures (<250K) acts in the opposite direction. This explains completely the "unusual" behavior of the $\gamma \to \varepsilon$ martensitic transformation during cooling. At very low temperatures there could even be partial reversion to an $\varepsilon \to \gamma$ transition. The smaller the concentration of Mn, the lower the T_N^γ values, the larger the temperature range where the $\gamma \to \varepsilon$ transition takes place and the larger the volume of γ phase which succeeds to transform. This is in accordance with experimental data on the amount of ε phase in quenched state. If the ε phase would be in a magnetically ordered state at 320K, then the driving force could be favorable to realization of the $\gamma \to \varepsilon$ transition even in alloys

with Mn $<$ 40%. Such a situation can exist for very small particles of the ε phase nucleated in alloys with Mn $>$ 30-33% in which T_N^γ > 300K and T_N^ε < 250K. At 300K ε particles in the bulk state (d > 10-22nm) display the weak paramagnetism of conductive electrons and the magnetic term in this state does not favor the $\gamma \rightarrow \varepsilon$ transition. But with particle size <10-20nm, there may be spatial alignment of most of its spins due to magnetic interaction with the boundary lattice planes of the antiferro-magnetic matrix phase. A common effect revealed by Néel et al [14]. It is now clear why only electron microscopy and Mössbauer spectroscopy but not a dilatometry, X-ray analysis and magnetometry, detected small amounts of the ε phase in alloys with Mn $<$ 37.2%. High pressure increases the driving force for $\gamma \rightarrow \varepsilon$ not only by increasing the sV.sp term, but also by reducing the magnetic barrier itself. The magnetic free energy of the γ phase reduces as a result of strong decrease of T_N^γ under pressure and even vanishes at 300K. As the magnetic barrier is minimal in the alloy with ~20-25% Mn, the pressure, needed to complete the $\gamma \rightarrow \varepsilon$ transformation, is minimal too. It has been shown that the alloy with ~25% Mn has a minimal elastic modulus E in the γ phase range [15]. The term due to external stresses in the thermodynamic driving force is ~$(\sigma.\varepsilon)/E$[16]. Also, the smaller E, the easier it is to generage faults in the γ matrix, i.e. potential nuclei for ε phase growth. Therefore, naturally, in the alloy with ~25% Mn both these favorable factors [9] reach maximal effectivness and promote complete $\gamma \rightarrow \varepsilon$ transition at minimal ψ.

References

[1] M. Hansen, "Constitution of Binary Alloys", Metallurgy and Metal. Eng. Ser., McGraw-Hill, p. 664, 1958.

[2] T.P. Ershova, E.G. Ponjatovski, Izv. Acad. Nauk, Metally, 4, N5.

[3] P.M. Giles, R. Marder, Met. Trans., 2, 1371 (1971).

[4] F. Trichter, A. Rabinkin, M. Ron, A. Sharfstein, Scripta Met., 12, N5, 431 (1978).

[5] H. Schumann, Pract. Metallographie, 12, 511 (1975).

[6] H. Schumann, Archiv fur Eisenhütten, 38, N8, 647 (1967).

[7] I. Bogachev, G. Zviginzeva, Dokl. Acad. Nauk, USSR, 215, N3, 570 (1974).

[8] J.F. Breedis, L. Kaufman, Met. Trans., 2, 2359 (1971).

[9] G.B. Olson and Morris Cohen, Met. Trans., 6A, 791 (1975).

[10] M. Ron, M.M. Stupel, B.Z. Weiss, Acta Met., 25, 1355 (1977).

[11] E. Gartstein, A. Rabinkin, Acta Met. (in publication), 1979.

[12] G.B. Olson and Morris Cohen, Met. Trans., 7A, 1897 (1976).

[13] A. Rabinkin, Calphad, 3, N2, 77 (1979).

[14] L. Néel, J. Phys. Soc. of Jap., 17, Suppl. B-1, 676 (1962).

[15] I. Bogachev, B. Ergolaev, T. Frolova, Phyz. Met. V. Metalloved., 29, 358 (1970).

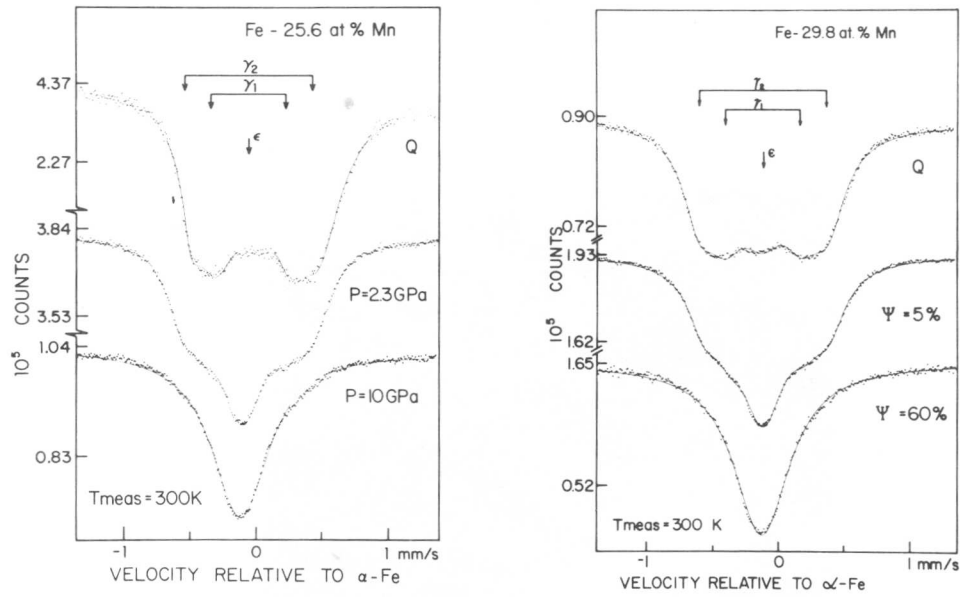[16] A.L. Roitburd, Physika Tverd. Tela, 19, N10, 2879 (1977).

Fig.1. Mössbauer spectra for a) Fe-25.6% Mn after hps, b) Fe-29.8% Mn after cold work.
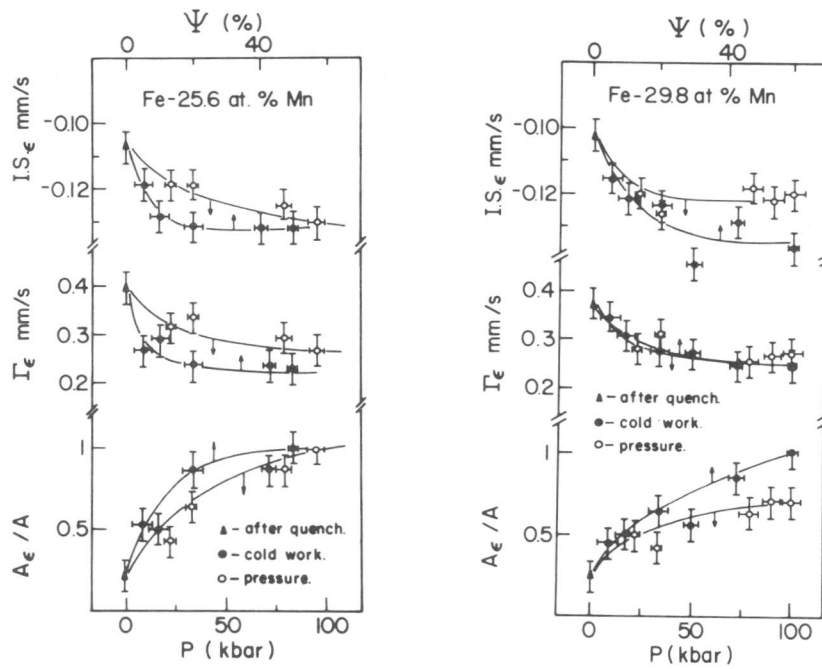

Fig.2. Changes in Mössbauer parameters after hps and cw for a) Fe-25.6% Mn, b) Fe-29.8% Mn.
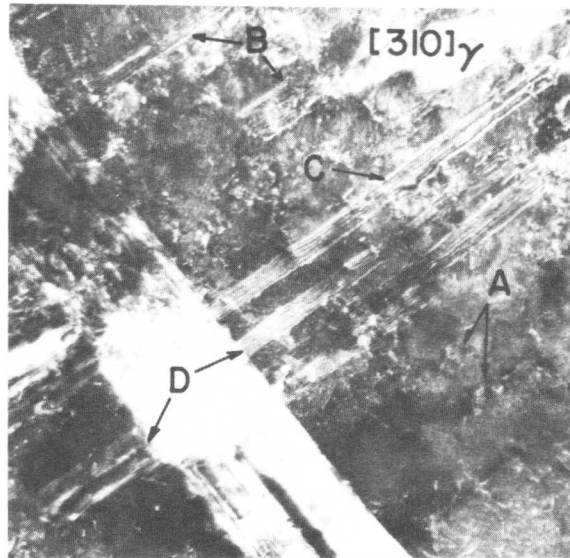
Fig.3. Successive stages of the ε phase formation in Fe-29.8% Mn sub-
jected to a uniform pressure of 8GPa (80 kbar). (A) A small
stacking fault formed by partial dislocations. (B) Wide
stacking faults. (C) "Stacking" faults, which may be thin ε-
plates. (D) The preferred growth of the new stacking faults or
thin ε plates from the interface on the existing martensite
plate.

A Thermal and Optical Study of the Transition between hcp ^{4}He and fcc ^{4}He from the Triple Point to 9 kbar

J. P. Franck

The phase diagram of solid ^{4}He was studied by thermal analysis, and by an elliptometric method, from the triple point at T = 14.99 K and P = 1129 bar to 9 kbar. The transition in heating and cooling shows temperature hysteresis varying from about 10 mK near the triple point to about 3 K at 9 kbar. The transition shows athermal behaviour. Detailed isothermal transformation studies were made in a crystal near 9 kbar. Isothermal transformation is observed in heating but not in cooling. Isothermal holding leads to pronounced stabilization of the cooling transition. The properties of the transition observed so far make it likely that the transition is martensitic.

I. Introduction

The transition between the two close-packed phases of helium (hcp-fcc) is one of the weakest first order transitions known. Because of this, both experimental and theoretical investigations of it are difficult. Calculations using molecular dynamics [1] have predicted a phase diagram which is in fair agreement with experiment over a limited density range. During attempts to extend the known part of the phase diagram it was discovered that the transition in ^{4}He has many aspects that are familiar from martensitic transformations, particularly temperature hysteresis and athermal behaviour of the transition [2,3]. In the present paper an extension of the phase diagram to 9 kbar is given, as well as a detailed kinetic investigation of one high density crystal.

II. Experimental

Thermal analysis was used to about 4 kbar. The helium crystal is grown under approximately constant pressure in a pressure cell, which can be operated as a calorimeter. The cell contained 7.44 cm^3 of helium, corresponding to between 0.60 and 0.79 mole of helium depending on the density. The transition could be observed at well-controlled rates in both heating and cooling. The calorimetric method also allows for a measurement of the latent heat. Above 4 kbar the thermal method becomes extremely difficult to use because of the increasing thermal width of the transition as well as the rising heat capacity of the vessel.

Department of Physics, University of Alberta, Edmonton, Alta T6G 2J1, Canada, and Department of Physics, University of Delaware, Newark, Del. 19711 USA

The optical method uses the birefringence of the hcp phase [4] to distinguish it from the optically isotropic fcc phase. The helium crystal is contained in an optical pressure cell which can be used in transmission. The pressure seal uses two sapphire windows of 2.4 mm thickness which are sealed using an inverted Bridgeman packing. The helium crystals are again grown at approximately constant pressure, they are 13mm long and 4mm in diameter. Linearly polarized light from a He-Ne laser traverses the cell, on emergence it is elliptically polarized due to the birefringence of the helium crystal as well as stress bire-fringence in the windows. The emerging beam is passed through a $\lambda/4$ plate and a second analyzer, which are both adjusted for extinction. In this setting the axis of the $\lambda/4$ plate are parallel to the axis of the elliptically polarized light. The phase transition corresponds then to the insertion and removal of an additional retardation plate into this system. The method in favorable cases can be very sensitive, it has the added advantage of high speed.
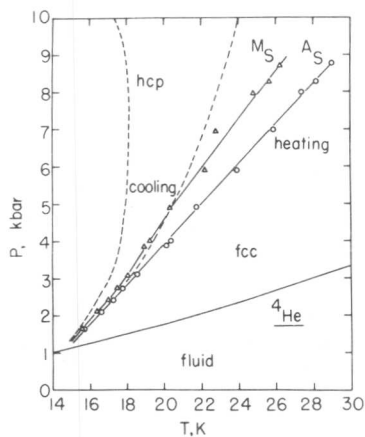

Fig. 1. Phase diagram of ^{4}He. Dashed lines theoretical calculations, Ref.[1].

III. The Phase Diagram

Fig. 1 shows the phase diagram from the triple point to about 9 kbar. Data up to 4 kbar were obtained using thermal analysis, the data above 4 kbar are from the optical study. The transition temperatures in heating and cooling are labelled A_S and M_S as is conventional for martensitic transformations. The temperature hysteresis increases from quite low values near the triple point ($\sim$10 mK) to about 3K at 7 kbar. Above 7 kbar the temperature hysteresis appears not to increase any more. As in the earlier work, it was found that the M_S temperature is much more susceptible to crystal quality than the A_S temperature. Close to the triple point, the transition line becomes very steep and possibly infinite, this was described in detail in Ref. [3]. Latent heat measurements were possible from the triple point to about 16K. They give the transition entropy as $\Delta S = 0.0183$ joule/mole K. As can be seen from Fig. 1, the experimental phase diagram deviates with increasing pressure from the theoretical predictions of Ref. [1].

IV. Kinetic Studies

Detailed kinetic studies using the optical method were made on a crystal of molar volume V = 7.82 cm^3/mole. The transition in this crystal was observed at A_S = 29.01 K and M_S = 26.23 K. The pressure at the transition is 8.76 kbar. Fig. 2 shows a number of cooling and heating transitions. These were taken in succession at various cooling and heating rates. Before the initial cooling transition the crystal had been held for 12 hours in the high temperature (fcc) phase about 12 K above A_S. The pronounced bursts during the cooling transition are very
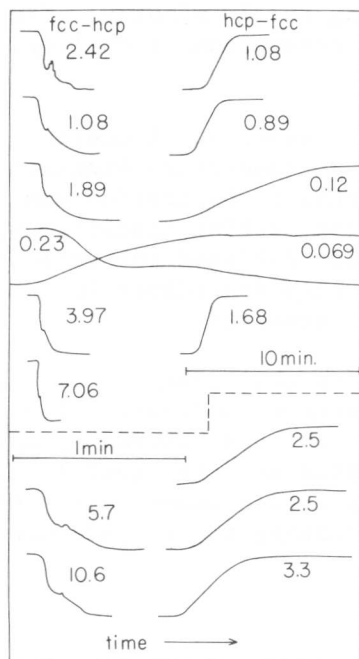
-307-

Fig. 2. Transmitted intensity of laser light (arbitrary scale). The transitions were traversed in order from left to right and downwards. Numbers indicate cooling resp. heating rates in K/min.

often observed after this type of thermal treatment. The athermal character of the transition is evident from the figure. Another interesting aspect of the results is the remarkable reproducibility of the signal for the transition during the 5 hours when those data were taken. It should be noted that the axis orientation and the amount of retardation of the effective retardation plate representing the hcp crystal depends on the orientation of the hexagonal axis relative to the laser direction. The reproducibility of the transition signal indicates that the c-axis orientation is faithfully reproduced during repeated transitions. This behaviour was generally also observed in other crystals that were investigated by the optical method. Deviations from this behaviour occur, however, if the crystal is held in the high temperature phase for prolonged times (e.g. in excess of one hour) and at temperatures considerably above the A_S temperature. After such heat treatment the optical signal is usually considerably different, indicating a different direction of the c-axis.

Isothermal transition rates were obtained by partially completing the athermal heating or cooling transition and then holding the temperature constant. Observation of the optical signal allowed us to estimate the fraction transformed as a function of time. Some of the results are shown in Fig. 3. For the heating transitions the transition was stopped at 15% and 33% complete. During isothermal holding the transition proceeds at gradually decreasing rates, sometimes in an irregular fashion. After 3 hours holding time the transition was 90% complete. When heating is resumed, the transition goes to completion without delay. In cooling, two curves are shown for partial transformations of 3% and 16%. During isothermal holding the transition appears to continue for about 50 minutes, and then stops. The final amount transformed was 50% and 33% respectively. When cooling is resumed, the transition proceeds to completion, but with considerable delay. This delay, or stabilization of the cooling transition is shown in Fig. 4. The cooling transition set in only
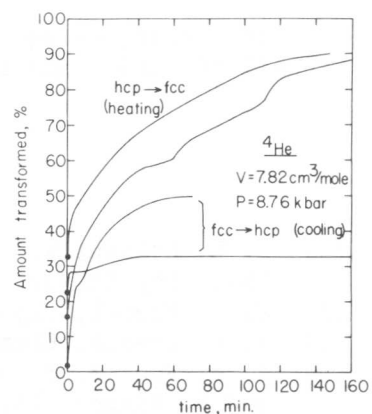

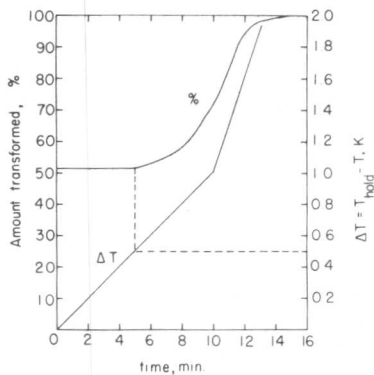Fig. 3. Isothermal transformation curves.

Fig. 4. Cooling transformation, after isothermal holding for 70 minutes. Time is measured from resumption of cooling.

5 minutes after resumption of cooling, corresponding to a temperature stabilization of 0.5 K. This stabilization was always observed for cooling transitions, although its amount differed for various pre-treatments. This dependence is at present not fully resolved.

In contrast to these isothermal transitions above A_S and below M_S, there is at present no indication that the transition can proceed isothermally in the interval between M_S and A_S, even when the transition was partially started and the crystal then taken back into the interval (M_S, A_S). Lowering of the temperature below A_S always stopped the heating transition, and raising the temperature above M_S always stopped the cooling transition.

V. Conclusion

The transition hcp ^{4}He to fcc ^{4}He shows gradually increasing temperature hysteresis from the triple point to 9 kbar. Above 7 kbar the hysteresis remains constant near 3K. The transition is athermal. The orientation of the hexagonal c-axis is reproduced repeatably after taking the crystal through the transition as long as prolonged heat treatment in the fcc phase is avoided. The heating transition can run to completion isothermally above A_S after several hours. The cooling transition does not run to completion on isothermal holding below M_S, although partial isothermal transformation is observed. No isothermal transformation is observed between M_S and A_S. These results give further evidence that the transition mechanism is most likely that of a martensitic transition.

References

[1] B. L. Holian, W. D. Gwinn, A. C. Luntz, and B. J. Alder, J. Chem. Phys. 59, (1973), 5444.
[2] J. P. Franck, Phys. Rev. Letters 40 (1978), 1272.
[3] J. P. Franck, Chem. Phys. Letters 63 (1979), 100.
[4] J. E. Vos. B. S. Blaisse, D. A. E. Boon, W. J. van Scherpenzeel, and R. Kingma, Physica 37, (1967), 51.

Nucleation Kinetics of the FCC→HCP Martensitic Transformation in Steels

G. B. Olson and M. Cohen

The isothermal nucleation kinetics of the FCC→HCP martensitic transformation in an Fe-Mn-Ni alloy are consistent with the same linear dependence of the activation energy on the chemical free-energy change as observed for the FCC→BCC martensitic transformation in the same alloy system. Since the lattice-invariant deformation is absent in the FCC→HCP transformation, it is concluded that the rate-controlling step is associated with the lattice deformation in both transformations. The kinetic behavior is consistent with the thermally-assisted motion of discrete interfacial dislocations accomplishing the lattice deformation with the same activation area as for slip.

I. Introduction

Both the lattice deformation (which converts one lattice to another) and the lattice-invariant deformation (which reduces strain energy) have been proposed as possible rate-controlling processes in the isothermal nucleation of the FCC→BCC martensitic transformation in steels. Theoretical calculations [1,2] have shown that, in principle, either process is capable of accounting for the experimentally observed linear dependence of the nucleation activation energy on the chemical free-energy change of the transformation. The FCC→HCP martensitic transformation allows a critical test between these two alternatives since, for this transformation, the lattice-invariant deformation is absent. In addition, the transformation occurs in the same Fe-Ni-Mn ternary alloy system in which the FCC→BCC isothermal kinetics have been studied extensively.

II. Materials and Procedures

Fe-Mn-Ni alloys were prepared with compositions selected to be stable against FCC→BCC transformation according to the thermodynamic parameters of Breedis and Kaufman [3]. The results to be reported here were obtained on an Fe-16.5Mn-6.7Ni alloy with additions of 0.05Ti and 0.01Al to getter the interstitials. In the annealed condition, the alloy was found to transform at room temperature, producing the HCP ε plate martensite shown in Fig. 1.

Transformation kinetics were studied by electrical resistivity measurements. In preliminary experiments, it was found that free surfaces had a strong stimulating influence on the kinetics; indeed, an Fe-17Mn-10Ni alloy which underwent substantial surface transformation below 200 K exhibited no bulk transformation down to 78 K. To eliminate this effect, the surfaces of the resistivity specimens were doped with Ni by Ni-plating and then annealing at 1000 C.

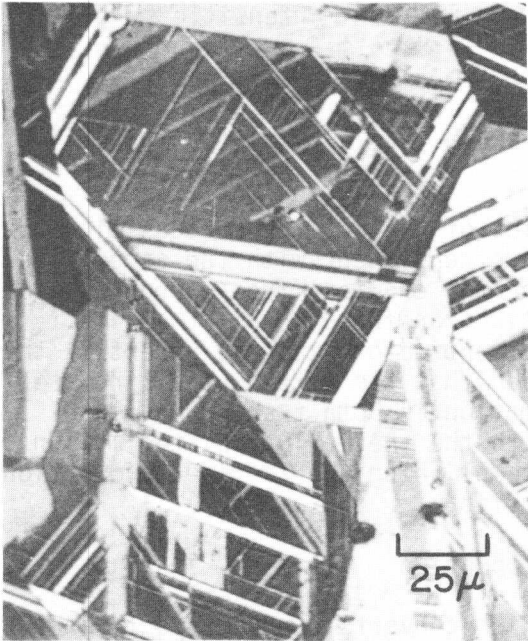Massachusetts Institute of Technology, Cambridge, Massachusetts, U.S.A.

Fig. 1 HCP plate martensite in
Fe-16.5Mn-6.7Ni alloy. Etchant:
10 g potassium metabisulfite in
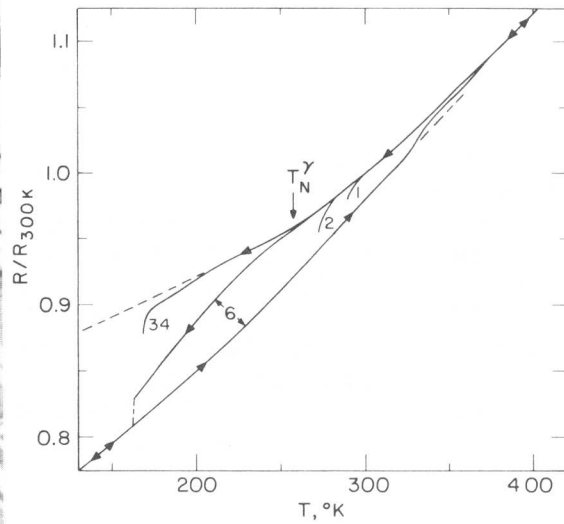100 cm^3 sat. sodium thiosulfate.

Fig. 2 Relative change in elec-
trical resistance on cooling and
heating. Numbers indicate ther-
mal cycles.

    The relative resistivity changes on cooling are plotted in Fig. 2.
Although the alloy initially transformed at room temperature, it was
found that thermal cycling had a stabilizing effect, lowering the for-
ward transformation temperature and increasing the hysteresis between
the cooling and heating transformations. On the sixth cycle, the
specimen was held in frozen ethanol for several hours, producing the
largest resistance change observed. For purposes of volume-fraction
estimates, this change was assumed to correspond to complete transforma-
tion; thus, the resistance curve obtained on heating was taken as that
of the HCP phase* (the reversion temperature for this cycle is also
indicated in Fig. 2). In subsequent cycles, isothermal measurements
were made. The stabilizing effect of cycling appeared to approach a
saturation level such that after twelve cycles the transformation rate
at a given temperature was reasonably reproducible. Isothermal trans-
formation runs were then carried out at different temperatures to
assess the temperature dependence of the transformation kinetics. After
each run, the specimen was completely reverted to austenite by heating
to 435 K. As Fig. 2 shows, the austenite resistivity displayed a
change of slope at 260 K. This anomaly correlates with the Néel tempera-
ture, T_N, for an antiferromagnetic transition in alloys of this type
[4,5].

----

*
 Incomplete transformation would introduce a constant pre-exponential
factor that would not significantly affect the activation-energy esti-
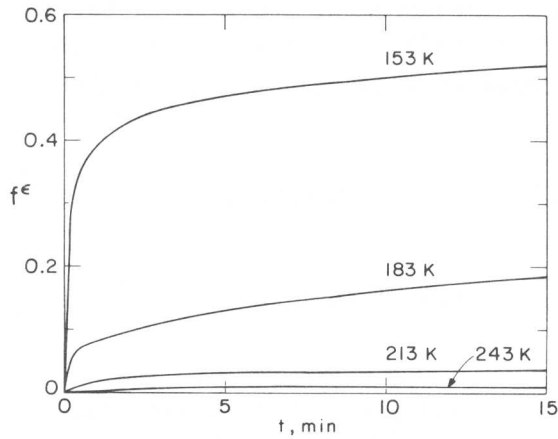mates to be discussed later.

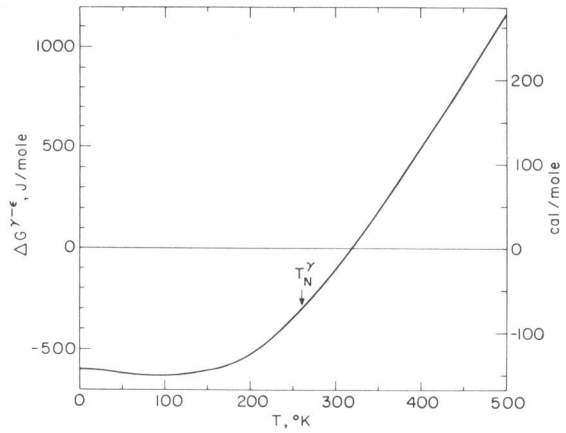Fig. 3 Isothermal transformation curves of volume fraction ε martensite, f^ε, vs. time, t.

Fig. 4 Calculated transformation free-energy change vs. temperature.

III. Results and Discussion

Typical isothermal transformation curves of the volume fraction of HCP martensite, f^ε, vs. time are given in Fig. 3. The curves are initially linear; the associated transformation rates were measured over a range of four orders of magnitude over a temperature range of about 100 K. The activation energy, Q, at a given temperature was obtained from the initial transformation rate according to the following equation [6]:

$$\dot{f} = n_i \overline{V}_0 \nu \, \exp\!\left(-\frac{Q}{RT}\right) \tag{1}$$

where n_i is the initial number of nucleation sites per unit volume, $\overline{V}_0$ is the initial average martensitic plate volume, and ν is the attempt frequency. As in previous such analyses of the FCC→BCC transformation, n_i is estimated as 10^6 cm^{-3} and ν is taken as 10^{13} sec^{-1}. A value for $\overline{V}_0$ of 4×10^{-10} cm^3 was obtained from measurements by Rémy [7] on a similar alloy of comparable grain size.

The shape of the chemical free-energy change, $\Delta G^{\gamma \to \varepsilon}$, vs. temperature was calculated using available parameters for the electronic and vibrational contributions of the pure metals [8-10]. Magnetic contributions were incorporated separately according to the model of Weiss and Tauer [11] using the observed T_N of the austenite, a magnetic moment of 0.7 μ_B for the austenite, and assuming the HCP phase to be effectively nonmagnetic. The curve was then fitted to the experimental $T_0^{\gamma \to \varepsilon}$ temperature bracketed by the forward and reverse transformation temperatures of the annealed alloy. The resulting curve is shown in Fig. 4.

The measured activation energies are plotted vs. the chemical free-energy change in Fig. 5. Numbers next to the points designate the

-312-

number of the thermal cycle at which the measurement was made. The behavior appears consistent with a linear relation between the activation energy and $\Delta G^{\gamma \to \epsilon}$. The solid line represents a least-squares fit which can be expressed as:

$$Q(J/mole) = 1.230 \times 10^5 (J/mole) + 146 \times \Delta G(J/mole) \qquad (2)$$

or

$$Q(erg/event) = 2.043 \times 10^{-12}(erg/event) + 1.70 \times 10^{-21}(cm^3) \times \Delta g_v (erg/cm^3). \qquad (3)$$
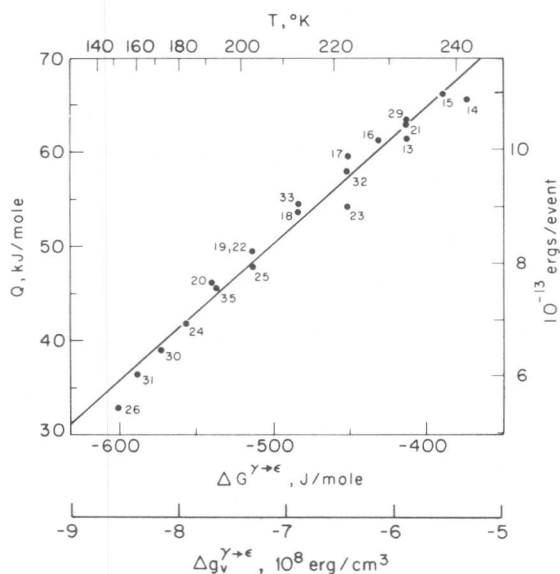

Fig. 5 Nucleation activation energy vs. chemical free-energy change. Numbers indicate thermal cycle at which isothermal measurement was made.

The slope of the line, $\partial Q/\partial \Delta g_v$, is compared with that obtained for previous FCC→BCC kinetic experiments in Table I. Shown are results from both bulk specimens [6,12] and small-particle experiments in which autocatalytic effects are circumvented [13]. The slope obtained for the FCC→HCP transformation is somewhat higher than that for the FCC→BCC transformation in Fe-Ni-Mn alloys but falls well within the range for Fe-base alloys in general. That the kinetics of the FCC→HCP transformation, in which the lattice-invariant deformation is absent, are consistent with a linear dependence of the activation energy on the chemical free-energy change, having a slope comparable to that of the FCC→BCC transformation,

Table I   Kinetic Parameters Derived from Isothermal Nucleation Experiments

	$\partial Q/\partial \Delta g_v$ cm^3	v^* cm^3	Ω	A^* cm^2
a) FCC→BCC				
Bulk Specimens				
Fe-24Ni-3Mn	1.05×10^{-21}	2.44×10^{-22}	21	4.98×10^{-14}
Fe-29.2Ni	3.69×10^{-21}	8.56×10^{-22}	73	17.5×10^{-14}
Small Particles				
Fe-24.2Ni-3.6Mn	1.20×10^{-21}	2.78×10^{-22}	24	5.67×10^{-14}
Fe-22.3Ni-0.49C	1.77×10^{-21}	4.11×10^{-22}	35	8.39×10^{-14}
b) FCC→HCP				
Bulk Specimens				
Fe-16.5Mn-6.7Ni	1.70×10^{-21}	6.03×10^{-22}	52	4.10×10^{-14}

strongly suggests that the rate-controlling step in isothermal martensitic nucleation is associated with the lattice deformation <u>in both cases</u>.

In a previous analysis of martensitic nucleation kinetics [1], isothermal kinetic data for the FCC→BCC transformation were interpreted in terms of the thermally-assisted motion[+] of discrete interfacial dislocations necessary to produce the transformation lattice deformation in a discrete crystal [14]. This interpretation is based on a dislocation-dissociation mechanism of martensitic nucleation [15,16] in which the partial dislocations bounding a nucleus are driven by a negative fault energy. For such a nucleus, n planes in thickness, the fault energy per unit area (in the plane of faulting) can be expressed as:

$$\gamma = n\rho_A(\Delta G^{ch} + E^{str}) + 2\sigma \tag{4}$$

where ρ_A is the number of moles of atoms per unit area in a close-packed plane, ΔG^{ch} and E^{str} are the molar chemical free-energy change and coherency strain energy, respectively, and σ is the particle-matrix interfacial free energy per unit area. Employing a simple model of thermally-activated deformation in which the activation energy for dislocation motion is linearly dependent on stress through an activation volume, v^*, and expressing the force exerted on the dislocations by the fault energy of eq. (4) yields the following expression for the activation energy for martensitic nucleation:

$$Q(\Delta G^{ch}) = Q_0 + \left[\tau_\mu + \frac{\Delta n\rho_A}{b}E^{str} + \frac{2\Delta n\sigma}{nb}\right]v^* + \left(\frac{\Delta n\rho_A}{b}v^*\right)\Delta G^{ch}. \tag{5}$$

Here, Q_0 is the stress-free activation energy for dislocation motion, τ_μ is the athermal friction stress, Δn is the number of planes transformed per dislocation ($\Delta n = 2$ for FCC→HCP, $\Delta n = 1$ for FCC→BCC), and b is the dislocation Burgers vector. A linear dependence of Q on ΔG^{ch} is then controlled by the activation volume for motion of the dislocations accomplishing the lattice deformation.

Values of the activation volume necessary to account for the transformation kinetic data are given in Table I expressed both in units of cm^3 and atomic volume, Ω. In order to compare the kinetic parameters of the FCC→HCP and FCC→BCC transformations which involve different Burgers vectors, a more appropriate basic quantity is the activation area, A^*, defined by $v^* = bA^*$. This parameter is given in the last column of Table I. Based on this quantity, the FCC→HCP result is in good agreement with that of the FCC→BCC transformation in the same Fe-Ni-Mn system. The activation area thus obtained is also in excellent agreement with that

---

[+]Calculations in ref. [1] indicate that dislocation motion is more likely to be thermally activated than is dislocation production in this case.

observed for slip in austenitic steels at low temperatures [17]. This activation area is thought to be controlled by dislocation-solute interactions. It is expected that the effect of thermal cycling in the FCC→ HCP experiments is to increase the dislocation density in the parent austenite, thereby providing an athermal back stress that would not significantly affect the activation area for the rate-controlling solute interaction. Hence, comparison of the kinetic behavior of the thermally-cycled alloys with that of the annealed alloys on which the FCC→BCC studies were previously made seems reasonable. Further FCC→HCP kinetic experiments on annealed alloys are planned.

IV. Conclusions

1. The basic nucleation-kinetics behavior of the FCC→HCP martensitic transformation is essentially the same as that of the FCC→BCC transformation in the same alloy system. Since the lattice-invariant deformation is absent in the FCC→HCP case, this strongly suggests that the rate-controlling step is associated with the lattice deformation in both instances.

2. As shown previously for the case of the FCC→BCC transformation, the observed linear dependence of the nucleation activation energy on the chemical free-energy change is consistent with the thermally-assisted motion of discrete interfacial dislocations accomplishing the lattice deformation with the same activation area as for slip in austenite at low temperatures.

References

[1] G.B. Olson and M. Cohen: Met. Trans., 7A(1976), 1915.
[2] V. Raghavan and M. Cohen: Acta Met., 20(1972), 333.
[3] J.F. Breedis and L. Kaufman: Met. Trans., 2(1971), 2359.
[4] M. Shiga and Y. Nakamura: J. Phys. Soc. Japan, 19(1964), 1743.
[5] I.N. Bogachev, V.F. Yegolayev, and B.M. Efros: Fiz. Metal. Metalloved, 29(1970), 424.
[6] S.R. Pati and M. Cohen: Acta Met., 17(1969), 189.
[7] L. Rémy: Met. Trans., 8A(1977), 253.
[8] L. Kaufman: Manlabs-NPL Thermochemical Databank, 1979.
[9] L. Rémy: Acta Met., 25(1977), 173.
[10] G.B. Olson: Sc.D. Thesis, MIT Dept. Mat. Sci. and Eng., June 1974.
[11] R.J. Weiss and K.J. Tauer: J. Phys. Chem. Solids, 4(1958), 135.
[12] V. Raghavan and M. Cohen: Met. Trans., 2(1971), 2409.
[13] C.L Magee: Met. Trans., 2(1971), 2419.
[14] G.B. Olson and M. Cohen: to appear in Acta Met. (1979).
[15] G.B. Olson and M. Cohen: Met. Trans., 7A(1976), 1897.
[16] G.B. Olson and M. Cohen: Met. Trans., 7A(1976), 1905.
[17] G.F. Bolling and R. H. Richman: Phil. Mag., 19(1969), 247.

Second and third order elastic constants and martensitic nucleation in a Cu-Zn-Al alloy

G. GUENIN and P.F. GOBIN

Various experiments were done on the same single crystal of β Cu-Zn-Al alloy in the vicinity of the M_s temperature and on a martensitic single crystal. Second and third order elastic constants were measured by ultrasonic technique, and phonon dispersion curves were deduced from neutron scattering experiments. The relative lattice instability of the crystal is seen through the low value of $C' = \frac{1}{2}(C_{11} - C_{12})$, second order elastic constant and its positive temperature derivative. Nevertheless the temperature derivative is not very high. The phonon branches study confirms this situation : the whole TA_2 phonon branch corresponding to C'(at q = 0) is located at very low frequencies and these frequencies weakly decrease with decreasing temperature but without critical behaviour even at the very vicinity of M_s temperature. From third order elastic constants measurements it was shown that the C' coefficient is very sensitive to uniaxial stresses. In particular a [001] uniaxial compression made to sharply decrease the (110) [1$\bar{1}$0] C' coefficient. This situation is shown to correspond to one of the stability criteria described in Clapp's calculation. It is shown that a shear strain (110) [1$\bar{1}$0] is well able to reduce the lattice stability. The result is used to calculate the instability region around dislocations. The consequences on the martensite nucleation are then examined.

I. Introduction

In the thermoelastic martensite alloys it is likely to think that the mechanical stability plays an important part in the nucleation process of the martensite. In this paper an extensive experimental stability study will be shown in the particular case of Cu-Zn-Al alloy, then will be presented a description of a possible nucleation process in this kind of alloys.

II. Experimental Results

<u>Elastic constants</u> : The figure 1 exhibits the values of the elastic constants and their variations with temperature in the β phase. In addition one of the sets of corresponding values in the martensite are presented [1, 2]. The outstanding features are :
- the now well known very low value of C' constant and its positive temperature dependance.
- the very different value of the corresponding elastic constant in the martensite and its large negative temperature dependance (larger than usual), whereas the other constants and their temperature derivatives are not very different from the corresponding ones in the β phase.

Groupe d'Etudes de Métallurgie Physique et de Physique des Matériaux
E.R.A. n° 463 - Institut National des Sciences Appliquées de LYON -
Bâtiment 502 - 20, avenue Albert Einstein - 69621 VILLEURBANNE CEDEX
FRANCE -

From this it can be concluded that the mechanical stability decreases as the transformation temperature range is approached in the martensitic phase as well as in the β phase [2]. However the derivatives are not very high and the situation is far from catastrophical.

<u>Phonon dispersion curves</u> : the principal result concerning the phonons branches measured by neutron scattering [3] is shown on figure 2. The result is in good agreement with those obtained on Au-Cu-Zn [4] and Cu-Al-Ni [5] alloys : the whole $TA_2[\zeta\zeta0]$ branch is very low in energy and decreases with decreasing temperature. A small anomaly at $q=\frac{2}{3}q$ max is seen on this branch and was also observed on Au-Cu-Zn alloy [4]. This anomaly can be related to the 9R structure of the martensite and appears therefore as a premartensitic effect. Nevertheless the behaviour, again is not critical near the M_s temperature.

<u>Third order elastic constants</u> : the set of the third order elastic constants was obtained from ultrasonic measurements under uniaxial and hydrostatic stresses of the sample [6]. Figure 3 illustrates the velocities variations with uniaxial stress. It is to be noticed a very high sensitivity of the "C'" velocity to the applied uniaxial stress in particular it is seen that a $|001|$ uniaxial stress induces a sharp decrease of the (110) $|1\overline{1}0|$ velocity (C'). This is the evidence of the large anharmonicity affecting the C' coefficient. It can, be imagined that for large strains identical to those produced by $|001|$ uniaxial stress the lattice could be made unstable (C'=o). In fact this extrapolation corresponds to one of the stability criteria described in Clapp's calculation [7].

<center>III. Discussion and theory</center>

From the elastic constant measurements and the phonon dispersion curves it is unlikely that the observed soft mode (C') should be responsible for the martensite nucleation in the perfect crystal. However as first pointed out by Clapp [7], the situation can be very different in strained regions, where, due to the anharmonic terms (third order elastic constants), the lattice can become locally unstable.

Some possible unstable sites will be now examined : the most effective strain for the lattice instability is the "Bain strain" [7] and only few percent strain of this type are necessary to produce the instability. This strain level can easily be found near lattice discontinuities and Clapp's idea was that the free surface is the best candidate. However the strain near the free surface is not Bain type and it seems difficult to encounter such a strain in the crystal. We believe that a simpler strain, a single shear for example if less effective than the Bain strain type, is much more frequently found and with higher level.

In b.c.c. alloys a single shear {110} <1$\overline{1}$0>may be considered as half a Bain strain. Indeed a Bain strain can be in first approximation considered as the combination of two shears of some amplitude on two {110} <1$\overline{1}$0> systems at 60° : for example the combination of (110) [1$\overline{1}$0] and (101) [10$\overline{1}$] shears gives a Bain strain in $|100|$ direction. The stability study as a function of (110) [0$\overline{1}$1] shear strain leads to the following results :

- Stability condition :

$$C_{11}-C_{12} \pm \frac{\sigma}{2\sqrt{3}}(a-2b) > 0 \qquad (1)$$

with $\qquad a = C_{111}-C_{112} \qquad \frac{\sigma}{2} = \eta_2 = -\eta_3$

$\qquad\qquad\quad b = C_{112}-C_{123} \qquad \eta_4, \eta_5, \eta_6, \eta_1 = 0$

which gives the critical strain

$$\sigma_c = \pm \frac{C_{11}-C_{12})2\sqrt{3}}{a-2b}$$

Strain energy density to produce the instability

$$F_c - F_o = \frac{3(C_{11}-C_{12})^3}{(a-2b)^2}$$

whereas the strain energy density to produce the instability in the case of the Bain strain (7) was

$$F_c - F_o = \frac{2(C_{11}-C_{12})^3}{(a-2b)^2}$$

Thus the strain energy density necessary to produce the instability is $\frac{3}{2}$ larger, for single shear than for Bain strain which is not very much if we consider the much higher probability of shear strain occurence in the crystal.

- A physical meaning of the stability criterium can be related to the restoring force for other {110} <1$\bar{1}$0> shears systems. This restoring force is the following :

$$F_r = \frac{C_{11}-C_{12}}{2} \pm \frac{\sigma}{8} (a-2b) \qquad (2)$$

+ or - depending on the shear system.
This restoring force is almost identical to the stability criterium (1) In fact the lattice becomes unstable a little before the restoring force vanishes).

To sum up : when a bias shear is done on a {110} <1$\bar{1}$0> system
- the restoring force in this system is not modified: $\frac{C_{11}-C_{12}}{2}$
- the restoring force in one equivalent system at 60° is enhanced whereas in the other equivalent system at 60° this restoring force is reduced.

As a result a single shear strain {110} <1$\bar{1}$0> is well effective to produce a lattice instability. Such a strain can be encountered around particular dislocation in b.c.c. alloys.

A theoretical calculus [8] has shown that one important consequence of high elastic anisotropy is the emergence of dislocations with b = a <110> as a stable perfect defect instead of the well observed b = $\frac{a}{2}$ <111> (the order is not here taken into account). Moreover we ob-

served in Cu-Zn-Al alloy 9 by X ray topography a dislocation extinction which can be interpreted as resulting from a <110> type Burgers vector Therefore it is likely that such dislocations are present in highly anisotropic alloys exhibiting martensitic transformation. Around these dislocations a relativity wide region of large {110} <1$\bar{1}$0> shear strain is observed [11] which can be considered as an instability zone [10].

Role of such instability zones in the martensitic nucleation :

In classical theories of nucleation [12] the strain energy term due to the transformation is unfavourable to the nucleation. In the case of β→9R transformation the homogeneous transformation strain is very close to a simple {110}<1$\bar{1}$0> shear [17]. Consequently the instability zones near the dislocations, where C' is zero or very small can relax this transformation strain resulting in a very small strain energy term However the interfacial energy term remains and a rough calculus applied to our case leads to critical nucleus with a large number of atoms (10^5-10^6) and a large energy hill even in case of coherent nucleation. Such a critical nucleus cannot be obtained by classical thermal activation.

Crussard [14] proposed a different formulation of the thermal activation especially axed on correlated movements of atoms (waves). Starting from this idea Crussard [15] made a theory of martensite nucleation activated by high amplitude shear wave. In his theory the high amplitude necessary wave was obtained by random interference of the lattice waves. This idea of wave triggering can be used, replacing the random interference by the enhanced shear vibrations in the vicinity of dislocations due to the very low value of C'. A simplified one dimensional calculus [16] shows that if a local soft region has a C'_1 value whereas the other parts of the crystal has the value C', the amplitude of a common shear mode governed by C' is enhanced by the factor $\sqrt{\frac{C'}{C'_1}}$ in the soft region and the corresponding energy density by the factor $\frac{C'}{C'_1}$. Therefore it is likely to think that the nucleation is assisted by the high amplitude waves generated by the low C' localized around the dislocations or around other defects inducing shear strain.

IV. Conclusion

A calculation based on second and third order elastic constants, shows that around dislocations (or other type of {110}<1$\bar{1}$0> shear defect) in β phase alloys an instability zone is present where C' is nul or very small. This zone is expected to play an important part in the nucleation of martensite :

- it reduces by a large factor the strain energy term of the transformation.
- large shear lattice waves are induced in this zone which can possibility overpass the remaining nucleus barrier due to the interfacial energy.

References

[1] G. Guenin, M. Morin, P.F. Gobin, W. Dejonghe, L. Delaey : Scripta. Met., 11, 1071 (1977)
[2] G. Guenin, D. Rios Jara, Y. Murakami, L. Delaey, P.F. Gobin : to be published in Scripta. Met.,(April 79)

[3] G. Guenin, S. Hautecler, R. Pynn, P.F. Gobin, L. Delaey : To be pu-
blished in Scripta. Met.

[4] M. Mori, Y. Yamada, G. Shirane : Sol. State Com. 17, 127 (1975)

[5] S. Hoshino, G. Shirane, M. Suezawa, T. Kajitani: Japan J. Appl. Phys.
14, 1233 (1975)

[6] G. Guenin, P.F. Gobin : Scripta. Met., 12, 351 (1978)

[7] P..C. Clapp: Phys. Stat. Sol. (b), 57, 561 (1973)

[8] L.K. France, C.S. Hartley, C.N. Reid, Met. Sci. Journal, 1, 65 (1967)

[9] C. Mai, G. Guenin, M. Morin, F. Livet, C. Esnouf, P.F. Gobin : to
be published

[10] G. Guenin, P.F Gobin : to be published

[11] J.W. Steeds:"Anisotropic elasticity theory of dislocations "Claren-
dond Press Oxford (1973)

[12] L. Kaufman, M. Cohen : Progree in metal physics 7, 165 (1958)

[13] J. DeVos, L. Delaey, E. Aernoudt, Z. Metallkde. 69, 511 (1978)

[14] C. Crussard; Physica XV, 184 (1949)

[15] C. Crussard: Inst. Interm. Phys., Solvay 9è conseil de Physique,
Brussels, 345 (1951)

[16] G. Guenin: These Doctorat, Lyon (France) (1979)
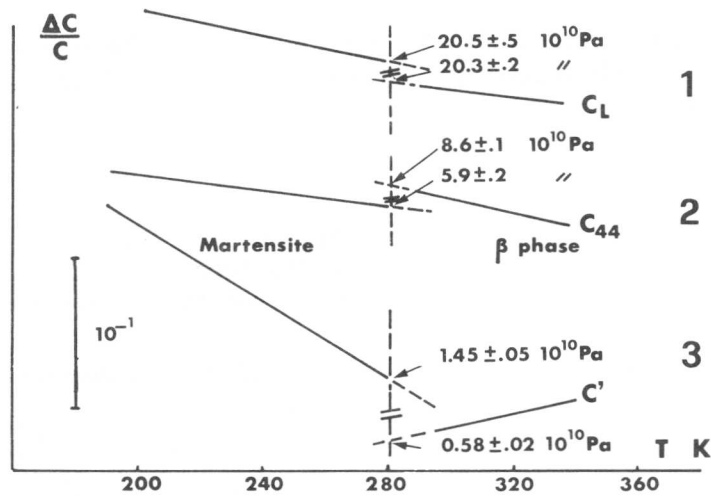
[17] M. Alhers: Z. Metallkde, 65, 636 (1974)

Figure 1 : Elastic constants and their temperature variations for
the β phase and the martensite. These elastic constants are deduced
from sound velocity measurements normal to $(011)_\beta$ plane in the β
phase and $(11\overline{4})_M$ plane in the martensite (see reference [2])

1 - Longitudinal wave (corresponding to $C_L = \frac{1}{2}(C_{11}+C_{12}+2C_{44})$ in
the β phase)

2 - Fast transverse wave (corresponding to C_{44} in the β phase)

3 - Slow transverse wave (corresponding to C' in the β phase)

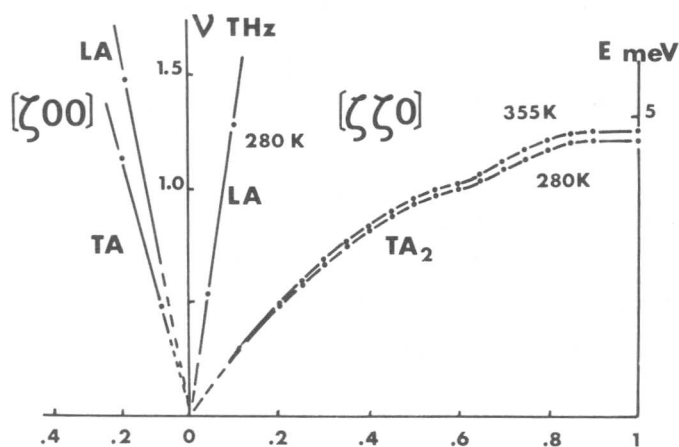Figure 2 : Some phonon branches of β Cu-Zn-Al alloy. Focussing is done on the TA$_2$ [ζζ0] branch which is very low in energy and decreases with decreasing temperature.
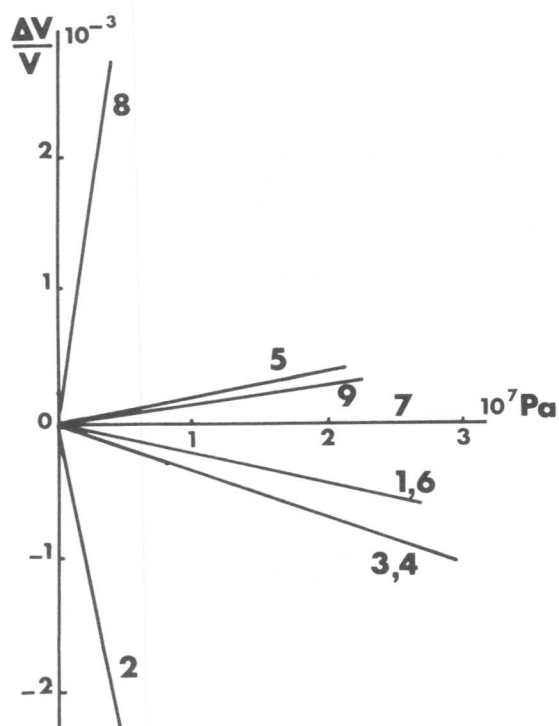

Figure 3 : Relative velocity variations with uniaxial compression static stress.

[001] compression
1-V$_\ell$ [1$\bar{1}$0]   (C$_L$)
2-V$_t$ [1$\bar{1}$0] shear [110]   (C')
3-V$_\ell$ [1$\bar{1}$0] shear [001]   (C$_{44}$)

[110] compression
4-V$_\ell$ [001]   (C$_{11}$)
5-V$_t$ [001] shear [110]   (C$_{44}$)
6-V$_t$ [001] shear [1$\bar{1}$0]   C$_{44}$
7-V$_\ell$ [1$\bar{1}$0]   (C$_L$)
8-V$_\ell$ [1$\bar{1}$0] shear [110]   (C')
9-V$_t$ |1$\bar{1}$0| shear |001| (C$_{44}$)

Molecular Dynamics Simulation of Martensite Nucleation

Philip C. Clapp* and Daniel J. McLaughlin**

Preliminary results of the simulated nucleation of a martensitic transformation in BCC and FCC lattices are presented. A Morse potential was used as the interatomic interaction and was adjusted to control the relative stability of FCC and BCC structures. A grain boundary was inserted in the FCC array and a stacking fault in the BCC array to provide nucleating heterogeneities.

I.   Introduction

As part of a larger program [1-3] to develop a general statistical mechanical theory of the heterogeneous nucleation of first order martensitic transformations, we are conducting molecular dynamics simulations of the static and dynamic motions of atoms in the vicinity of lattice defects at temperatures close to the transformation temperature. It is expected that by studying the evolution of the static displacements during the transformation a concrete picture of the critical path for nucleation will emerge in atomistic terms. In addition, by monitoring the velocity auto-correlations of selected regions of the atomic array it is possible to deduce the local phonon spectrum and thereby study what role localized soft modes may play in the nucleation process.

II.   Molecular Dynamics Simulations

The method of molecular dynamics consists in providing input to the computer for the initial spatial configuration of an array of atoms as well as their initial velocities, along with data giving the details of the interatomic interaction derived either from experiment or from theoretical calculations. The computer is "taught" Newton's laws of motion and then calculates the position and velocity of each atom in the array at subsequent time intervals.

The temperature of the system is determined by the average kinetic energy and may be changed when desired by scaling the atom velocities and waiting a suitable time interval for equilibrium to be re-established. Either the pressure or volume may be controlled by suitable manipulations of the boundary conditions of the atom array.

The boundary conditions on the outer atoms of the array must be chosen carefully or surface effects will distort the results. We have used periodic boundary conditions, which means that atoms on opposite surfaces of the array are made to interact as if they were nearest neighbors in each neighbor shell. We have initially used arrays of about 300 atoms which extend about 20 atom spacings in the z direction, and

---

*Department of Metallurgy and Institute of Materials Science, University of Connecticut, Storrs, CT 06268. **Department of Physics and Institute of Materials Science, University of Connecticut, Storrs, CT 06268.

about 4 atom spacings in the x and y direction. For the first trial
FCC array a grain boundary has been inserted at the 10th atomic level in
the z direction lying in the x-y plane. For the BCC array the {110} planes
are parallel to the x-y plane and the upper 10 planes are sheared in the
$\langle 1\bar{1}0 \rangle$ direction by $\sqrt{2}\ a/4$ relative to the lower 10 planes to introduce a
stacking fault that is expected to be an effective nucleating site for
the BCC $\rightarrow$ FCC transformation. (a is the BCC lattice parameter).

For our first simulations a normalized Morse potential (represented
by Eq. 1) is being used although we soon expect to utilize more realistic
interatomic potentials fitted to empirical elastic constant and stacking
fault energy data.

$$V(r) = e^{-A(r-r_0)} - 2e^{-2A(r-r_0)} \tag{1}$$

The Morse potential is a useful trial form because it is a reasonable
approximation to the actual interaction in many metals [4] and the two
adjustable parameters can be easily varied to make a variety of lattice
structures stable, metastable or unstable. The parameter, r_0, gives the
radial distance of the minimum of $V(r)$ and the parameter, A, controls the
curvature of the potential. $V(r)$ has positive curvature for r less than
$r_i = r_0 + A^{-1}\ln 2$ and negative curvature for r greater than r_i.

This fact is important in determining the stability of any initial
atomic array at 0°K or, equivalently, its proximity to the strain spinodal
[1]. For instance, in the case of the BCC lattice, when A has been
adjusted to make interactions with third and higher neighbors negligible,
we found that the average second neighbor distance must be less than r_i,
or the lattice is immediately unstable with respect to shear on {110}
planes implying that the strain spinodal has been crossed and $C_{11}-C_{12}<0$.
This instability problem of BCC lattices with pairwise interactions is
well known and arises because the first neighbor distance remains constant
to first order in the shear displacement whereas half the second neighbor
distances increase while half decrease. Hence if the second neighbor
distances are in a region of negative curvature of the potential, a
lowering of energy occurs as a result of the shear, initially. Milstein [5]
has given a general treatment of this problem for FCC and BCC lattices.

An interesting feature emerges in studying the BCC slightly unstable
lattice (i.e. when the second neighbor distance is larger than r_i but very
close to it). This is that shear of only a few per cent of the {110}
planes produces a stable minimum of the lattice energy. Since the shear
can be in either the $\langle 1\bar{1}0 \rangle$ direction or its opposite, a double well
minimum of the lattice energy exists for this case, a situation of consid-
erable interest in much of the recent theoretical work on higher order
displacive transitions of an anharmonic lattice [6,7]. However, for the
time being we have confined our simulations to initial arrays of BCC that
are in the locally stable condition.

One further parameter at our disposal is the volume per atom of the
array which, once set, remains constant throughout the simulation of the
transformation. As a consequence, the small volume changes that occur in
an actual first order martensitic transformation are not reproduced in our
simulations. However, by choosing an atomic volume different than that
which minimizes the lattice energy (as set by the interatomic potential),
a volume force is added to the simulation which can represent the volume

force produced by conduction electrons in a real metal. This allows for matching to the individual elastic constants and avoidance of the Cauchy relation restrictions that would apply to a lattice with only pair-wise central force interactions present.

In our results to date we have not yet tried to adjust the inter-atomic potential or other parameters to fit a real martensitic system, but have simply chosen the parameters to obtain some initial demonstration of a displacive transformation. These perhaps could be regarded as simulations of the nucleation event in "martensitium." So far, we have not observed a transition in FCC martensitium. This may be because we have not yet established a high enough driving force, or because the grain boundary is not a sufficiently potent nucleus, or because we have not waited sufficiently long in the simulations as yet. We plan to vary all three conditions in the future to determine how the transformation can be induced.

In the case of BCC martensitium we have just seen some initial evidence that upon steadily cooling from 1000°K to 500°K, the average atomic positions near the stacking fault are shifting into a regularly faulted structure approximating a FCC region that is propagating outward from the original stacking fault. We have not yet had time to watch the transformation develop completely or to study the phonon spectrum prior to and during the transformation, but this will be very shortly carried out.

References

[1] P. C. Clapp: phys. stat. sol. (b), 57(1973), 561.
[2] P. C. Clapp: J. Mat. Sci. and Eng., 38(1979), 193.
[3] P. C. Clapp: to appear in Met. Trans. (1979).
[4] L. A. Girifalco and V. G. Weizer: Phys. Rev., 114(1959), 687.
[5] F. Milstein: Phys. Rev., B2(1970), 512.
[6] A. R. Bishop and J. A. Krumhansl: Phys. Rev., B12(1975), 2824.
[7] T. Schneider and E. Stoll: Phys. Rev., B13(1976), 1216.

An Atomic Model of Strain Induced Martensitic Transformations

Douglas E. MacDonald

A jellium model of the alkali metals applicable to finite deformation is employed in the determination of the uniaxial extensions and contractions which trigger the martensitic transformation (bcc → fcc) and the reverse transformation (fcc → bcc). A Born stability criteria based on infinitesimal elasticity is used to detect the onset of the transformation during a homogeneous deformation along [001]. For the (bcc → fcc) transformation, the effective elastic coefficient ($V_{11} - V_{12}$) vanishes at c/a(bcc) $\cong$ 0.90 while the minor $V_{33}(V_{11}+V_{12})-2V_{13}^2$ vanishes at c/a(bcc) $\cong$ 1.05. For the (fcc → bcc) transformation, the effective elastic coefficient V_{66} vanishes at c/a(fcc) $\cong$ 0.66 and the coefficient ($V_{11}-V_{12}$) vanishes at c/a(fcc) $\cong$ 1.04. The symmetry and lack of it between the (bcc → fcc) transformation and its reverse is explained in terms of the effect of the deformation on the volume and structure dependent terms in the expressions for the effective elastic coefficients. The finite values found for the uniaxial strains necessary for the transformations substantiates the need for a model which can sustain such deformations. While the present stability criteria falls in the area of infinitesimal deformations superimposed on finite deformations, it is pointed out that a criteria based on finite excursions from equilibrium may be more appropriate and physically meaningful.

I. Introduction

The goal of the research described herein is to assess the applicability of the stability analysis of strained atomic models of metallic lattices to martensitic transformations. A simple yet fundamental model for metallic cohesion is adopted in order to clarify the interpretation of the underlying causes for the transformation. The stability of the strained model is investigated as a possible indicator of the onset of the transformation. The results are discussed in relation to future directions of this and similar studies.

II. Jellium Model

As a starting point the alkali metals represent a group of metals whose atomic bonding can be described by simple yet realistic models. The pseudopotential theory and its modifications give an excellent description of the cohesion in the alkali metals. In the pseudopotential theory the cohesive energy consists of the free-electron energy, the electrostatic energy and the perturbation energy. The free-electron energy consists of the Fermi, exchange, and correlation energies of the

Metal Science and Standards Division, Center for Materials Science, National Bureau of Standards, Washington, DC 20234, USA. Former address: Department of Engineering Science and Mechanics, The Pennsylvania State University, University Park, PA 16801, USA.

electron gas and depends only on the volume. The electrostatic energy is evaluated for the jellium model, i.e. a lattice of positive point ion-cores embedded in the uniform compensating sea of valence electrons. The first-order perturbation theory result, i.e. the ground state, energy [1], depends solely on the volume, whereas the second-order perturbation theory result, the band structure energy, is structure dependent. Another structure dependent energy term, the core-core replusion, is sometimes included in the expression for the cohesive energy for the alkali metals [1]. It accounts for the exchange and correlation interactions of the ion-core electrons.

For the initial calculation for the alkali metals, the core-core repulsive and band structure energy terms are omitted. Neglecting core-core repulsion assumes zero core overlap, whereas neglecting the band structure energy implies zero screening of the ion-ion interaction by the valence electrons. The model used in this research does contain, however, the effects of the Fermi, exchange, correlation, ground state and electrostatic energies. It is called the jellium model after the electrostatic energy component. Although this simple model is not the best available one for the alkali metals, it is a fundamental part of any upgraded model and it represents a vast improvement over empirical interatomic force models. For the application to martensitic transformations, it is important that the electrostatic energy term yields precisely the correct variation for the finite excursion of the bcc lattice to fcc and vice-versa [2]. In addition, the model exhibits excellent agreement with the experimental pressure-volume curves (see for example reference [1]). The jellium model adopted here is then uniquely suited to investigations of finite deformations of metallic lattices, while incorporating the volume effects of these deformations self-consistently.

III. Stability

The onset of the martensitic transformation after a prescribed finite strain is determined from a stability criterion. The strained lattice is taken to be stable if for each infinitesimal displacement the work by the applied forces does not exceed the change in the total potential energy of the system [3]. For the case of homogeneous virtual deformations under dead loading the criterion for stability can be written

$$[T_{jm}\delta_{ik} + C_{ijkm}]u_{i,j}u_{k,m} > 0 \qquad (1)$$

where T_{jm} and C_{ijkm} are the stress and the second-order coefficients in the initial strained state and the $u_{i,j}$ are the displacement gradients from that state. The quantities in the brackets are the effective elastic coefficients, B_{ijkm}, describing infinitesimal displacements from the strained state. Recognizing, of course, that deformation under initial stress is fundamentally different from the stress-free case with the related symmetry [4]. The lattice is stable then if the 9x9 elastic coefficient matrix $[[B_{ijkm}]]$ is positive definite.

In order to obtain these elastic coefficients for the homogeneously deformed state, a strain energy density function is developed from the cohesive energy expression for the jellium model. To accomplish this

the deformed atomic sphere radius, r_s', and the direct and reciprocal lattice vectors, $\overline{R}_n'$ and $\overline{K}_m'$ in the cohesive energy are written in terms of the Green deformation tensor and the whole expression divided by the atomic volume in the undeformed state [1,2]. General expressions for the thermodynamic tensions and coefficients in the deformed state can be obtained by successive differentiations of the strain energy density. The stress, T_{ij}, and the coefficients C_{ijkm} follow directly [5].

As it stands, the above criterion senses stability with respect to rigid body rotations as well as pure deformations. Assuming for now that rigid body rotations (i.e. finite strain effects) do not affect the onset of the transformation, only symmetric displacement gradients, $u_{i,j}$ are employed in Eq. (1) and the criterion can be written in terms of the 6x6 matrix $[[V_{ijkm}]]$ [6].

$$V_{ijkm} u_{i,j} u_{k,m} > 0 \qquad (2)$$

IV.   Results

The onset of martensitic transformations for homogeneous deformation along [001] have been established using Eq. (2). The results for sodium are summarized in Table I. There the moduli are now written in reduced notation.

Table I.   Strain Induced Martensitic Transformations

Initial Structure	Critical Modulus/Minor	c/a	Eigenstrain	Maximum Stress(GPa)
BCC	$V_{33}(V_{11}+V_{12})-2V_{13}^2$	1.0535	$e_{11}=e_{22}$ $e_{33}\cong-2e_{11}$	0.3936
BCC	$V_{11}-V_{12}$	0.9018	$e_{11}=-e_{22}$	-1.156
FCC	$V_{11}-V_{12}$	1.0441	$e_{11}=-e_{22}$	0.3549
FCC	V_{66}	0.6614	e_{12}	-6.331

Upon [001] extension the (110) planes of bcc become more like the (100) planes of fcc and the Bain strain eigenmode instability accelerates the change over to the fcc lattice. During contraction the (110) bcc planes begin to resemble the close packed planes of fcc and the shear instability ($e_{11}=-e_{22}$) provides the proper stacking for the transformation to fcc. Starting with fcc sodium, [001] extension carries (110) planes into similarity with the (112) planes of bcc. The shear of the (110) fcc planes at the instability produces the stacking found for (112) planes of bcc. Under contraction the fcc lattice remains stable until it reaches the same instability as for bcc. Of course, the change in the critical modulus and strain is consistent with the relative orientations of the basis cells used to define the structures (e.g. $V_{66_{fcc}} \leftrightarrow (V_{11}-V_{22})_{bcc}$). The observed instabilities correspond to the phase transformations bcc $\leftrightarrow$ fcc in the strained lattices in agreement with a referee for reference [6] and not to some mechanical failure of the lattice.

To examine any symmetries in the bcc→fcc and the fcc→bcc transformations the concurrence of the condition $V_{33}=V_{13}$ with the Bain instability is utilized. In Figure 1, $V_{11}-V_{12}$, V_{66} and $V_{33}-V_{13}$ are plotted versus c/a for the bcc and fcc sodium lattices. (Note $(V_{33}-V_{13})_{fcc}= V_{33}-V_{13})bcc$). This figure displays the range of stability for lattices under uniaxial extension-contraction. Note that while $V_{33}-V_{13}$ goes negative for bcc on extension, it only softens for fcc on contraction. This is related to the fact that on extension the lattice volume increases whereas on contraction it decreases. Since the model has a volume instability upon expansion but lacks one on compression, this helps to explain the absence of symmetry between the bcc→fcc transformation during extension and the fcc→bcc transformation for contraction. In effect, the hydrostatic pressure has stabilized the fcc lattice against transformation. As to the symmetry in the shear instabilities, it is interesting that just before the bcc lattice becomes stable again with respect to the Bain strain (i.e. c/a ≅ 1.50) the lattice is at the shear instability of the fcc lattice.

The individual contributions of the cohesive energy terms to coefficients $V_{11}-V_{12}$ and $V_{33}-V_{13}$ for bcc sodium are plotted in Figure 2. It is evident from this figure that the martensitic transformations are driven primarily by the variation in the electrostatic energy contribution to the moduli. In detail, the Bain instability of Figure 2a comes from there being a minimum of the negative electrostatic energy contri-
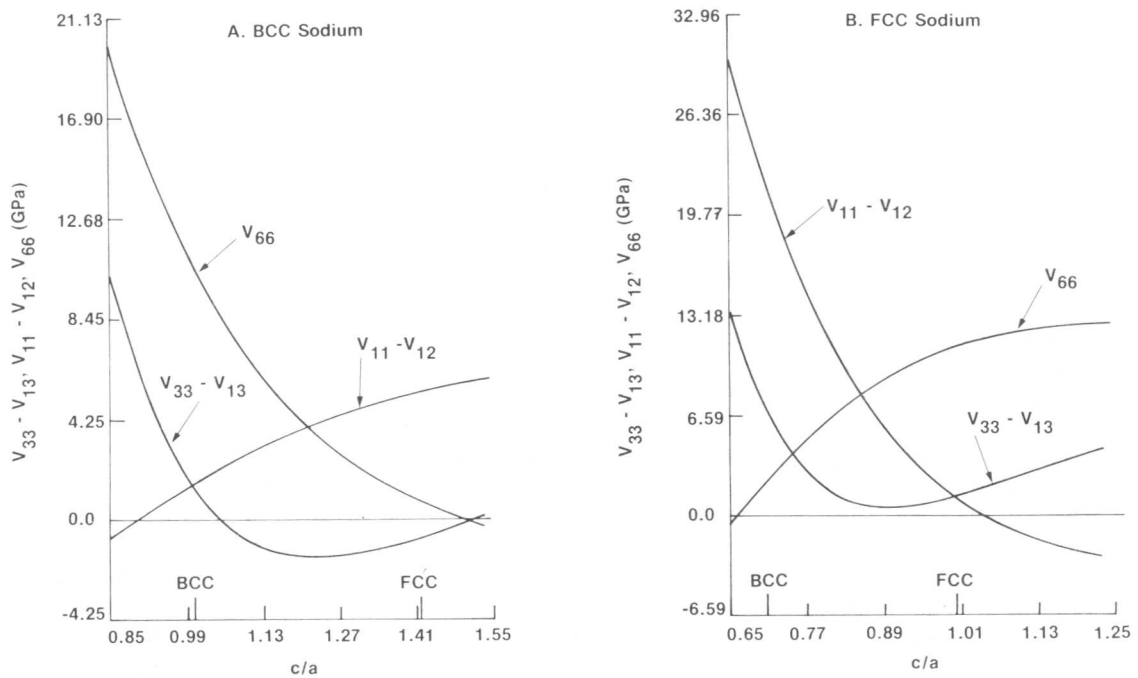

Figure 1. Variation of the moduli governing strain induced martensitic transformations. A. BCC Sodium. B. FCC Sodium.

bution during extension while the positive ground state energy term is
decreasing. For the fcc lattice on the other hand, the increase of the
ground state energy upon contraction compensates for the minimum in the
electrostatic energy contribution resulting in the softening observed
in Figure 1b. Due to the exponential factors [2] in the expression for
the electrostatic energy contribution to $V_{11}-V_{12}$, it decreases faster
than the increase in the r_s^{-3} dependence [1] of the ground state energy;
yielding the shear instability shown in Figure 2b and the transformation
to bcc during contraction.

V. Discussion

The present stability criterion falls in the area of infinitesimal
deformations superimposed on finite deformations and the eigenstrains
are identified with martensitic transformations and not mechanical
failure. In that sense, the association between instability and marten-
sitic transformations is valid. Apart from possible improvements in the
model of atomic cohesion, the crucial point is the assessment of sta-
bility. By testing for stability for virtual pure strain from the
reference state (Eq. (2)), the resulting eigenstrains may be incompatible
with dead loading [7]. In addition, the criteria in Eq. (2) or Eq. (1)
determine strictly the critical points on the loading path; stability at
these points can only be established by consideration of higher order
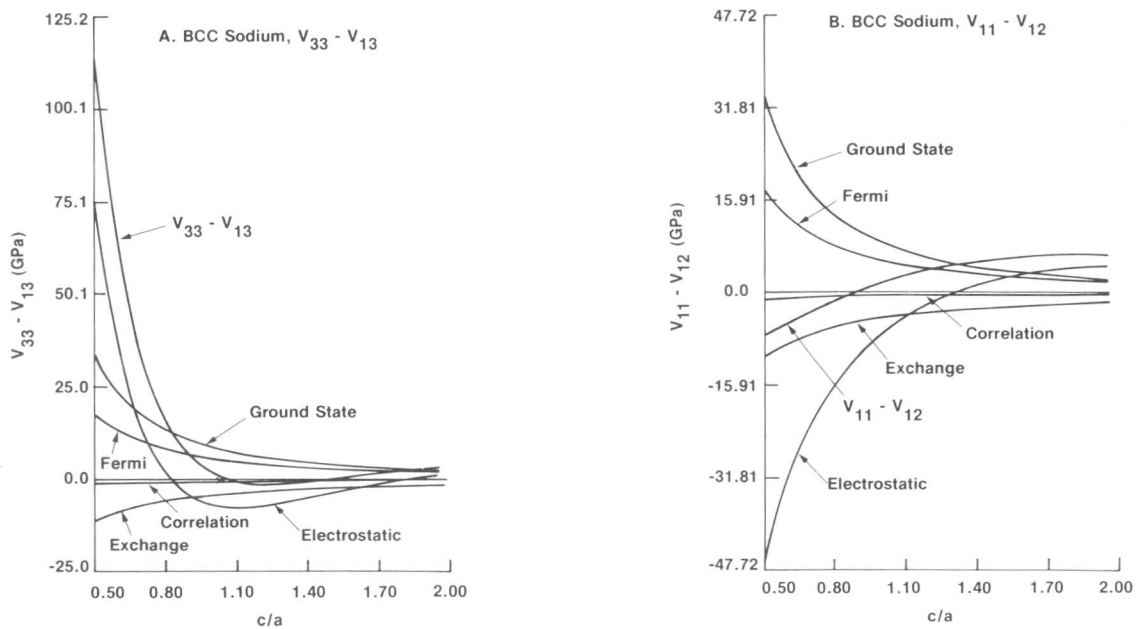variations in the energy [8]. Relatedly, the critical eigenmodes should

Figure 2. Individual contributions to the moduli for BCC Sodium which
initiate the instabilities. A. $V_{33}-V_{13}$. B. $V_{11}-V_{12}$.

be followed to assure the transformation is completed. Thus, finite excursions from the pre-strained state must be considered to determine the stability. For example, the modes where the lattice rotates with respect to the dead loads as well as deforms should be included in the criterion (i.e. Eq. (2)). All of these considerations are distinct from the implicit assumption that only relative near field stability be tested [9] in order to model martensitic transformations.

References

[1] J. Eftis, D. E. MacDonald and G. M. Arkilic: Mater. Sci. Eng., 7 (1971), 141.
[2] D. E. MacDonald: Phys. Res. B, 12 (1975), 2055.
[3] C. E. Pearson: Q. Appl. Math., 14(1956), 133.
[4] M. A. Biot: J. Appl. Phys., 11(1940), 522.
[5] R. N. Thurston: J. Acoust. Soc. Am., 37(1967), 348.
[6] N. H. MacMilliam and A. Kelly: Proc. R. Soc. Lond. A, 330(1972), 309.
[7] R. Hill: Math. Proc. Camb. Phil. Soc., 77(1975), 225.
[8] R. Hill and F. Milstein: Phys. Rev. B, 15(1977), 3087.
[9] Z. S. Basinski et al: Can. J. Phys., 48(1970), 1480.

Stess Induced Martensitic Transformation
of Fe-Ni-C Alloy Single Crystals

A. Sato*, M. Kato** and T. Mori*

Temperature and orientation dependences of transformation stress and crystallography of stress induced martensites are examined on Fe-30%Ni-0.5%C alloy single crystals. The transformation stress, defined as the stress at which first stress drop is noted on a stress-strain curve, is found to exhibit steep inverse temperature dependence in both tension and compression tests. The direction and sense dependences of a critical temperature, below which the martensitic transformation occurs by the applied stress, have indicated that the $\{111\}_f<112>_f$ shear plays an important role in the initiation of the fcc → bcc (bct) martensitic transformation. The orientation relationships, determined by an x-ray weissenberg method and an electron diffraction analysis, have also given further confirmation on this account.

I. Introduction

Under external stress fcc → bcc (bct) martensitic transformation occurs at a temperature, Md, higher than the usual Ms temperature. The transformation products, then, take particular orientations and the yield stress determined by the transformation shows an inverse temperature dependence [1]. These characteristic features of the stress effects have been studied sxtensively in recent years.

In one view it has been suggested [2,3] that interaction between external stress and total shape change associated with the transformation is essential in describing the stress effects. According to the phenomenological crystallographic theory of martensitic transformation, the shape change is calculated to meet an invariant plane condition at the final stage of the transformation so that the elastically stored energy due to the transformation becomes zero [4,5] in absence of external stress. Since evaluation of the interaction energy becomes possible only when a transformation process is completed in some volume element, such a view may be adequate if nuclei of various martensite variants are formed in advance and some of the lowest energy variants are selected to grow under the stress. Most of the reports advancing this view are, however, concerned with polycrystalline materials and the description of the stress field is not straight forward.

On the other hand, another view demonstrated by using single crystalline materials [6 ∿ 9] have suggested that the lattice change is affected by the external stress. None of these materials, however,

---

* Department of Materials Science and Engineering, Tokyo Institute of Technology, Ookayama, Meguro, Tokyo 152, Japan.

** Presently at Department of Materials Science, The Technological Institute, Northwestern University, Evanston, Illinois 60201, U.S.A.

transform in a form of a plate martensite leaving a question how this view compares with the former in conjunction with the application of the phenomenological theory [10]. The present study attempts to answer this question, by examining stress induced martensitic transformation on Fe-30%Ni-0.5%C alloy single crystals.
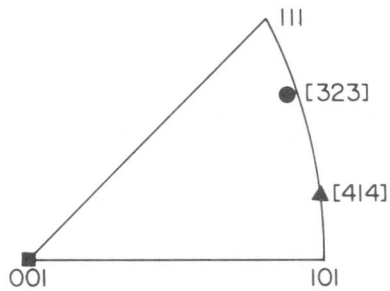
II. Experimental Procedure

Fig. 1 Stereographic projection of stress axes.

Single crystals grown by the Bridgeman method were cut to have the tensile or compressive axes as shown in Fig. 1. The tensile specimens were shaped to have shoulders at the ends and the final dimension was 1 x 1.5 x 7 mm in the gage portion. The dimension of the compressive specimen was 1 x 2.5 x 3 mm. These specimens were annealed in an argon atmosphere at 1273K for 1h, water quenched and electrolytically polished. Mechanical tests were made on an Instron type testing machine at an approximate strain rate of 3 x 10^{-4}/s in the temperature range 100 $\sim$ 293K. Some of the deformed specimens were examined in detail by an optical microscope and a monochromatic interference microscope. Orientation of martensites were determined by the x-ray Weissenberg method and a 200 kV microscope equipped with a 60° tilt and 360° rotation goniometer.

III. Experimental Results and Discussion

Yielding and plastic flow of the present crystal at a low temperature is characterized by the appearance of a large stress drop upon the martensitic transformation, in contrast to the smooth stress-strain curves at a higher temperature, as shown in Figs. 2(a) and (b). According to the surface observation, the magnitude of the individual stress drop was found to be in good correspondence with the size and the number
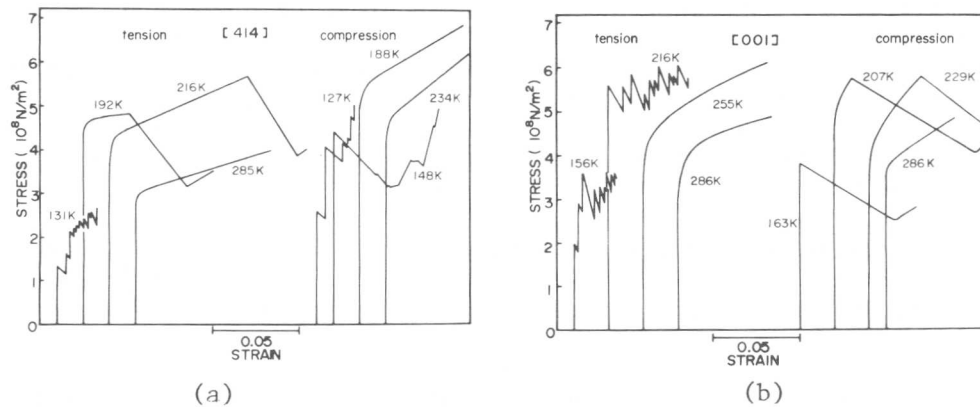

(a)

(b)

Fig. 2 Stress-strain curves obtained by tension and compression tests at various temperatures. (a) [414]. (b) [001].
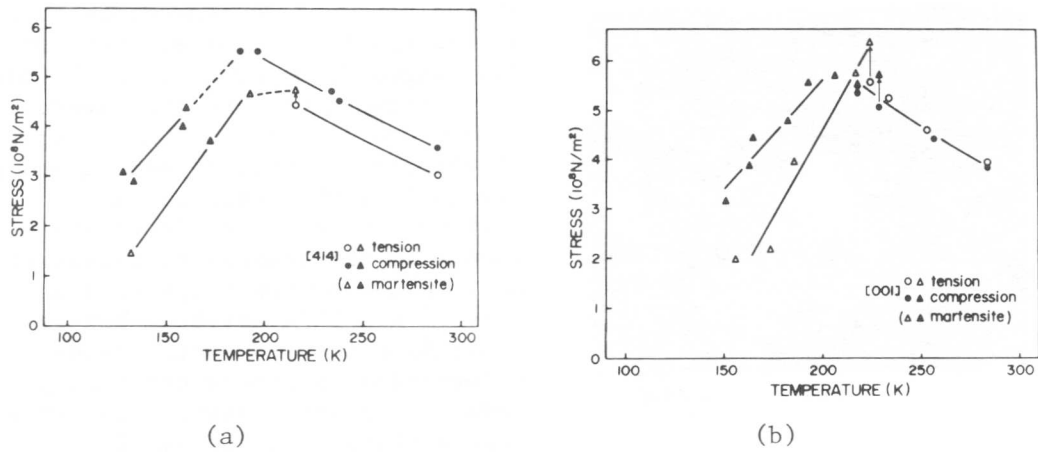
Fig. 3 Temperature dependences of transformation stress (triangle) and usual yield stress. Filled and open symbols show the tension and compression tests, respectively. (a) [414]. (b) [001].

of the martensites formed by each burst. It was found that the specimens undergone large single stress drop contained a single deformation band consisting of a number of plate martensites with identical orientation, indicating that only a single variant[†] of α-martensites formed by the burst. On the other hand, those showed small serrations contained several variants, some of which could not be incorporated with the direct influence of the applied stress. Formation of these irrational variant can be explained by considering the effect of internal stress developed around the pre-formed martensites.

We define the stress at which the first stress drop is noted as the "transformation stress", and show how it depends on the temperature and on the direction and sense of the applied stress, in Figs. 3 (a) and (b). The two data points noted "creep" in Fig. 3(a) were obtained by cooling a specimen under a constant load, showing good accordance with the results of usual tensile tests. A steep inverse temperature dependence of the transformation stress is seen clearly in the figures for both tension and compression. More interestingly it is noted that a critical temperature below which the martensitic transformation occurs is apparently higher for tension than for compression in the [414] specimen, while the situation is reversed in the [001] specimen. Such an orientation and sense dependences provide strong evidence that the $\{111\}_f<112>_f$ shear plays an importantrole as it has been demonstrated in the previous works [9,11].
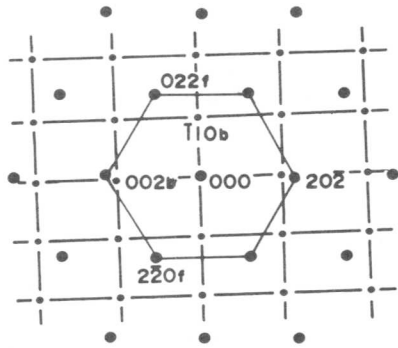
According to the surface analyses, habit planes of the martensites were found to be all in the neighbourhood of $\{145\}_f$ plane and the shape deformation was 0.21 along the $<4\ 15\ 14>$ direction which is slightly off the right angle with respect to the habit plane. The number

---

† Correctly, the plate is composed of alternating fine twinned variants.
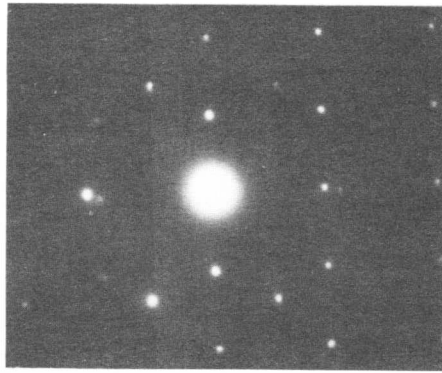
(a)

(b)

Fig. 4 Diffraction pattern of a [323] specimen deformed by tension. Projection of the tensile axis is parallel to the vertical.

of the variants decreased drastically by the application of external stress and ranged from one to a few. This is an indication that the external stress assists or prohibits formation of certain variants depending on the crystallographic orientation. However, there was no detectable change in the indices of either the habit plane or the shape deformation direction. This may be taken as an indication that the total shape deformation is determined solely by an invariant plane condition and stress contribution to it is small.

Orientation relationships of the stress-induced martensites were determined by the x-ray Weissenberg method and an electron microscopy. Figure 4 and Figure 5 show the representative diffraction patterns of the most highly populated variants in the [323] specimens, deformed 6% by tension at 180K and 4% by compression at 182K. In both micrographs the beam direction is taken along the [1$\bar{1}$1] direction, parallel to the plane normal of the primary shear system. From the indices shown in the figure, one can find the approximate orientation relationships. With reference to the x-ray results they were identified to be


(a)
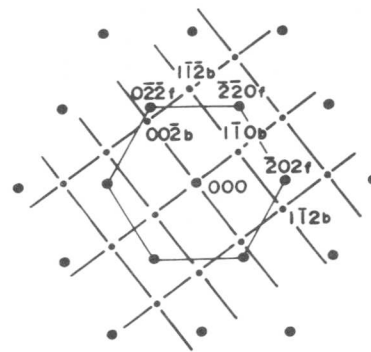
(b)

Fig. 5 Diffraction pattern of a [323] specimen deformed by compression. Projection of the compression axis is parallel to the vertical.

$$(1\bar{1}1)_f // (110)_b; \quad [121]_f // [\bar{1}10]_b \qquad\qquad \text{Fig. 4}$$

$$(1\bar{1}1)_f \overset{1°}{\sim} (110)_b; \quad [\bar{1}01]_f \overset{2.5°}{\sim} [1\bar{1}1]_b \qquad\qquad \text{Fig. 5}$$

where the former and the latter are the N and the G-T relationships, respectively. A representative Weissenberg photograph is shown in Fig. 6 where the twin related martensite of the N variant can be identified in the illustration. According to these x-ray patterns orientation relationship of the twin related N-variant was established to satisfy

$$(111)_f // (110)_{tw}; \quad [1\bar{2}1]_f // [1\bar{1}4]_{tw}$$
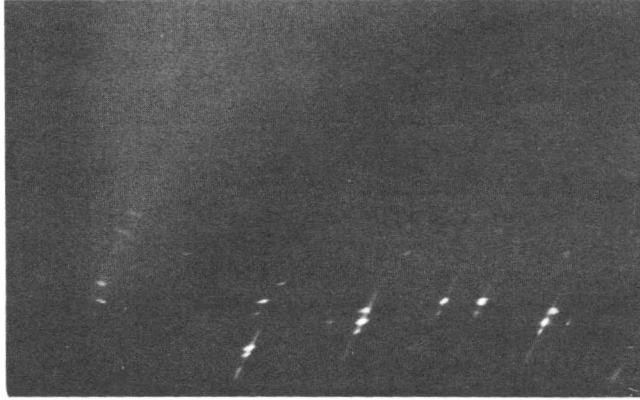
(a)
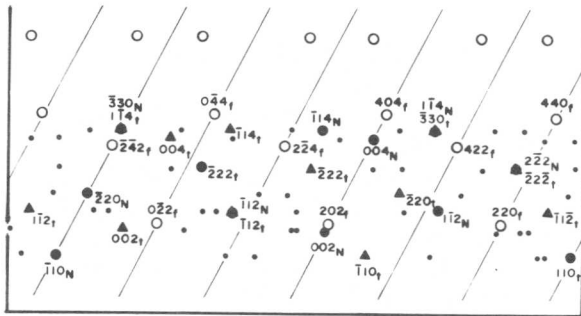
(b)

Fig. 6 An x-ray Weissenberg photograph showing a twin related Nishiyama variant.
○ Austenite. ● Other variants.
● N-variant. ▲ Twinned N-variant.

By examining the Schmidt factor for the {111} <121> shear system, preferential nucleation of these variants can be explained well by adopting the Bogers-Burgers double shear mechanism [12]. By analyzing the similar diffraction patterns of the [001] specimens, the reversal in the sense dependence of the transformation temperature (Fig. 3) is also found to be in good accordance with the previous interpretation [9].

Onodera et al [13] examined and analyzed the stress induced martensitic transformation in Fe-Ni-C and Fe-Mn-C alloys in view of the former approach described in section I. They have reported that there is a good correlation between the calculation and the experimental observation. However, If one realizes that the driving force for the transformation comes from the lattice change but not strictly from the total shape deformation, the stress effect may be discussed better by the stress-strain relationship itself, which provides direct information on the starting point of the transformation. According to the recent calculation by Mura et al [4], the elastically stored energy due to presence of alternating thin twin plates is extremely large. This energy might contribute to prohibit spontaneous propergation of martensitic transformation. Thus, one has

to pay attention to this energy, especially when the information is limited to a final state observation alone.

In order to describe the stress effect correctly, it is necessary to determine how the atomic movement is influenced by the stress and to know how the saddle point configuration is altered by the stress. In this regard, temperature, orientation and sense dependences of the stress-strain diagram provide useful information. These observations can not, however, be correlated with the phenomenological theory. For the factorized expressions used in the theory have nothing to do with the actual atomic movement. In other words, the thory does not care how the saddle point would be but discusses only the final state. Since the present study has shown that either the habit plane or the total shape deformation is hardly affected by the application of stress, it is difficult to imagine that the observed severe discrimination of the variants comes from the interaction such as considered in the earlier works [2,3,13].

Summarizing the preceding results and discussions, it is our contention that an external stress acts as a triger to nucleate certain variants, which are favoured by the stress effect on a $\{111\}_f <112>_f$ lattice shear, in fcc → bcc (bct) martensitic transformation, and the subsequent growth occurs almost spontaneously with the aid of large chemical free energy gain. The additional energy gain such as due to the interaction between the stress and the total shape change is not considered to be essential in determining the nucleation of a particular martensite variant.

REFERENCES

[1]   G. F. Bolling andR. H. Richman: Acta Mat., 18(1970), 673.
[2]   J. R. Patel and M. Cohen: Acta Met., 1(1953).
[3]   J. W. Christian: "The Theory of Transformation in Metals and Alloys", Pergamon, Oxford, (1965), 819.
[4]   T. Mura, T. Mori and M. Kato: J. Mech. Phys. Solids, 24(1976), 305.
[5]   M. Kato, T. Miyazaki and Y. Sunaga: Scripta Met., 11(1977), 915.
[6]   A. J. Bogers: Acta Met., 10(1962), 260.
[7]   G. H. Olsen and W. A. Jesser: Acta Met., 19(1971), 1009,1299.
[8]   G. Stone and G. Thomas: Met. Trans., 5(1974), 2095.
[9]   M. Kato and T. Mori: Acta Met., 24(1976), 853 and 25(1977), 951.
[10] J. S. Bowles and J. K. Mackenzie: Acta Met., 2(1954),129,138,224.
[11] A. Sato, Y. Sunaga and T. Mori: Acta Met., 25(1977), 627.
[12] A. J. Bogers and W. G. Burgers: Acta Met., 12(1964), 255.
[13] H. Onodera, H. Oka and I. Tamura: J. Japan Inst. Metals, 42(1978), 898.

Effect of Pre-Straining on Martensitic Transformation

Hidehiro Onodera* and Imao Tamura**

The effect of deformation twins which were introduced by pre-straining at 298K (above the M_d temperature) on the martensitic transformation was examined using an Fe-25%Ni-0.65%C alloy. The M_s temperature first rose up to about 10% pre-strain and then fell slowly with increasing degree of pre-straining. The maximum increase of the M_s is about 30K. From optical microscopic observations, it was found that martensites formed preferentially at the grain boundaries or the annealing twin boundaries on which deformation twins (that were introduced by pre-straining) impinged. From the crystalographic analysis, it was concluded that such martensites were formed by the aid of residual internal stress at the boundaries on which deformation twins impinged.

I. Introduction

It is well known that martensitic transformation takes place by heterogeneous nucleation. The defects in austenite have been considered to be preferential nucleation sites for the transformation. There are two different views about the effect of defects on the martensitic transformation. Magee [1] suggested that the strain fields of the incoherent steps or ledges on the annealing twin boundaries are the actual nucleation site. Eastering and Thören [2] showed that dislocations in the austenite are suitable sites for martensite nucleation by calculating the interaction energy between the nucleous and the dislocations. On the other hand, Jaswon [3] and Olson and Cohen [4] reported that the martensitic transformation takes place by dissociation of perfect dislocations in the austenite. However, it has not been confirmed what kind of defect acts as the nucleation site for the martensitic transformation and how the defect acts, since it is difficult to observe microscopically such defects as incoherent steps or ledges on the annealing twin boundaries and dislocations in the austenite.

The authors [5] reported that deformation twinning can occur in austenite of Fe-Ni-C alloys. Deformation twins can be observed by optical microscopy, so they are the most suitable to examine the effect of defects on the martensitic transformation. Therefore, in this study, the effect of deformation twins which were introduced by pre-straining above the M_d temperature on the martensitic transformation were examined.

II. Experimental Procedure

An Fe-25%Ni-0.65%C alloy was prepared by vacuum induction melting. Chemical compositions were listed in Table 1. The ingot was hot-rolled at 1473K and then cold-rolled to make a sheet of 0.8 mm thickness. The

---

* Graduate Student, Kyoto University.
** Department of Metal Science & Technology, Faculty of Engineering, Kyoto University, Sakyo-Ku, Kyoto, Japan.

specimens for tensile deformation were cut from the sheet. Specimens were austenitized at 1423K for 1h in a vacuum furnace, and were quenched in water. The specimens were pre-strained to various strain by tension at 298K (above the M_d temperature), and then the M_S temperatures were determined by electric resistivity measurment. The microstructure of the specimen was examined by optical microscopy. 35% $Na_2S_2O_5$ solution was used as an etching solution.

The variant of martensite was determined by two surface analysis. In this alloy, lenticular martensite or thin plate martensite were formed, and the habit plane was reported as $\{3\ 15\ 10\}_\gamma$ for both martensites [6, 7]. Maki et al [8] reported that the morphology of martensite depends mainly on the formation temperature. The orientation of the austenite matrix was determined by the method which was proposed by Shugo et al [9] using the four $\{111\}_\gamma$ traces of annealing or deformation twins.

III. Results

(1) Effect of pre-straining on the M_S temperature

Fig. 1 shows the variations of the M_S temperature with increasing degree of pre-straining. The M_S first rises up to about 10% strain, and then falls with increasing degree of pre-straining. The maximum increase of the M_S is about 30K.

When austenite is plastically deformed, the regions which have high internal stress are introduced. Such internal stress was suggested to aid the martensitic transformation by Kurdjumov et al [10] and Tokizane [11]. On the other hand, plastic deformation results in the strain-hardening of austenite. The strain-hardening of the austenite was suggested to lower the M_S by Tokizane [11]. It seems that the variation of the M_S in Fig. 1 can also be explained by both the effects.

(2) Optical microscopic observation

The optical microstructure observation was performed on the Fe-25%Ni-0.65%C specimen which formed a few martensite plates after cooling just below the M_S, to reveal the effect of microstructure of austenite on the martensitic transformation.

In Photo.1, (a), (b) and (c) show optical microstructures of the specimen which was deformed to 30% strain at 298K and then cooled to 130K. Martensite (M) are often observed at the grain boundary (GB) on which deformation twins impinged (Photo.1(a)), at the annealing twin boundary (AT) on which deformation twins (DT) impinged (Photo.1(b)) and at the deformation twin boundary (DT) on which deformation twins (DT) impinged (Photo.1(c)). From this observation, it was made clear that martensite was tend to form at the region which had high internal stress that formed by the impingement of deformation twins. To confirm this, the next experiment was performed.

Photo.2(a) shows optical microstructure of the specimen which deformed to 30% strain at 298K. Photo.2(b) shows optical microstructure

of the same area as (a) which was cooled to 120K. Martensite (A) and (B) are considered to be formed from the annealing twin boundary (AT) on which deformation twins (DT,A) impinged. Martensite (C) and (D) are considered to be formed from the grain boundary (GB) on which deformation twins (DT,C) and (DT,D) impinged, respectively.

From these observations, it can be concluded that the region which has high internal residual stress due to the impingement of deformation twins (that were introduced by pre-straining) is quite effective to make nucleation site for the martensitic transformation.

IV. Discussion

The stress is concentrated at the grain boundary or the annealing twin boundary on which deformation twins impinged, and such concentrated stress can not be released completely by unloading. The direction of such residual stress is crystalographically fixed by the shear system of impinging twin, and then the variant of martensite which forms by the aid of such residual stress will be restricted by the direction of the residual stress. Then the relation between the variant of martensite and the direction of residual stress was examined.

Photo.3 shows an optical microstructure which was deformed to 30% strain at 298K and then cooled to 130K. Martensites (A,B and C) are considered to be formed from the annealing twin boundary (AT) on which deformation twins (DT) impinged. The variants of these martensites were decided by two surface analysis. Twin plane of the annealing twin (AT) was decided as $(111)\gamma$ from trace analysis. That of the deformation twins (DT) was decided as $(\bar{1}\bar{1}1)\gamma$. Schmid factor for each twinning system is shown in Table 2. From Table 2, the twinning direction of the impinging deformation twins was decided as $[2\bar{1}1]\gamma$ on the $(\bar{1}\bar{1}1)\gamma$ plane. The direction of residual shear stresss was assumed the same as the twinning direction of the impinging deformation twins.

According to Livingston and Chalmers [12], if deformation twinning of system (i) (which has an unit vector e_i as its twinning plane normal and g_i as its twinning direction) has occurred in crystal A, and impinges on the grain boundary between crystal A and crystal B, and if the acting stress is P_i, the resultant shear stress P_j on twinning system (j) (which has an unit vector e_j as its twinning plane normal and g_j as its twinning direction) will be as follows.

$$P_j = P_i \times N_{ij} = P_i[(e_i \cdot e_j)(g_i \cdot g_j) + (e_i \cdot g_j)(e_j \cdot g_i)] \qquad (1)$$

N_{ij} value (stress coupling factor) between the twinning system $[2\bar{1}1]\gamma$, $(\bar{1}\bar{1}1)\gamma$ and the shear of martensitic transformation on the habit plane was calculated for 24 martensite variants. The calculated results are shown in Table 3. The shear system $\{3\ 15\ 10\}\gamma$, $<.\overline{24}\ .60\ .\overline{77}>\gamma$ was used as the shear system of martensitic transformation which was calculated by W-L-R [13]. Since martensite was formed inside $(111)\gamma$ annealing twin, the shear system was transformed to the indices of matrix by equation (2). The variants of observed martensites were marked by -o in Table 3. In Table 3, martensite variants are listed from the larger value of N_{ij}. Observed martensite variants have

$$[h \; k \; l]_M = \frac{1}{3} \; [h \; k \; l]_T \begin{pmatrix} \bar{1} & 2 & 2 \\ 2 & \bar{1} & 2 \\ 2 & 2 & \bar{1} \end{pmatrix} \qquad\qquad (2)$$

relatively large N_{ij} values. The same analyses as above were done for other 3 martensite plates. The results are shown in Table 4. In Table 3 and 4, every observed variant has large N_{ij} value. From these results, it can be concluded that martensite was formed by the aid of the residual stress which formed by the impingement of deformation twins.

Such internal residual stress can also be introduced by pile-up dislocations at the obstacles, and the residual stress is considered to have the same effect as above.

V. Conclusion

(1) The M_S temperature of the Fe-25%Ni-0.65%C alloy rose up to about 10 % pre-strain and then fell slowly with increasing degree of pre-straining.

(2) In the specimen which formed a few martensite plates after cooling just below the M_S, martensites were often observed at the grain boundaries or the annealing twin boundaries on which deformation twins (that were introduced by pre-straining) impinged.

(3) For such martensites, the N_{ij} value (stress coupling factor) between the twinning system which impinged on the boundaries and the shear of martensitic transformation on the habit plane was large. From the analysis, it was concluded that such martensites were formed by the aid of residual stress at the grain boundaries or the annealing twin boundaries on which deformation twins (that were introduced by pre-straining) impinged.

References

[1] C. L. Magee: Phase Transformation, ASM, Chapman and Hall Ltd., London, (1970), 115.
[2] K. E. Easterling and A. R. Thölen: Acta Met., 24(1976), 333.
[3] M. A. Jaswon: Inst. Metals Monograph and Rep. Series No. 18 (1955), 173.
[4] G. B. Olson and M. Cohen: J. Less-Common Metals, 28(1972), 107.
[5] H. Onodera and I. Tamura: Scripta Met., 11(1977), 1057.
[6] A. B. Greninger and A. R. Troiano: Trans. AIME, 145(1941), 289.
[7] T. Maki and C. M. Wayman: Proc. of the First JIM Int. Symposium (1976), 69.
[8] T. Maki, S. Shimooka, M. Umemoto and I. Tamura: Trans. JIM, 13 (1972), 400.
[9] Y. Shugo et al: Research Institute of Mineral Dressing and Metallurgy Report, Tohoku University, 32(1976), 109.
[10] G. V. Kurdjumov: JISI, (1960), 26.
[11] M. Tokizane: Scripta Met., 10(1976), 459.
[12] J. D. Livingston and B. Chalmers: Acta Met., 5(1957), 322.
[13] M. S. Wechsler, D. S. Lieberman and T. A. Read: Trans. AIME, 197(1953), 1503.

Table 1 Chemical compositions (wt%), M_S and M_d temperatures (K).

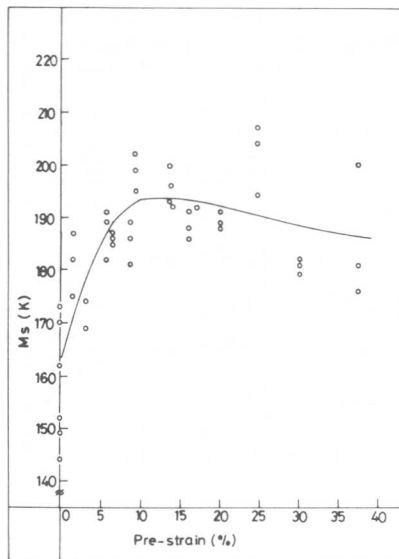| Alloy	C	Si	Mn	P	S	Ni	Fe	M_S	M_d
Fe-25%Ni-0.65%C	0.65	0.067	0.17	0.010	0.009	25.31	bal.	163	250

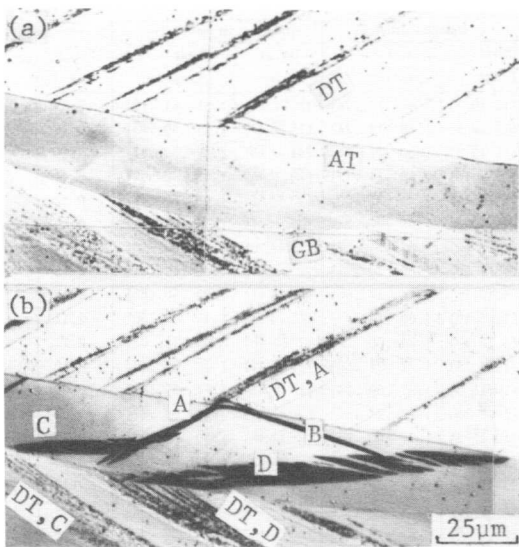Fig. 1 Variation of the M_S temperature with increasing degree of pre-straining.

Photo.2 (a):Microstructure of the specimen which deformed to 30% strain at 298K. (b):Microstructure of the same area as (a) which was cooled to 120K.
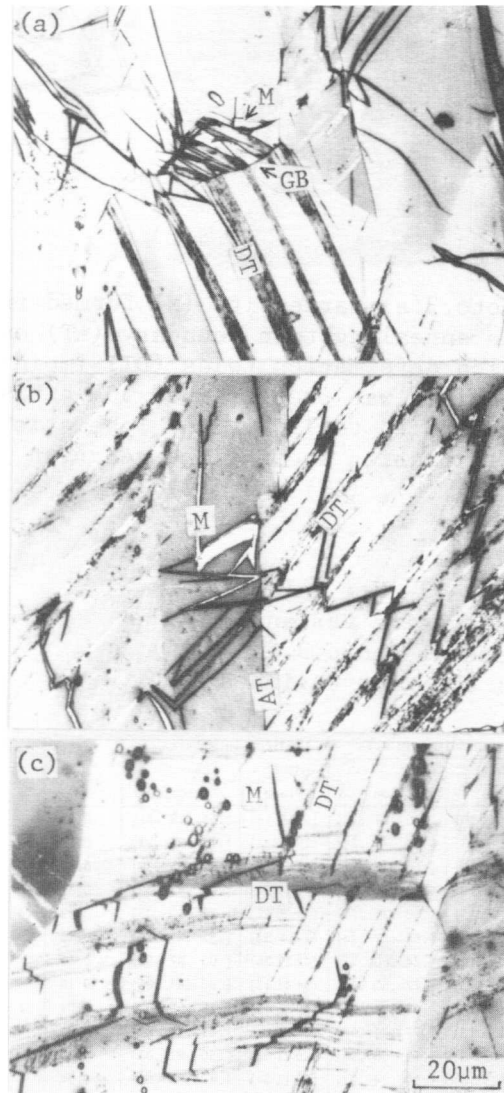

Photo.1 Microstructures of the specimen which deformed to 30% strain at 298K and cooled to 130K. (a):martensite(M) which formed from the grain boundary(GB), (b):martensite(M) which formed from the annealing twin boundary (AT), (c):martensite(M) which formed from the deformation twin boundary(DT) on which deformation twins(DT) impinged.
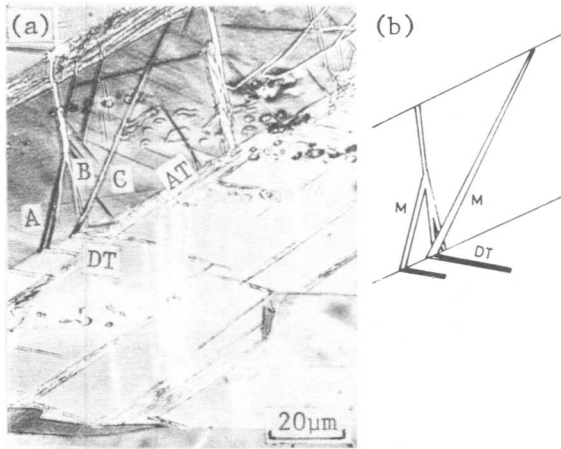
(a) (b)

Photo.3(a) Martensite (M) formed from the annealing twin boundary (AT) on which deformation twins (DT) impinged. Specimen was pre-strained 30% at 298K and cooled to 130K. (b) Schematic illustration showing the relation among (M), (AT) and (DT).

Table 2 Calculation of the Schmid factor for the shear system $\{111\}\gamma$, $<112>\gamma$ in the case of Photo.3.

Shear Plane	Shear Direction	Schmid Factor
(111)	[11$\bar{2}$]	−0.22
	[1$\bar{2}$1]	0.32
	[$\bar{2}$11]	−0.11
($\bar{1}$11)	[$\bar{1}$2$\bar{1}$]	−0.09
	[211]	−0.07
	[$\bar{1}$1$\bar{2}$]	0.17
(1$\bar{1}$1)	[$\bar{2}$$\bar{1}$1]	0.14
	[1$\bar{1}$$\bar{2}$]	−0.17
	[121]	0.03
($\bar{1}$$\bar{1}$1)	[2$\bar{1}$1]	0.41 ─o
	[$\bar{1}$1$\bar{2}$]	−0.25
	[$\bar{1}$21]	−0.16

Table 3 N_{ij} value for 24 martensite variants in the case of Photo.3.
o: observed variants.

Indices in A.T.		Indices in Matrix		S.C.F.	
Habit Plane	Shear Direction	Habit Plane	Shear Direction		
($\bar{15}$ 3 10)	[.$\bar{60}$.$\bar{24}$.$\bar{77}$]	(1 $\bar{53}$ 14)	[.55 .19 .81]	0.65	
($\bar{15}$ 10 3)	[.$\bar{60}$ .77 .$\bar{24}$]	(29 $\bar{46}$ 7)	[.15 .02 .99]	0.59	
($\bar{15}$ $\bar{3}$ 10)	[.$\bar{60}$ .24 .$\bar{77}$]	($\bar{11}$ $\bar{47}$ 26)	[.87 .03 .50]	0.48	─o
($\bar{3}$ 15 10)	[.24 .60 .$\bar{77}$]	(13 $\bar{41}$ $\bar{34}$)	[.83 .47 .$\bar{30}$]	0.37	
($\bar{15}$ $\bar{10}$ 3)	[.$\bar{60}$ .77 .$\bar{24}$]	($\bar{11}$ $\bar{26}$ 47)	[.87 .$\bar{50}$.$\bar{03}$]	0.21	─o
(15 10 3)	[.60 .77 .$\bar{24}$]	($\bar{1}$ 14 $\bar{53}$)	[.$\bar{55}$ .81 .19]	0.18	─o
($\bar{3}$ $\bar{15}$ 10)	[.24 .$\bar{60}$.$\bar{77}$]	($\bar{47}$ $\bar{11}$ 26)	[.03 .87 .50]	0.17	
($\bar{10}$ 15 3)	[.77 .60 .$\bar{24}$]	(34 $\bar{41}$ $\bar{13}$)	[.30 .47 .$\bar{83}$]	0.10	
(15 3 10)	[.60 .$\bar{24}$.$\bar{77}$]	($\bar{29}$ 7 $\bar{46}$)	[.15 .99 .02]	0.09	
($\bar{10}$ 3 15)	[.77 .$\bar{24}$ .60]	($\bar{14}$ $\bar{53}$ $\bar{1}$)	[.$\bar{81}$ .19 .$\bar{55}$]	0.05	
($\bar{10}$ $\bar{15}$ 3)	[.77 .$\bar{60}$.$\bar{24}$]	($\bar{26}$ $\bar{11}$ 47)	[.$\bar{50}$ .87 .$\bar{03}$]	−0.03	
(15 $\bar{3}$ 10)	[.60 .24 .$\bar{77}$]	($\bar{41}$ 13 $\bar{34}$)	[.47 .83 .$\bar{30}$]	−0.04	
($\bar{10}$ $\bar{3}$ 15)	[.77 .24 .60]	($\bar{26}$ $\bar{47}$ 11)	[.$\bar{50}$ .03 .$\bar{87}$]	−0.07	
(3 10 15)	[.$\bar{24}$.$\bar{77}$ .60]	($\bar{13}$ $\bar{34}$ $\bar{41}$)	[.$\bar{83}$.$\bar{30}$ .47]	−0.11	
(3 15 10)	[.$\bar{24}$ .60 .$\bar{77}$]	(7 $\bar{29}$ $\bar{46}$)	[.99 .15 .02]	−0.11	
($\bar{3}$ $\bar{10}$ 15)	[.24 .77 .60]	($\bar{47}$ $\bar{26}$ 11)	[.03 .$\bar{50}$.$\bar{87}$]	−0.13	
(3 $\bar{10}$ 15)	[.$\bar{24}$ .77 .60]	($\bar{53}$ $\bar{14}$ 1)	[.19 .$\bar{81}$ .55]	−0.24	
(3 $\bar{15}$ 10)	[.$\bar{24}$.$\bar{60}$.$\bar{77}$]	($\bar{53}$ 1 14)	[.19 .55 .81]	−0.26	
(15 $\bar{10}$ 3)	[.60 .77 .$\bar{24}$]	($\bar{41}$ 34 $\bar{13}$)	[.$\bar{47}$ .30 .83]	−0.33	
(10 $\bar{15}$ 3)	[.$\bar{77}$.$\bar{60}$.$\bar{24}$]	($\bar{46}$ 29 7)	[.02 .$\bar{15}$ .99]	−0.42	
(10 15 3)	[.$\bar{77}$ .60 .$\bar{24}$]	(14 $\bar{1}$ $\bar{53}$)	[.81 .$\bar{55}$ .19]	−0.43	
($\bar{3}$ 10 15)	[.24 .$\bar{77}$ .60]	(7 $\bar{46}$ $\bar{29}$)	[.99 .02 .15]	−0.51	
(10 $\bar{3}$ 15)	[.$\bar{77}$ .24 .60]	($\bar{46}$ 7 $\bar{29}$)	[.02 .$\bar{99}$ .15]	−0.54	
(10 3 15)	[.$\bar{77}$.$\bar{24}$ .60]	($\bar{34}$ 13 $\bar{41}$)	[.$\bar{30}$.$\bar{83}$ .47]	−0.55	

Table 4 N_{ij} value for 24 martensite variants.
o: observed variants.

Indices in A.T.		Indices in Matrix		S.C.F.	
Habit Plane	Shear Direction	Habit Plane	Shear Direction		
(15 10 3)	[.60 .$\bar{77}$.$\bar{24}$]	($\bar{1}$ 14 $\bar{53}$)	[.$\bar{55}$ .81 .19]	0.65	
($\bar{15}$ $\bar{10}$ 3)	[.$\bar{60}$ .77 .$\bar{24}$]	($\bar{11}$ $\bar{26}$ 47)	[.87 .$\bar{50}$.$\bar{03}$]	0.48	─o
($\bar{15}$ $\bar{10}$ 3)	[.60 .77 .$\bar{24}$]	($\bar{41}$ 34 $\bar{13}$)	[.$\bar{47}$ .30 .83]	0.46	
(15 3 10)	[.60 .$\bar{24}$.$\bar{77}$]	($\bar{29}$ 7 $\bar{46}$)	[.15 .99 .02]	0.44	
(3 10 15)	[.$\bar{24}$.$\bar{77}$ .60]	($\bar{13}$ $\bar{34}$ $\bar{41}$)	[.$\bar{83}$.$\bar{30}$ .41]	0.32	
($\bar{15}$ 10 3)	[.$\bar{60}$ .77 .$\bar{24}$]	(29 $\bar{46}$ 7)	[.15 .02 .99]	0.29	
($\bar{15}$ $\bar{3}$ 10)	[.$\bar{60}$ .24 .$\bar{77}$]	($\bar{11}$ $\bar{47}$ 26)	[.87 .03 .50]	0.21	─o
($\bar{15}$ 3 10)	[.$\bar{60}$.$\bar{24}$.$\bar{77}$]	(1 $\bar{53}$ 14)	[.55 .19 .81]	0.18	─o
($\bar{3}$ $\bar{10}$ 15)	[.24 .77 .60]	($\bar{47}$ $\bar{26}$ 11)	[.03 .$\bar{50}$.$\bar{87}$]	0.17	
(15 $\bar{3}$ 10)	[.60 .24 .$\bar{77}$]	($\bar{41}$ 13 $\bar{34}$)	[.47 .83 .$\bar{30}$]	0.12	
(3 15 10)	[.$\bar{24}$ .60 .$\bar{77}$]	(7 $\bar{29}$ $\bar{46}$)	[.99 .15 .02]	0.11	
(10 3 15)	[.$\bar{77}$.$\bar{24}$ .60]	($\bar{34}$ 13 $\bar{41}$)	[.$\bar{30}$.$\bar{83}$ .47]	0.10	
(10 15 3)	[.$\bar{77}$ .60 .$\bar{24}$]	(14 $\bar{1}$ $\bar{53}$)	[.81 .$\bar{55}$ .19]	0.05	
($\bar{10}$ $\bar{3}$ 15)	[.77 .24 .60]	($\bar{26}$ $\bar{47}$ 11)	[.$\bar{50}$ .03 .$\bar{87}$]	−0.03	
($\bar{10}$ $\bar{15}$ 3)	[.77 .60 .$\bar{24}$]	($\bar{26}$ $\bar{11}$ 47)	[.$\bar{50}$ .87 .$\bar{03}$]	−0.07	
($\bar{3}$ 10 15)	[.24 .77 .60]	(7 $\bar{46}$ $\bar{29}$)	[.$\bar{99}$ .02 .15]	−0.12	
($\bar{3}$ 15 10)	[.24 .60 .$\bar{77}$]	(13 $\bar{41}$ $\bar{34}$)	[.83 .47 .$\bar{30}$]	−0.13	
(3 $\bar{15}$ 10)	[.$\bar{24}$.$\bar{60}$.$\bar{77}$]	($\bar{47}$ $\bar{11}$ 26)	[.03 .87 .50]	−0.14	
(3 $\bar{15}$ 10)	[.$\bar{24}$.$\bar{60}$.$\bar{77}$]	($\bar{53}$ 1 14)	[.19 .55 .81]	−0.24	
(3 $\bar{10}$ 15)	[.$\bar{24}$.$\bar{77}$.$\bar{60}$]	($\bar{53}$ $\bar{14}$ 1)	[.19 .$\bar{81}$ .55]	−0.26	
(10 $\bar{3}$ 15)	[.$\bar{77}$ .24 .60]	($\bar{46}$ 7 $\bar{29}$)	[.02 .$\bar{99}$ .15]	−0.42	
($\bar{10}$ 3 15)	[.77 .$\bar{24}$ .60]	($\bar{14}$ $\bar{53}$ $\bar{1}$)	[.$\bar{81}$ .19 .$\bar{55}$]	−0.43	
(10 $\bar{15}$ 3)	[.$\bar{77}$ .60 .$\bar{24}$]	($\bar{46}$ 29 7)	[.02 .$\bar{15}$ .99]	−0.54	
($\bar{10}$ 15 3)	[.77 .60 .$\bar{24}$]	(34 $\bar{41}$ $\bar{13}$)	[.30 .47 .$\bar{83}$]	−0.55	

Martensitic Transformations in Iron-Nickel-Carbon Alloys

T. N. Durlu* and J. W. Christian**

Small austenitic single crystals of two alloys with sub-zero M_s (burst) temperatures were spark-machined from recrystallized samples and used in both the undeformed and deformed conditions to investigate the subsequent transformation. The M_s temperature as a function of reduction in area by rolling increased to a broad maximum at 40-50% deformation and then decreased again. Crystallographic investigations were made of the preferred habit plane variants formed in the first burst in single crystals of many different orientations predeformed in compression. Most of the crystals were orientated for single slip and the initial transformation occurred by the co-operative formation of a single group of plates with four habit plane variants. It is believed that the results indicate that an active slip system stimulates particular habit plane variants rather than inhibits others. Studies were also made of deformation-induced martensite in polycrystalline samples of Fe-Ni-C alloys. Different morphologies were found for stress-induced and strain-induced martensites.

I. Introduction

Burst transformations in Fe-Ni and Fe-Ni-C alloys are believed to involve the autocatalytic formation of groups of plates with four different variants of the habit plane at equal angles to a {110} plane of the austenite [1-2]. The kinetics of the burst transformation were studied by Brook and Entwisle [3] and many workers have published information on the effects of prior deformation and of thermal stabilization on the subsequent course of the transformation in polycrystalline materials [4-9]. Bokros and Parker [2] investigated single crystals of an Fe-31.7% Ni alloy predeformed in tension and found that the dominant habit planes in the subsequent transformation were crystallographically related to the active slip systems. Fearon and Bevis [10] have made a detailed study of the crystallography of the transformation in single crystals of Fe-Ni alloys, but no work on Fe-Ni-C single crystals has been reported.

In the temperature range immediately above M_s, the application of an external stress may result in the formation of martensite before the yield stress of the austenite is reached. This is now termed "stress assisted" martensite and the upper temperature limit at which it can form was denoted M_s^σ by Bolling and Richman [11]. At higher temperatures, slip in the austenite precedes the formation of martensite which is now "strain-induced" and has a different morphology [6,11-13]. There is some confusion in the literature about the definition of the M_d temperature,

---

* Science Faculty, Ankara University, Turkey; formerly Department of Metallurgy and Science of Materials, Oxford.

** Department of Metallurgy and Science of Materials, Oxford; temporarily at National Bureau of Standards, Washington, D.C.

especially since Guimaraes showed that small amounts of strain-induced martensite can form at temperatures appreciably above the previously accepted M_d. In his usage and that of Maxwell et al [13], M_d is regarded as the highest temperature at which plate-martensite with the normal morphology is observed and this corresponds at least approximately to the upper limit of stress-assisted martensite.

II. Experimental

Recrystallized austenitic samples of compositions Fe-26.4% Ni -0.24% C and Fe-24.0% Ni-0.45% C were obtained with grain diameters exceeding 6mm and small single crystal compression specimens were prepared by spark machining and electrolytic polishing. Some of these crystals were subsequently deformed by rolling and were then examined metallographically after cooling to various temperatures in the transformation range. Other crystals were deformed in compression, the slip traces were analyzed and then the specimens were cooled to produce transformation. Habit planes were determined from metallographic observations made with a scanning electron microscope and crystal orientations were determined from selected area channelling patterns.

Compression tests at different temperatures were carried out to investigate the formation of stress-assisted martensite in polycrystalline specimens of the Fe-26.4% Ni-0.24% C alloy and in an alloy of composition Fe-17.1% Ni-0.81% C. Habit planes were determined by means of single and two surface analyses and orientation relations from electron diffraction patterns from thin foils. Large plastic deformation of 10-70% were given to specimens of the Fe-17.1% Ni-0.81% C alloy at a temperature of 80 °C and the volume fractions of strain-induced martensite were then determined from measurements of electrical resistivity.

III. Results

The temperatures corresponding to the first burst of martensite forming during continuous cooling were -35 °C for crystals of Fe-26.4% Ni-0.24% C and -42 °C for crystals of Fe-24.0% Ni-0.45% C. Figs. 1 and 2 show the variation of these M_s temperatures with the reduction in area produced by rolling the austenite crystals at room temperature on {210} and {321} respectively. The M_s temperatures were reproducible to ±1.5 °C and no dependence on rolling direction was detected. For both alloys, the M_s temperature was initially raised by the prior plastic deformation and reached a maximum value, $\Delta M_s \approx 25$ °C, after 40-50% reduction in area. Depression of M_s, i.e. mechanical stabilization, was only observed for deformations greater than about 70%.

In the undeformed crystals, the volume fractions of martensite produced by cooling to M_s and to -80° and -140° were measured metallographically as ~10, 30 and 75% respectively. Single crystals rolled by 10% or 20% before cooling showed a small reduction in volume fraction transformed at M_s but no further effect was detected after higher strains.

Six single crystals were examined for surface slip traces after
∿5% strain in compression. Four of these crystals had widely varying
"centre triangle" orientations of the compression axis and they all
showed a single set of slip traces which corresponded to the expected
{111} plane. The other two crystals had <211> and <111> orientations
and slipped on two and three sets of {111} planes respectively. Other
control crystals were used to check the stress vs. strain behaviour. As
shown in Fig. 3, parabolic hardening was observed, rather than the three-
stage hardening characteristic of f.c.c. pure metals. The results in
Fig. 3 are plotted as true normal stresses rather than as resolved shear
stresses, and Fig. 4 shows a comparison between the stress vs. strain
curves of a single crystal and of a polycrystalline specimen of the same
composition.

Crystals of Fe-26.4% Ni-0.24% C of ten different orientations
(Fig. 5) were deformed ∿20% in compression, cooled to just below the M_s
temperature and then examined at room temperature. In each transformed
crystal, a single group of habit plane variants appeared to form over
most of the volume of the crystal, although in a few cases additional
martensite plates were observed near the edges of the specimens. The
habit planes were all approximately of the {259} type and with one
exception the dominant group consisted of four variants of this habit
centered on a particular {110} plane of the austenite. The exception
was a crystal with its compression axis close to <001> which contained
only two prominent habit planes, but a second crystal of this orienta-
tion was transformed and examined after only 8% prior strain and was
then found to contain a group of four variants.

Crystallographic analysis showed that for most crystals the pre-
ferred habits for a compression axis in the [001] - [011] - [$\bar{1}$11] unit
triangle were (2$\bar{5}$9) ($\bar{2}$59) (2$\bar{9}$5) and ($\bar{2}$95) and thus grouped about (0$\bar{1}$1).
The crystal with axis near [001] slipped on the (111) [$\bar{1}$01] and the ($\bar{1}$11)
[101] systems, and the habit planes for both crystals tested were
grouped around ($\bar{1}$10); for the crystal with only two habits, these were
($\bar{5}$92) and (59$\bar{2}$).

In polycrystalline specimens of both the Fe-26.4% Ni-0.24% C and
Fe-17.1% Ni-0.81% C alloys, the upper limit at which stress-induced
martensite was formed was 10 °C, i.e. approximately M_s+50 °C. The
plates had the typical "butterfly" or "bracket" appearance previously
described by Tamura et al [14]. Fig. 6 shows the metallographically
determined volume fraction of martensite in the Fe-26.4% Ni-0.24% C
alloy as a function of temperature after straining to just beyond the
elastic limit. Continued deformation into the plastic range resulted
in the formation of more elongated plates and the bracket effect was
less noticeable, but the morphology and crystallography were still
typical of stress-assisted rather than of strain-induced martensite.
Fig. 7 shows the mean ratio of radius to semi-thickness of the plates
derived on the assumption that the shape is lenticular. The habit
planes of five different plates were all found to be close to the {259}
type habits of the martensite formed on cooling, and the orientation
relation was of the Greninger-Troiano type. The accuracy of the de-
terminations did not justify a detailed comparison with the crystallo-
graphic theory.

Strain-induced martensite was found to occur in parallel bands as described by Maxwell et al [13] and electron microscopy of individual plates showed that these contained high dislocation densities. The volume fraction of martensite formed at 80 °C in the Fe-17.1% Ni-0.81% C alloy is shown in Fig. 8. Observations on the crystallography and substructures of the strain-induced martensite are presented in a separate note.

IV. Discussion

The results shown in Figs. 1 and 2 are in general agreement with those of Guimaraes and Shyne [5-6] and Wollmann and Guimaraes [7] but differ somewhat from those obtained for iron-nickel alloys by Gooch and West [4] and Reed [15]. Presumably, there are two competing effects in a plastically deformed region, namely a stimulation of the nucleation because of either the internal stresses or the formation of favorable defect configurations and an inhibition of growth by the deformation substructure. The increase and subsequent decrease in M_s indicates that the former dominates at low strains and the latter at very high strains.

A similar conclusion is obtained from the determinations of the preferred habits in the single crystals tested in compression. Bokros and Parker [2] used mainly multiple slip orientations and found that the preferred habit plane groups were those in which the {110} plane characterizing a group of four habits was normal to one or other of the active slip planes but was not normal to the slip directions. This rule would allow two groups of habits for the single slip orientations used in the present work, but in fact a single group, consistent with the rule, was always observed. For a crystal with duplex slip, it might be expected that only one group of habits would develop and that this would be centered on the {110} plane which is normal to both slip planes. This would be the $(0\bar{1}1)$ plane for the crystals which slipped on (111) and $(\bar{1}11)$ but in fact the group was centered on $(\bar{1}10)$. This observation that a group of variants favored by one slip plane can develop despite appreciable slip on another plane not normal to the group suggests that the role of the deformation substructure may be in stimulating some groups of variants rather than in inhibiting the growth of others. It also seems probable that the stimulation is attributable to some features of the defect configuration rather than directly to the internal stress field of the dislocation distribution. This is consistent with the observation that the volume occupied by an individual group of variants increased rather than decreased in a deformed crystal.

Maxwell et al [13] have suggested that the morphology of stress-assisted martensite is determined by a condition of maximum relief of the externally applied stress. Presumably, the accommodation stresses around one plate of a pair force nucleation of the second plate, but because of the applied stress there is no need for the formation of a full group of four variants. In the present work, the plates formed at higher strains (and stresses) became more elongated and were formed singly rather than in pairs, but the observed habit remained identical with one of the pairs in a bracket. This may be a result only of the larger magnitude of the applied stress in relation to the accommodation

stresses. All the indications are that the strain-induced martensites
ar appreciably higher temperatures form by a different mechanism.

References

[1]   E. S. Machlin and M. Cohen: Trans. AIME, 191(1951), 744, 1019.
[2]   J. C. Bokros and E. R. Parker: Acta Met., 11(1963), 1291.
[3]   R. Brook and A. R. Entwisle: J. Iron Steel Inst., 203(1065), 905.
[4]   T. G. Gooch and D.R.F. West: J. Iron Steel Inst., 205(1967), 555.
[5]   J.R.C. Guimaraes and J. C. Shyne: Scripta Met., 4 (1970), 1019.
[6]   J.R.C. Guimaraes and J. C. Shyne: Met. Trans., 2(1971), 2063.
[7]   D. R. Wollmann and J.R.C. Guimaraes: Scripta Met., 7(1973), 355.
[8]   J.R.C. Guimaraes and R. M. Brito: Scripta Met., 7(1973), 621.
[9]   M. Tokizane: Scripta Met., 10(1976), 459.
[10] E. O. Fearon and M. Bevis: Acta Met., 22(1974), 991.
[11] G. F. Bolling and R. H. Richman: Met. Trans. 2(1971), 2451.
[12] G. B. Olsen and M. Cohen: J. Less-Common Met., 28(1972), 107.
[13] P. C. Maxwell, A. Goldberg and J. C. Shyne: Met. Trans., 5(1974),
      1305.
[14] I. Tamura, T. Maki and H. Hato: Trans. Jap. Iron Steel Inst.,
      10(1970), 165.
[15] R. P. Reed: Acta Met., 15(1967), 1287.
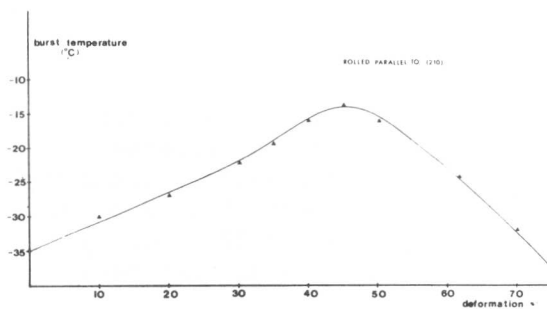
Fig. 1. M_s temperatures of crystals of Fe-26.4% Ni-0.24% C after predeformation by rolling.
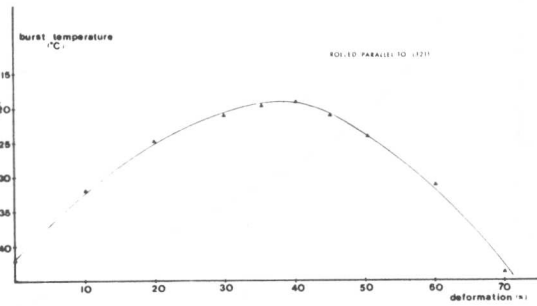

Fig. 2. M_s temperatures of crystals of Fe-24.0% Ni-0.45% C after predeformation by rolling.
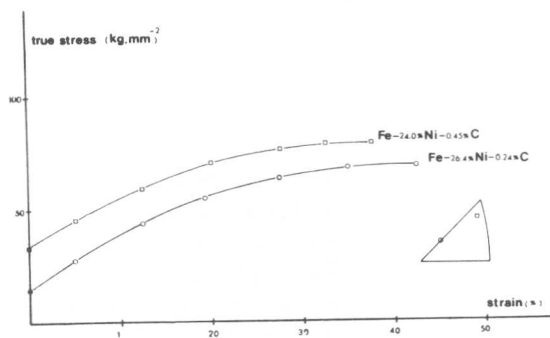

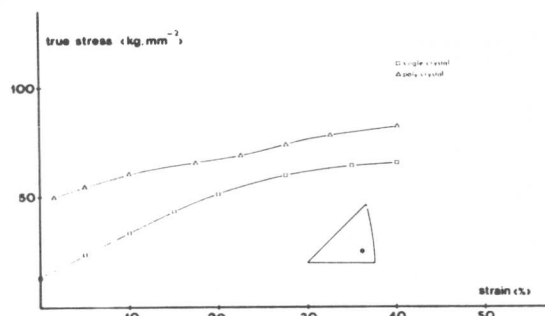Fig. 3. Compressive stress vs. strain curves of austenite single crystals.

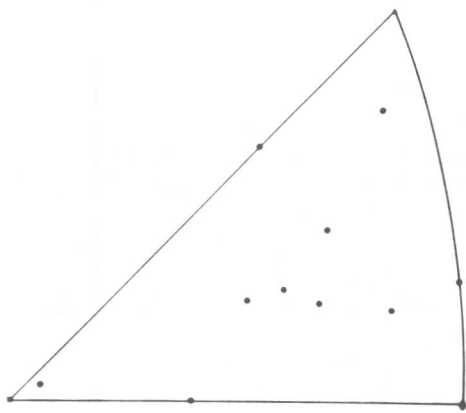Fig. 4. Stress vs. strain curves of Fe-26.4% Ni-0.24% C.

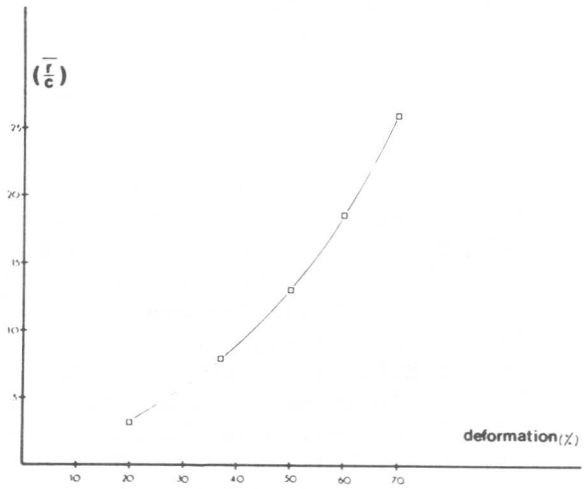Fig. 5. Compression axes of Fe-26.4% Ni-0.24% C crystals.

Fig. 7. Mean aspect ratio of stress-assisted martensite plates in Fe-26.4% Ni-0.24% C after various strains at 0°C.
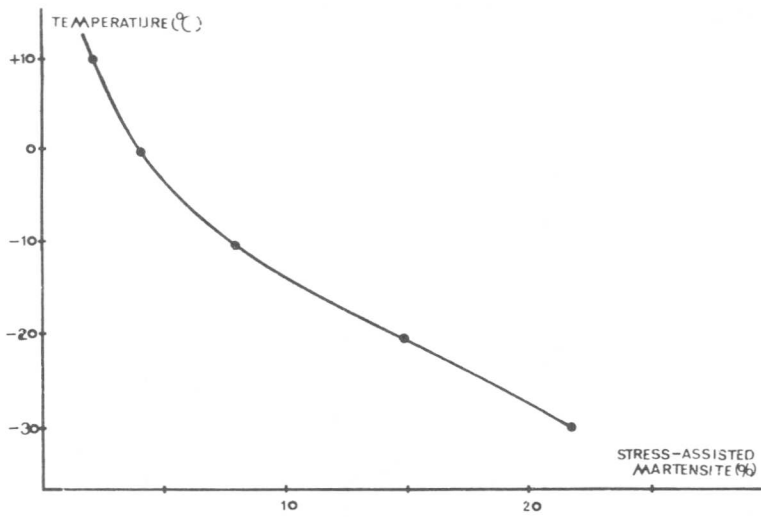

Fig. 6. Vol.% of stress-assisted martensite formed in Fe-26.4% Ni-0.24% C after 2% strain at various temperatures.
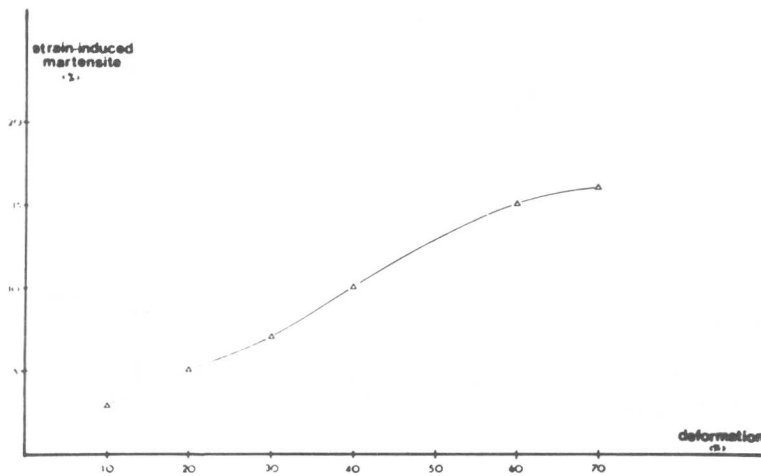

Fig. 8. Vol.% of strain-induced martensite formed in Fe-17.1% Ni-0.81% C after various strains at 80°C.

-348-

Direct observation of the nucleation of ε- and α-martensite in

stainless steels

M. H. Loretto, J. W. Brooks and R. E. Smallman

Department of Physical Metallurgy and Science of Materials,
The University, Birmingham B15 2TT, UK.

Abstract

The nucleation and growth of α- and ε-martensites have been observed in a

high voltage electron microscope during both cooling and straining of some

high purity stainless steels. It is clear from these observations that

stacking faults, which are produced either by single partial-dislocations,

or arrays of partial-dislocations, are themselves ε-martensite nucleii.

Analysis of single and overlapping faults has shown that the interplanar

spacing of the close-packed planes in the faulted volume changes to

that characteristic of ε-martensite before h.c.p. diffraction spots

can be detected. The formation of α-martensite is always observed to be

associated with dislocation pile-ups and the observations allow a very

simple·model for the nucleation and subsequent growth to be put forward.

(Paper will appear elsewhere.)

The Effect of Austenite Strength on the Transformation to Martensite in Fe-Ni and Fe-Ni-C Alloys

G.S. Ansell, P.J. Brofman, T.J. Nichol* and G. Judd

Abstract

The effect of austenite yield strength on the martensite transformation in a series of Fe-Ni and Fe-Ni-C alloys was investigated. The strength of the austenite was varied independently of composition via additions of inert yttrium oxide particles. Austenite yield strength was extrapolated down to the experimentally determined M_S temperature. As the austenite yield strength at M_S increased, both the M_S and the amount of martensite present at room temperature decreased. Thus it is confirmed that the energy required to overcome the resistance of the austenite to plastic deformation is a substantial portion of the non-chemical free energy opposing the transformation to martensite.

I. Introduction

Several investigators have discussed the relationship between the resistance of the austenite to plastic deformation and the nature of the martensite transformation [1-8, 16, 17]. In a recent work by Pradhan and Ansell [5], a calculation of the energy necessary to deform surrounding austenite (in order to accommodate transformational volume and shear strains) was compared with the chemical driving force at M_s in a series of lath forming Fe-Ni-Cr-C alloys. This comparison demonstrated that the resistance of austenite to plastic deformation represents a substantial portion of the non-chemical free energy for that alloy series.

From the above supposition [1, 4, 5] it follows that increases in austenite yield strength at M_S would increase the non-chemical free energy opposing the transformation, thus requiring an increase in the magnitude of the chemical free energy term for the transformation to proceed. This would be manifest in terms of decreasing M_S temperatures with increasing austenite yield strength at M_S [1, 4].

Changes in austenite yield strength via shifts in austenitizing temperature [3] and degree of work hardening [1, 6], have generally shown an inverse relationship between M_S and austenite yield strength. Additionally, decreases in austenite grain size have been associated with reduced M_S [10, 11, 14, 15].

The purpose of the present study [7, 12] was to investigate the effect of austenite yield strength on the martensite transformation at constant chemical composition. By adding inert oxide particles to the austenite matrix it was possible to develop a different grain size to austenitizing temperature relationship without varying alloy chemistry.

Department of Materials Engineering, Rensselaer Polytechnic Institute, Troy, N.Y. 12181.
*Allegheny-Ludlum Steel Research Center, Brackenridge, Pa.

This removed austenitizing temperature as a controlling variable and allowed increments in austenite strength due both to grain size and dispersion strengthening to be evaluated.

II. Experimental Procedure

Alloys were fabricated using powder metallurgical techniques. Raw materials were high purity carbonyl iron and nickel powder in the size range 4-8μ, graphite powder, and yttrium oxide powder (0.05-0.10 μm). Compositions of the alloys studied are given in Table I. Fe, Ni and C weight percents are calculated for the metallic matrix, while dispersed yttria contents are given in percent by volume.

Table I

Alloy Compositions

Alloy	Metal Matrix* (weight %)			Y_2O_3 Content (volume %)
	Fe	Ni	C	
Fe-Ni-C/0 Y_2O_3	bal	9.87	0.57	–
Fe-Ni-C/0.14 Y_2O_3	bal	9.79	0.57	0.14
Fe-Ni/1 Y_2O_3	bal	32.06	0.002	1.0
Casting of Fe-Ni/1 Y_2O_3	bal	32.03	0.004	–

*Analyzed

The two Fe-Ni-C alloys were prepared by wire blending for five hours while the Fe-Ni alloy was mechanically alloyed [9] in a Svegari Attriting Mill for 48 hours. Both sets of alloy powders were then packed in plain carbon steel cans, evacuated at 538°C, sealed and extruded with an extrusion ratio of 25 to 1 at 1120°C.

In the carbon-bearing alloys, M_S was determined by a search coil technique described elsewhere [18]. Prior austenite grain size was varied by austenitizing each alloy at four different temperatures. Hot tensile tests (conforming to ASTM A370) were performed at three test temperatures above the M_d for each grain size in each of the two alloys. Retained austenite measurements were made by a two peak X-ray technique [13].

M_S in the Fe-Ni alloys was measured by a resistivity technique [19]. For comparison, a section of the mechanically alloyed and extruded material was induction melted under an argon blanket in an alumina crucible. This casted piece was then homogenized for one week at 1150°C in a fused quartz ampule.

III. Results

(A) Fe-Ni-C Alloys

Fig. 1 shows the effect of austenitizing temperature on prior austenite grain size for the 0 and the 0.14 v/o Y_2O_3 alloys. Grain

growth was inhibited by the oxide dispersion, producing a more finely grained austenite at the same austenitizing temperature.
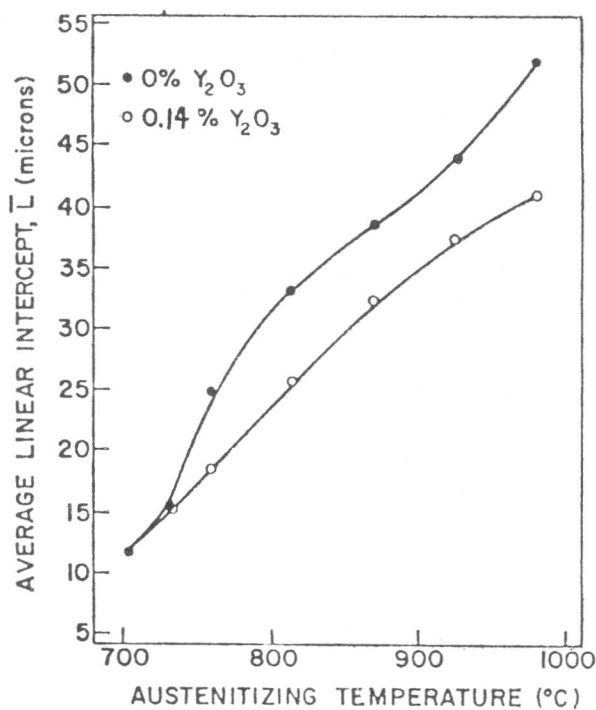

Fig. 1. Average linear intercept vs. austenitizing temperature.

M_S temperatures measured for each alloy and for each austenitizing temperature, are shown plotted against grain size in Fig. 2. These results are similar to those of Umemoto and Owen [11].

An example of the yield strength data is given in Fig. 3. The 0.2 percent offset yield stress for each austenitizing temperature, T_a, (and thus for each grain size), was fit to an equation of the form

$$\sigma_{0.2} = a + bT(°C), \quad T_a = \text{constant} \tag{1}$$

These coefficients are tabulated below:

Table II*

Yield Stress as a Function of Test Temperature

Alloy	Coefficients	Austenitizing Temperature (°C)			
		704	760	871	982
0% Y_2O_3	a	310.5	256.6	230.4	216.6
	b	−23.3	−25.6	−25.0	−25.6
0.14% Y_2O_3	a	300.6	259.4	230.5	207.0
	b	−15.6	−15.1	−16.8	−15.5
	a = MPa	b = 10^{-2}MPa/°C			

*Note: This table is a correction of previously published data [7, 12].

Figs. 4 and 5 show the variation in M_s and in percent retained austenite at room temperature with the extrapolated 0.2 percent offset yield stress at M_S. These figures suggest that varying austenite yield strength (rather than grain size per se) controls both M_s and percent transformed at room temperature, respectively [1].

The variation of austenite yield strength with grain size is shown more clearly in Fig. 6. Using the data from Table II, yield strength vs. $(\bar{L})^{-1/2}$ was plotted for several hypothetical temperatures near M_S. Hall-
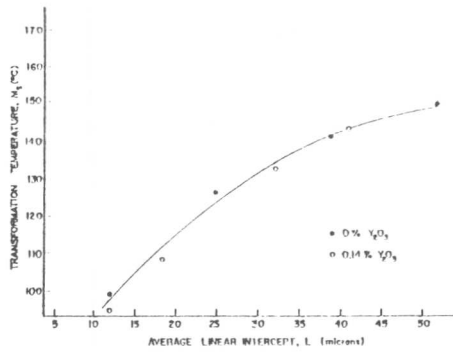
Fig. 2. M_s temperature vs. average linear intercept.

Petch strengtnening, via the expression $\sigma_{y.s} = \sigma_i + k_y(\bar{L})^{-1/2}$, clearly accounts for the observed strengthening behavior. In order to better understand the effect of the oxide dispersion, a two-dimensional linear regression analysis was computed using yield strength, temperature, and grain size data. The results of this analysis are:

0 v/o Y_2O_3: $\sigma_{0.2} =$
$(123.6-0.248T) + 658.4(\bar{L})^{-1/2}$ (2)

0.14 v/o Y_2O_3: $\sigma_{0.2} =$
$(104.4-0.158T) + 676.7(\bar{L})^{-1/2}$ (3)

The correlation coefficients for the above expression both have the value $r^2 > 0.99$, indicating that grain size is indeed controlling flow stress in this temperature regime. It is interesting to note that the slope, k_y, is relatively insensitive to oxide content (the slopes differ by < 3%). However the friction stress term, σ_i, decreases with temperature at a considerably slower rate in the oxide-bearing alloy.

(B) Fe-Ni Alloys

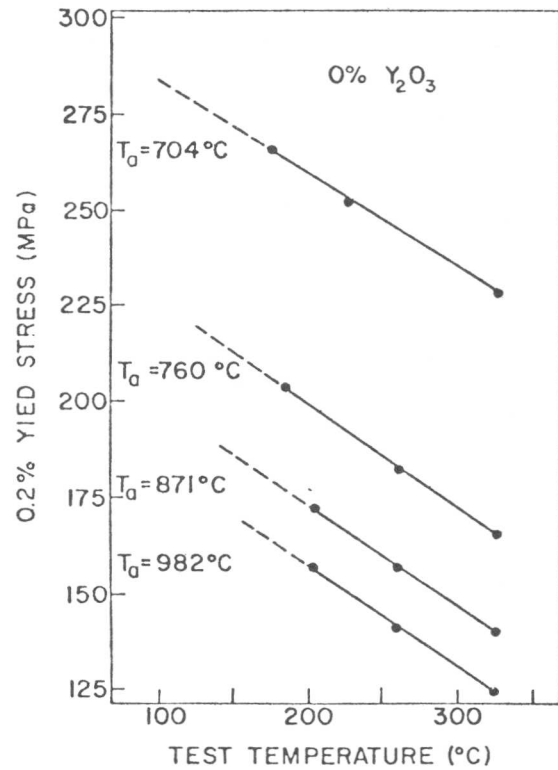Although tensile data were not obtained for the mechanically

Fig. 3. Yield stress vs. test temperature for 0 v/o yttria Fe-Ni-C alloy.
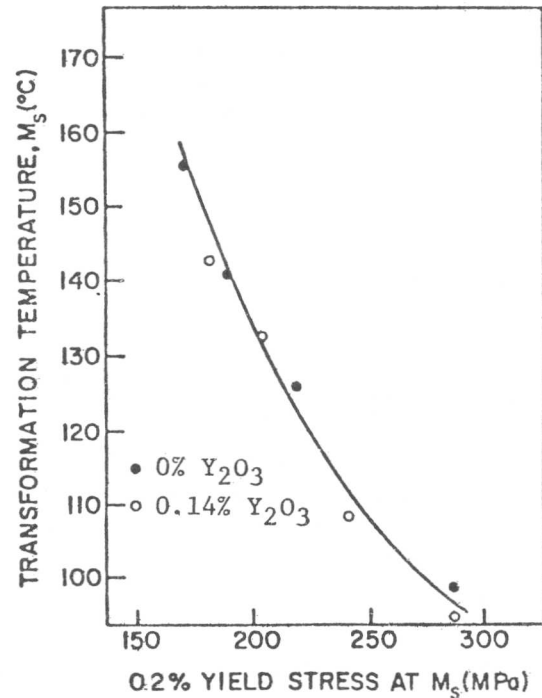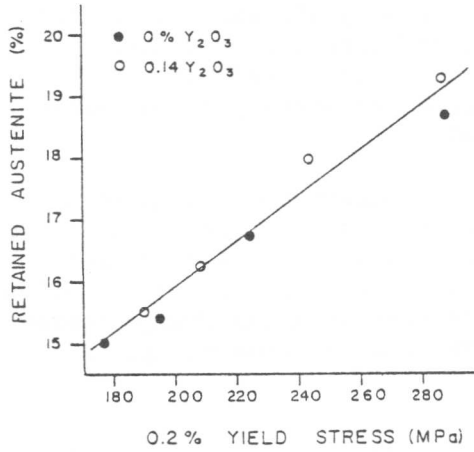

Fig. 4. M_s temperature vs. yield stress at M_s.

-353-

Fig. 5. Percent retained austenite vs.
yield stress at M_S.

Fig. 6. Calculated effect of grain size on
austenite yield stress at various
temperatures.

alloyed Fi-Ni alloy, similar
trends were observed. Table III
compares the grain size, M_S, and
room temperature hardness for the
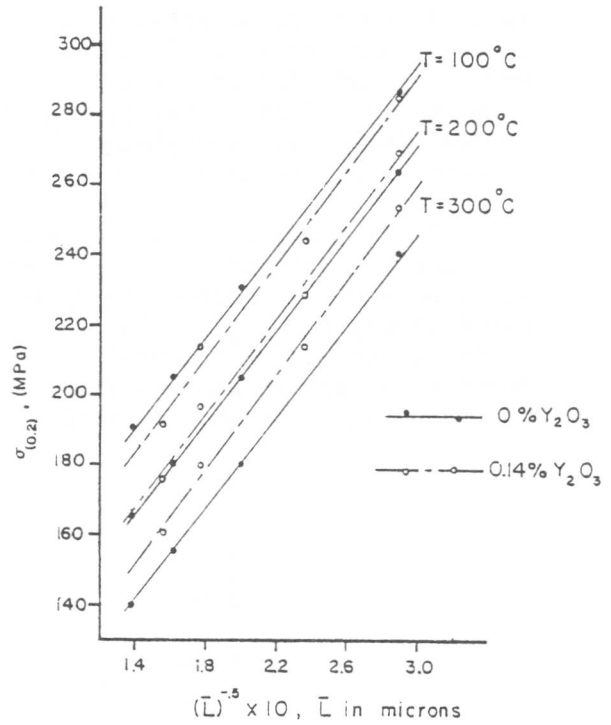extruded and cast alloys of Fe-32
Ni-1 v/o Y_2O_3.

Table III (Fe-32 Ni)

Condition	Grain Size ($\overline{L}$, μm)	M_S (°C)	Hardness (DPHN)
Mechanically Alloyed and Extruded	9	-131	144
Casting and Extruded Material	220	-32	97

The nearly 100°C drop in M_S in the extruded relative to the cast
alloy is in contrast with a 35-40°C drop in M_S observed by Umemoto and
Owen [11] in an Fe-31.3w/o Ni alloy undergoing a comparable grain re-
finement. The enhanced stabilization in the present alloy is most
likely due to dispersion strengthening.

IV. Discussion and Conclusions

In the present study, it has been shown that grain boundary
strengthening of the austenite leads to lower M_S temperatures. This is
readily explained in terms of the increased chemical driving force
(thus lower M_S) needed to offset the increased resistance to plastic
deformation.

Umemoto and Owen [11] indicated that above the 150 μm, M_S appeared

-354-

to be independent of grain size. Indeed, Fig. 2 of the present work clearly suggests a leveling off of M_S at larger grain diameters. This was explained [11] in terms of the "bursting" nature of the alloys studied. In light of the present findings, however, this apparent plateau in M_S may be explained by the decreasing potency of Hall-Petch strengthening for coarser grained material.

Fig. 7 summarizes much of the available information on M_S as a function of austenite yield strength in ferrous alloys [12]. The trend is clearly one of decreasing M_S temperature with increasing austenite yield strength at M_S. This confirms [1, 4, 5] that plastic deformation of the austenite to accommodate the transformation shape change represents an important contribution to the non-chemical free energy opposing the transformation to martensite.
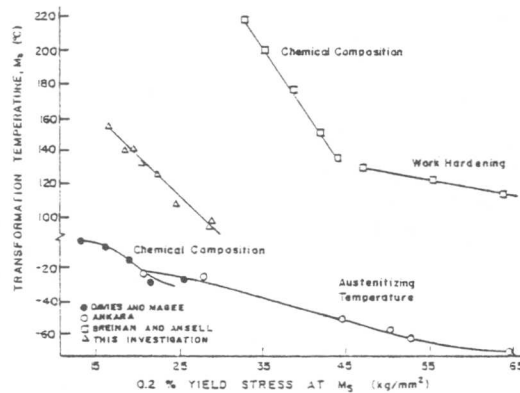

Fig. 7.   Summary of available M_S vs. austenite yield strength at M_S.

Bibliography

[1] E.M. Breinan & G.S. Ansell: Met. Trans., 1970, vol. 1, p. 1513.

[2] A.S. Sastri & D.R.F. West: J.Iron Steel Inst., 1966, vol.203, p. 138.

[3] O.A. Ankara: J. Iron Steel Inst., 1970, vol. 208, p. 819.

[4] S.J. Donachie & G.S. Ansell: Met.Trans. A, 1975,vol. 6A, p. 1863.

[5] R.Pradhan & G.S.Ansell: Met. Trans. A, 1978, vol. 9A, p. 793.

[6] J.R.Strife,M.J.Carr & G.S.Ansell: Met.Trans.A,1977,vol.8A,p.1471.

[7] T.J. Nichol, G.Judd & G.S.Ansell: Met.Trans.A,1977,vol.8A,p.1877.

[8] R.G. Davies & C.L. Magee: Met. Trans., 1971, vol. 2, p. 1939.

[9] J.S. Benjamin: Scientific American, 1976, vol. 234, p. 40.

[10] M.R. Meyerson & S.J. Rosenburg: Trans. ASM, 1954, vol. 46, p. 1225.

[11] M. Umemoto & W.S. Owen: Met. Trans., 1974, vol. 5, p. 2041.

[12] T.J. Nichol: Ph.D. Thesis, Rensselaer Polytechnic Institute, 1973.

[13] R.L. Miller: Trans. ASM, 1964, vol. 57, p. 892.

[14] Y. Inokuti & B.Cantor: Scripta. Met.,1976, vol. 10, p. 655.

[15] Y. Inokuti & B. Cantor: J. Mat.Sci., 1977,vol.12, p. 946.

[16] E.S. Machlin & M. Cohen: Trans.AIME,1951,vol.191, p. 746.

[17] J.C. Bokros & E.R. Parker: Acta.Met.,1963, vol.11, p. 1291.

[18] H.R. Woehrle, W.R.Clough & G.S.Ansell: Trans.ASM,1966,vol.59,p.784.

[19] K.A. Thornburg, D.P.Dunne & C.M. Wayman: Met.Trans.,1971,vol.2,p.2302.

Kinetics of Strain-Induced Martensitic Transformation :
the case of fcc Deformation Twinning

Luc Rémy[*]

Abstract

The kinetics of fcc deformation twinning (the variation of the amount
of twins versus strain) were determined by quantitative microscopy at
different temperatures in a Co-33Ni alloy. The stereological characteri-
zation of the twin distribution has enabled to propose a nucleation model
for twinning based on the formation of microtwin nuclei from the inter-
action of total slip dislocations. The kinetic curves have been described
by two parameters which are temperature dependent through the temperature
variation of stacking fault energy.

I. Introduction

The study of strain-induced martensitic transformations has received
considerable attention in particular since the discovery of TRIP pheno-
menon (Transformation Induced Plasticity). Most works were concerned with
the fcc-bcc transformation in stainless steels. The transformation kine-
tics, i.e. the variation of the amount transformed with strain, were
experimentally determined in some instances [see e.g.1.3]. However with
the exception of recent work by Olson and Cohen [4] only empirical equa-
tions were given to account for these results. Further transformation mecha-
nisms in stainless steels are complex with bcc martensite arising from an
intermediate transformation of the fcc matrix into twins or hcp marten-
site. Both transformation are very simple cases of martensitic transforma-
tion with transformation dislocations which are simply Shockley disloca-
tions, and direct kinetic measurements are necessary for a correct model-
ling of fcc→bcc transformation in stainless steels. Nevertheless it is
only recently that such kinetic data were established in Fe-Mn-C alloys for
the γ(fcc)→ε(hcp) transformation and in a Co-Ni alloy for fcc twinning [5,6].

In both cases the transformation kinetics were found to be largely
temperature dependent. This was attributed to the variation of stacking
fault energy (SFE) with temperature which describes the stability of the
parent fcc phase with respect to both transformations. More precisely
there is a close correlation between the temperature derivative of SFE
and the entropy change associated with the fcc→hcp transformation at
constant composition [7-9].

Though this is not always properly recognized, kinetic experiments
are a powerful means of examining the validity of nucleation mechanisms.
However before entering subtle nucleation details as those invoked in
the kinetics of isothermal fcc→bcc transformation [see e.g. 10], it is

Laboratoire de Metallurgie Mécanique, ERA CNRS 767, Centre des Matériaux
de l'Ecole des Mines de Paris, B.P. 87, 91003 EVRY CEDEX France.

necessary to have first a good description of the growth effects i.e. of stereological properties of the martensite plate distribution. Accordingly the present work reconsiders the kinetic data obtained for fcc twinning in a Co-33Ni alloy [6] with a large temperature derivative of intrinsic SFE of +0.05 mJ m^{-2} K^{-1} [7,9]. Thanks to a better stereological description of twins, a new kinetic model is proposed for twinning based on dislocation interaction.

II. Experimental Procedure

The composition of the alloy used in this study is Co-33.05% Ni with 200 ppm C in wt % as the major impurity. Tensile specimens were solution treated at 1273K for 30 min and then water-quenched, which gives a 80μm grain size. This alloy exhibits a spontaneous γ(f.c.c.)$\rightarrow\varepsilon$(h.c.p.) martensitic transformation on cooling below $E_s \sim 140K$ [7]. The transformation can be induced by straining at temperatures below $E_d \sim 280K$ [7]. However the alloy deforms only by slip and twinning at room temperature and above; twins can be observed at temperatures as high as 623K.

Cylindrical tensile specimens were tested at various temperatures as previously described [6]. The volume fraction of twins f was determined by point counting on optical micrographs on the basis of preliminary experiments with ε martensite [6]. A complete characterization of twin distribution was carried out. Since fcc twins can be considered as thin circular disks, this requires the determination of the number of twins per unit length $N_L = f/2\bar{t}$ with $\bar{t}$ the average thickness of twins [11] and of the number of twins per unit area. The average diameter of twins was obtained from $\bar{d} = 2N_L/N_A$. This definition was preferred to the harmonic mean of inverse lengths derived by Fullman [11] and previously used [5,6] which is unfortunately too much sensitive to inaccuracies in the determination of the size distribution in the range of small sizes.

III. Experimental Results

The volume fraction measurements are reported versus true strain in Fig. 1, as indicated by points, at the various temperatures studied. At variance with the strain-induced fcc-hcp transformation which starts for very small strains [5], twinning appears only after a critical strain ε_c which increases with increasing temperature. It is worth noting that only moderate volume fractions of twins are observed (lower than 0.5) as for ε martensite while the amount of strain induced α' martensite in stainless steels may reach values near unity [1].

The average size measurements of twins are illustrated in Figs. 2 and 3. The number of twins per unit length which gives an estimate of the average thickness, increases quite parabolically with the volume fraction (Fig. 2). The results can be described by the following relationship :

$$N_L = f/2\bar{t} = f/2t_o \cdot (1-f)^n \qquad (1)$$

where t_o the thickness of the first twins to form is 1.73μm and 1.04μm at 293K and 473K respectively, and the corresponding value of the exponent n is 1.9 and 1.3. Thus the thickness of twins is shown to be not